Control of Synaptic Transmission through SNARE Complex Regulation

BY

SUSAN MARIE KLOSTERMAN
B.S., Loyola University Chicago, 2006
M.S., DePaul University, 2008

THESIS

Submitted as partial fulfillment of the requirements
for the degree of Doctor of Philosophy in Biological Sciences
in the Graduate College of the
University of Illinois at Chicago, 2013

Chicago, Illinois

Defense Committee:

Janet Richmond, Advisor
David Featherstone, Chair
Liang-Wei Gong
Peter Okkema
John Larson, Psychiatry

ACKNOWLEDGMENTS

It is a great pleasure to thank the many people who made this thesis possible. Foremost, I would like to thank my Ph.D. advisor Janet Richmond for investing so much time, thought, and energy into this thesis over the past four years. Her enthusiasm and creativity continues to drive me and has made my Ph.D. experience productive and stimulating. I'm also thankful for all the memories Janet and I share outside of the lab, especially from our summer in Germany. In addition, I would like to thank the other members of my thesis committee: David Featherstone, Liang-Wei Gong, Peter Okkema, and John Larson. Their insightful suggestions and contributions have definitely improved my work.

I will forever be thankful for all the great members (past and present) of both the Richmond and Featherstone labs. I can't imagine what this experience would have been like without them. A special thanks to Anna Burdina who helped me get started, to Szi-Chieh Yu who provided all the EM for my projects, and to Ashley Martin who has been by my side since the day we joined the lab together.

Lastly I would like to thank my friends and family for all of their love and encouragement, especially my parents and fiancé Michael Territo. I will always be grateful for their faithful support and patience throughout my entire academic career. SMK

TABLE OF CONTENTS

LIST OF TABLES

LIST OF FIGURES

Chapter I

Chapter II

Chapter III

Chapter IV

LIST OF ABBREVIATIONS

ACh	Acetylcholine
BLOC	Biogenesis of lysosome-releated organelle complex
CHCR	Clathrin heavy chain repeat
DNC	Dorsal nerve cord
EJC	Evoked junctional current
EM	Electron microscopy
GFP	Green fluorescent protein
qRT-PCR	Quantative real-time PCR
HOPS	Homotypic fusion and vacuole protein sorting
HPF	High-pressure freeze fixation
LNC	Lateral nerve cord
MLD	Membrane localization domain
NEM	N-ethylmaleimide
NMJ	Neuromuscular junction
NSF	NEM-sensitive factor
PD	Presynaptic density
PKA	Protein kinase A
PS	Phosphatidylserine
RBD	Rab binding domain
RNAi	RNA interference
ROCK	Rho-associated serine/threonine kinase
SDS	Sodium dodecyl sulfate
SNAP-25	Synaptosome-associated protein of 25 kDa
SNARE	Soluble *N*-ethylmaleimide-sensitive factor attachment receptor
SV	Synaptic vesicle
VAMP	Vesicle-associated protein

VNC	Ventral nerve cord
VPS	Vacuole protein sorting
WT	Wild-type
Y2H	Yeast-two hybrid

SUMMARY

Chemical synaptic transmission is the mechanism by which animals transfer information between neurons and their targets, to process and integrate sensory inputs and produce appropriate behavioral responses. The rapid release of neurotransmitter-filled synaptic vesicles underlying this process absolutely requires the assembly of SNARE (soluble *N*-ethylmaleimide-sensitive factor attachment receptor) complexes, which represent the core fusion machinery. Consequently, proteins that regulate SNARE complex formation can profoundly alter the strength of synaptic connections. This thesis will focus on three synaptic proteins that interact with the SNARE complex, and explores their function. Specifically, the results presented establish that full-length tomosyn is required for its inhibitory function in *C. elegans*, that Snapin stabilizes the SNARE complex to promote fusion, and that VPS-39 alters Syntaxin conformation to enable fusogenic SNARE complex assembly.

I. INTRODUCTION

1.1 The synaptic vesicle cycle

In order to sustain synaptic transmission vesicles have to be locally recycled, refilled, and prepared for subsequent rounds of release as depicted in Figure 1. Neurotransmitters, synthesized within the presynapitc terminal, are loaded into vesicles via integral neurotransmitter transporters. The acidification of the vesicle lumen by proton pumps provides the driving force for vesicle refilling. Loaded synaptic vesicles are then translocated to active zones where they become docked and primed for release. Fusion competent vesicles subsequently undergo exocytosis in response to a calcium trigger, releasing their contents into the synaptic cleft. After fusion, the vesicle membranes are retrieved via endocytosis so that they can be refilled for another round of exocytosis. This precisely regulated cycle is dependent upon the highly orchestrated activity of numerous synaptically enriched proteins, which regulate the basic fusion machinery described in the following sections.

1.2 The fusion machinery: SNAREs

Synaptic vesicle fusion is critically dependent upon the formation of SNARE (soluble *N*-ethylmaleimide-sensitive factor attachment receptor) complexes. This complex has been extensively studied and is comprised of three proteins: synaptobrevin (also known as vesicle-associated protein [VAMP]), syntaxin, and SNAP-25, which are each members of an evolutionally conserved protein family implicated in membrane fusion events. Synaptobrevin was purified from synaptic

vesicles (Trimble et al., 1988) and syntaxin and SNAP-25 (synaptosome-associated protein of 25 kDa) were found to be localized on the neuronal plasma membrane (Oyler et al., 1989; Bennett et al., 1992). Synaptobrevin is often referred to as the v-SNARE because of its vesicle association, while SNAP-25 and syntaxin are referred to as t-SNAREs since they are located on the target membrane.

The SNARE proteins contain conserved 60-70 amino acid SNARE motifs (Fasshauer et al., 1998). These motifs come together to form a four alpha-helical parallel bundle known as the core complex (Sutton et al., 1998a). All three SNAREs are anchored to membranes: both synaptobrevin and syntaxin have a transmembrane domain, while SNAP-25 is anchored by the palmitoylation of cysteines located in the linker region between its two SNARE motifs. Since synaptobrevin is on synaptic vesicles and the t- SNAREs (syntaxin and SNAP-25) are on the plasma membrane, when the four-helical bundle assembles to form the *trans* SNARE complex, this brings the vesicle into close apposition with the plasma membrane. Upon calcium influx and fusion, the core complex is incorporated into the plasma membrane and referred to as a *cis* SNARE complex. In order for the SNARE proteins to be recycled, they must first be dissembled by NEM-sensitive factor (NSF) prior to sorting to their respective membranes during endocytosis.

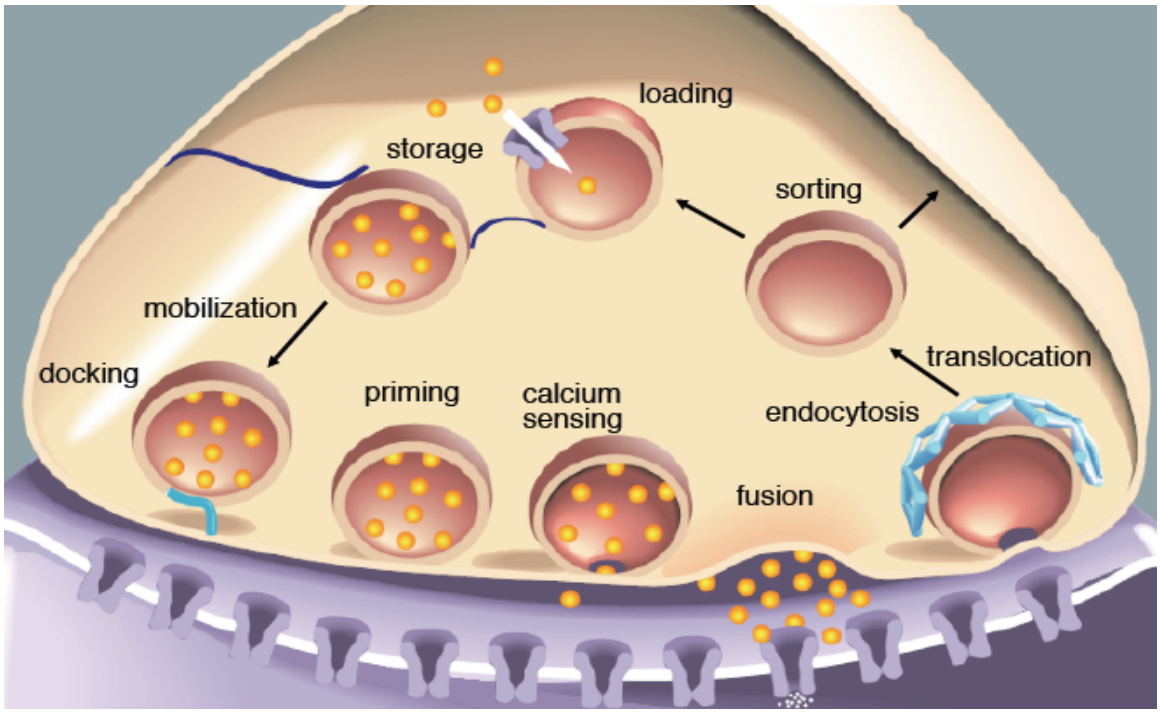

Figure 1: The synaptic vesicle cycle. Vesicles are filled with neurotransmitter and are then translocated to release sites near calcium entry where they become fusion competent. Upon calcium influx, they fuse and release their contents into the synaptic cleft. After fusion they are coated with clathrin and undergo endocytosis and the cycle can begin again.

1.3 SNARE complex assembly

Membrane fusion is a highly energetic event due to the repulsive forces of the two phospholipid bilayers. Therefore, it is necessary to overcome this energy barrier in order for bilayer mixing to occur. There are many reasons to believe that SNAREs play an important role in this process. The SNARE complex is very stable, and can only be disassociated by boiling in the presence of sodium dodecyl sulfate (SDS) (Fasshauer et al., 2002). The temporal sequence of events leading to full SNARE complex assembly is unresolved, but evidence suggests that initially the t-SNARE motifs interact to form a SNAP-25/syntaxin dimer that acts as a docking platform for vesicle interactions. At this stage, non-fusogenic dead-end SNARE complexes composed of one SNAP-25 and two syntaxin molecules can also form (Fasshauer and Margittai, 2004; Pobbati et al., 2006). In order for vesicles to become primed and fusion competent, the t-SNARE dimer must partner with the v-SNARE, synaptobrevin. The SNARE complex assembles in a parallel orientation starting at the N- terminals of the SNARE motif, "zippering'" towards the C-terminal transmembrane anchors of synaptobrevin and syntaxin (Hanson et al., 1997; Poirier et al., 1998). Evidence suggests that SNARE complexes form in two sequential stages, and can arrest in a semi-zippered state, in which only the N-terminal half of each SNARE is zippered. This is based on mutational analyses in which C terminal mutations lead to a partially unfolded configuration in which the N terminal regions of the SNARE motifs remain zippered but vesicles are in a non-fusion competent state (Sorensen et al., 2006). Consistent with this model clostridial toxin and

SNARE antibody disruption experiments indicate that the N-terminus of SNAREs are protected from cleavage at early stages, but the C-terminus is only protected at late stages of SNARE complex formation (Hayashi et al., 1994; Xu et al., 1999). This has given rise to the hypothesis that N terminal zippering occurs first and independently of the C terminal motif creating a meta-stable complex that subsequently fully zippers to trigger fusion in response to calcium.

1.4 Membrane Fusion

In order for vesicle fusion to proceed, a series of transitional steps are thought to occur; starting with the formation of a stalk bridging the vesicle and plasma membranes which has an hourglass appearance in x-ray scattering images (Yang and Huang, 2002). This stalk is comprised of a few dozen lipid molecules that eventually expand into a hemi-fused state where the outer membrane leaflet of the vesicle has merged with the inner leaflet of the plasma membrane. Hemi-fused vesicles have been observed at central synapses by conical electron tomography (Zampighi et al., 2006). Following hemifusion, further membrane mixing allows a fusion pore to develop through which neurotransmitter can exit the vesicle lumen. Alternative models suggest that the transmembrane domain of the SNARE complexes may generate a proteinaceous fusion pore in the absence of membrane mixing. While there is much debate, its likely that more than one SNARE complex is required for vesicle fusion. The minimal number of SNARE complexes required to overcome the energy barrier for exocytosis varies from as few as 2 to 15 and

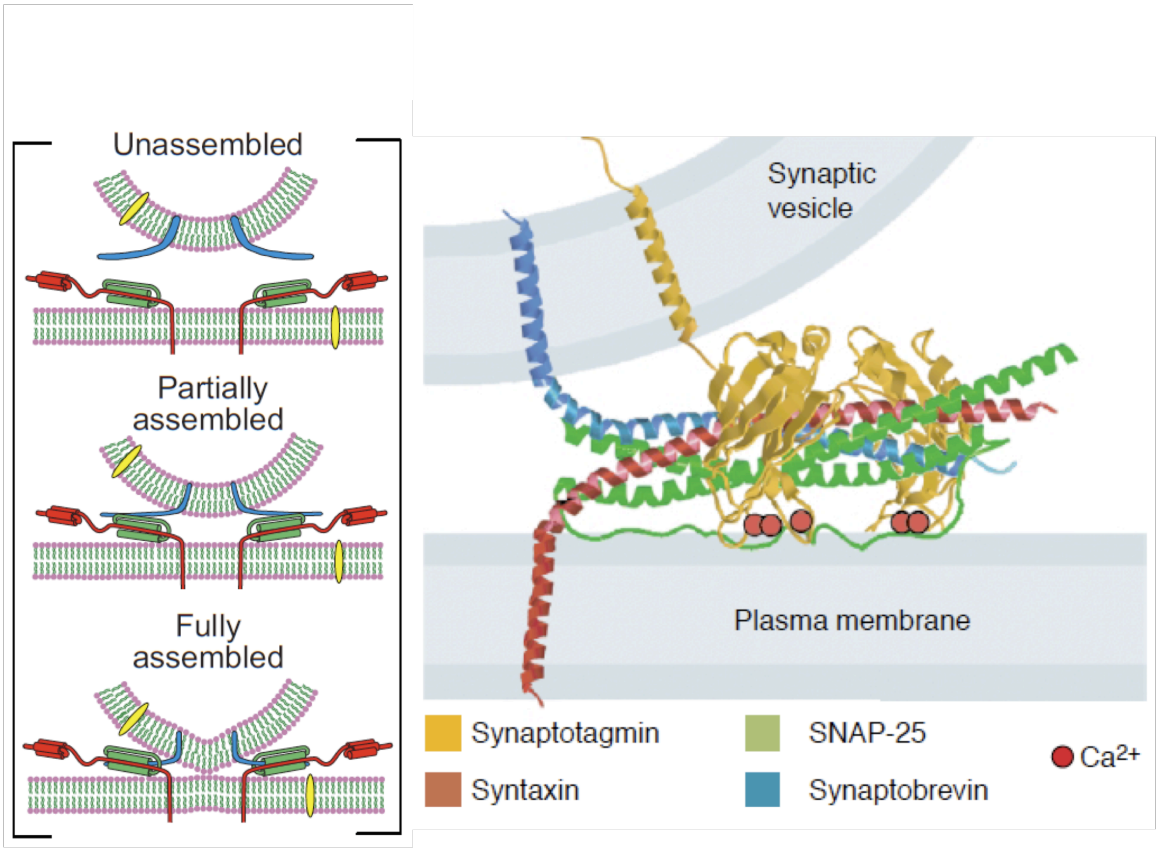

Figure 2. SNARE complex formation and association with Synaptotagmin. The series on the left depicts the SNARE complex components at various stages of assembly. The schematic on the right shows the ribbon structure of the SNAREs as well as Synaptotagmin. Adapted from (Koh and Bellen, 2003; Chapman, 2008).

appears to depend on vesicle type and experimental conditions (van den Bogaart and Jahn, 2011). There is also some evidence that SNARE complexes may form multimers which could act together to induce fusion (Montecucco et al., 2005). Such multimers have been observed at the EM level to form star-shaped structures (Rickman et al., 2005).

1.5 SNAREs and calcium sensing

Calcium influx through voltage-gated calcium channels triggers synaptic vesicle exocytosis, and is sensed by Synaptotagmin, a protein which was identified as a 65 kDa protein that associates with both synaptic vesicles and large dense core vesicles (Matthew et al., 1981). Synaptotagmin contains a transmembrane domain, and a large cytoplasmic domain comprised of two C2 domains (C2A and C2B) which bind calcium ions (Perin et al., 1991). In neurons, the main calcium sensor appears to be synaptotagmin-1, but many other isoforms have been identified (Craxton, 2007). In addition to calcium sensing, Synaptotagmin directly interacts with the SNARE complex, and likely facilitates membrane fusion.

Initial studies established binding between Synaptotagmin and syntaxin as well as assembled SNARE complexes in the absence of calcium using brain detergent extracts (Bennett et al., 1992; Sollner et al., 1993a). Subsequently, it was found that calcium binding to the Synaptotagmin C2 domains enhanced its binding affinity with Syntaxin, SNAP-25, assembled t-SNARE heterodimers, and fully assembled SNARE complexes using purified recombinant proteins (Chapman et al., 1995; Bai et al.,

2004b; Tang et al., 2006). These data suggest that Synaptotagmin can interact with the t-SNAREs at all stages of SNARE complex assembly while never binding directly to the v-SNARE Synaptobrevin (Bai et al., 2004b). The enhanced interaction between Synaptotagmin and the SNARE complex in the presence of calcium may induce full zippering, favoring vesicle fusion.

The C2 domains (C2A and C2B) of Synaptotagmin also interact with the anionic phospholipid, phosphatidylserine (PS) to penetrate membranes and aid in membrane fusion (Bai et al., 2004a; Herrick et al., 2006). The PS binding activity of C2B is enhanced when C2A is adjacent which suggests that C2A and C2B cooperate to bind membranes (Hui et al., 2006). The C2 domains of Synaptotagmin partially penetrate the plasma membrane resulting in a bulge at the site of vesicle contact, this induced membrane curvature lowering the energy barrier for membrane fusion to proceed (Chernomordik and Kozlov, 2003).

Given the essential role that the SNARE complex and the calcium sensor play in exocytosis; proteins that regulate this core exocytic machinery can have a critical impact on the level of synaptic transmission. The roles of three proteins that have been implicated in the regulation of the core machinery are examined in the following chapters.

II. *In vivo* analysis of conserved *C. elegans* tomosyn domains

Anna O. Burdina[1*], Susan M. Klosterman[1*], Ludmila Shtessel[2], Shawn Ahmed[2], and Janet E. Richmond[1] PLOS ONE 2011

1 Department of Biological Sciences, University of Illinois at Chicago, Chicago, Illinois, USA

2 Department of Biology, The University of North Carolina at Chapel Hill, Chapel Hill, North Carolina, USA

*These authors contributed equally to this study

Corresponding author: Janet E. Richmond Department of Biological Sciences, Science and Engineering Labs, 840 W. Taylor St. Chicago, IL 60607

Email: jer@uic.edu

2.1 Abstract

Neurosecretion is critically dependent on the assembly of a macromolecular complex between the SNARE proteins syntaxin, SNAP-25 and synaptobrevin. Evidence indicates that the binding of tomosyn to syntaxin and SNAP-25 interferes with this assembly, thereby negatively regulating both synaptic transmission and peptide release. Tomosyn has two conserved domains: an N-terminal encompassing multiple WD40 repeats predicted to form two β-propeller structures and a C-terminal SNARE-binding motif. To assess the function of each domain, we performed an *in vivo* analysis of the N- and C- terminal domains of *C. elegans* tomosyn (TOM-1) in a *tom-1* mutant background. We verified that both truncated TOM-1 constructs were transcribed at levels comparable to rescuing full-length TOM-1, were of the predicted size, and localized to synapses. Unlike full-length TOM-1, expression of the N- or C-terminal domains alone was unable to restore

inhibitory control of synaptic transmission in *tom-1* mutants. Similarly, co-expression of both domains failed to restore TOM-1 function. In addition, neither the N- nor C-terminal domain inhibited release when expressed in a wild-type background. Based on these results, we conclude that the ability of tomosyn to regulate neurotransmitter release *in vivo* depends on the physical integrity of the protein, indicating that both N- and C-terminal domains are necessary but not sufficient for effective inhibition of release *in vivo*.

2.2 Introduction

Tomosyn was initially isolated from rat cerebral cytosol in a syntaxin pull-down assay(Fujita et al., 1998). It was subsequently shown to form a novel SNARE complex with syntaxin and SNAP-25 displacing synaptobrevin (Hatsuzawa et al., 2003). Based on these observations, inhibition by tomosyn is thought to involve assembly of non-fusogenic tomosyn SNARE complexes at the expense of fusogenic SNARE complexes. Several mechanisms modulate the interaction between tomosyn and the SNARE complex. Rho-associated serine/threonine kinase (ROCK) stimulates the formation of tomosyn SNARE complexes (Sakisaka et al., 2004). Further activation of ROCK can enhance the inhibitory function of tomosyn, this inhibition requires the SNARE domain of tomosyn (Gladycheva et al., 2007). Tomosyn can also be phosphorylated by protein kinase A within the hypervariable linker region, which reduces the tomosyn/syntaxin interaction (Baba et al., 2005). Another SNARE-interacting protein, (M)UNC-13 might have an antagonistic role to tomosyn. Both UNC-13 and tomosyn interact with syntaxin, but have different effects. UNC-13 promotes docking as genetic deletion mutants in *C. elegans* show a

significant reduction of docked synaptic vesicles, which can be rescued by expressing an open form of syntaxin (Richmond et al., 1999a; Richmond et al., 2001; Hammarlund et al., 2007). Additionally, *unc-13* mutants can be rescued by crossing into a *tom-1* mutant background (Gracheva et al., 2007). There is also evidence that tomosyn and synaptotagmin interact, and this interaction could potentially regulate fusogenic SNARE complex formation (Fujita et al., 1998).

Overexpression of tomosyn in PC12 cells (Hatsuzawa et al., 2003), chromaffin cells (Yizhar et al., 2004) and neurons (Gracheva et al., 2006) was shown to down-regulate exocytosis indicative of an inhibitory function for this protein. Consistent with this interpretation, the first characterization of tomosyn (*tom-1*) mutants, performed in *C. elegans* demonstrated abnormally enhanced levels of neurotransmitter release in the absence of TOM-1 (Gracheva et al., 2006; McEwen et al., 2006). This exuberant release was shown to be associated with an increase in the readily releasable vesicle pool, supporting the notion that tomosyn down regulates release by interfering with the priming process. A similar phenotype has subsequently been documented in mouse tomosyn knock-outs (Sakisaka et al., 2008).

Current evidence suggests that the inhibitory function of tomosyn may involve multiple domains (Yizhar et al., 2007; Sakisaka et al., 2008). The highly conserved C-terminal SNARE domain which resembles the coiled-coil motif of synaptobrevin, is a high-affinity binding site for syntaxin (Ashery et al., 2009) capable of assembling into a tomosyn SNARE complex along with SNAP-25 (Pobbati et al., 2004). However, expression of the tomosyn C-terminal alone does not inhibit

release from chromaffin cells (Yizhar et al., 2007). The N terminal region of tomosyn is also highly conserved and contains WD40 repeats comprised of about 40 amino acids beginning with glycine-histidine and ending with tryptophan-aspartic acid. Interestingly, over-expression of this domain potently inhibits release in cultured cells (Yizhar et al., 2007; Sakisaka et al., 2008). The crystal structure of yeast Sro-7 reveals that the WD40 repeats fold into two seven-bladed ß-propeller protein interacting domains (Hattendorf et al., 2007). In mouse, the WD40 domains have been shown to interact with both syntaxin and SNAP-25, promoting non-fusogenic SNARE complex oligomers that may contribute to the inhibition of synaptic transmission (Sakisaka et al., 2008). Furthermore, recent experiments indicate that the N terminal WD40 repeats exhibit intramolecular interactions that may regulate the availability of the C terminal SNARE domain at exocytic sites (Hattendorf et al., 2007; Yamamoto et al., 2009). In summary, both N and C terminal domains of tomosyn appear to be involved in its inhibitory function.

However, while full-length tomosyn inhibits secretion in all cell types examined, expression of the C-terminal SNARE domain alone has produced variable results. For example, expression of the SNARE domain in chromaffin cells had no effect on the primed vesicle pool, and actually enhanced sustained release (Yizhar et al., 2007), whereas in cultured neurons and semi-intact PC12 cells, this domain produced partial inhibition (Hatsuzawa et al., 2003; Sakisaka et al., 2008). These data suggest that additional tomosyn domains may contribute to its inhibitory function. Consistent with this notion, tomosyn lacking a SNARE motif promotes SNARE complex oligomerization *in vitro* and inhibits secretion from chromaffin cells

and superior cervical ganglion (SCG) neurons (Yizhar et al., 2007; Sakisaka et al., 2008; Yamamoto et al., 2009). Similarly, tomosyn with mutations in the SNARE domain that impair syntaxin binding, retains inhibitory function in PC12 secretion assays (Constable et al., 2005). Brain extracts from mouse tomosyn mutants exhibit reduced levels of SNARE complex oligomers. Together, these observations suggest the tomosyn N terminus contributes to the regulation of secretion, possibly by limiting the availability of monomeric SNARE proteins. The tomosyn N terminus has also been shown to bind and inhibit synaptotagmin (Yamamoto et al., 2010). Thus, the current literature implicates both tomosyn domains in the regulation of secretion via several distinct molecular mechanisms. However, these roles have only been assayed *in cellulo*, and their interpretation is compounded by the presence of endogenous tomosyn. Here, we analyzed the independent and combined functionality of tomosyn N- and C-terminal domains at the *C. elegans* NMJ in a tomosyn mutant background.

2.3 Materials and Methods

Genetics

Nematode strains were maintained at 20-25°C on standard NGM media plates seeded with OP50 bacteria. The wild type used was Bristol N2 and the *tom-1* mutant *KP3293, tom-1(nu468)*. TOM-1 constructs were SY1229, *tom-1(nu468)*;*jaIs1078*[*Punc17*:*tom-1A*(+);*Pmyo-2:GFP*]; SY1242, *tom-1(nu468)*;*jaIs1052*[*Punc17*:*tom-1A*(+);*Pmyo-2:GFP*]; SY1230, *tom-1(nu468)*;*jaIs1079*[*Punc17:tom-1A SNARE*;*Pttx:RFP*]; SY1231, *tom-1(nu468)*; *jaIs1080*[*Punc17*:*tom-1A* ΔSNARE;*Pttx:RFP*]; SY1513, *tom-*

1(nu468);jaI1098[*Punc17;tom-1A TOM1A(1-989);Pttx:RFP*]; SY1232, *tom-1(nu468);jaIs1081*[*Punc17:tom-1A SNARE:FLAG;pmyo-3:GFP*]; SY1233, *tom-1(nu468);jaIs1082* [*Punc17: tom-1A* Δ*SNARE:FLAG;pttx-3:GFP*]; SY1234, N2;*jaIs1079***;** SY1235, N2;*jaIs1080*; SY1237, N2;jaIs1052; SY1239, *tom-1(nu468);jaIs1079***;***jaIs1080;* SY1240, N2;*jaIs1079***;***jaIs1080*.

Crosses were performed using standard genetics techniques, and the presence of the *tom-1(nu468)* mutation was confirmed by sequencing.

Tomosyn constructs and transgenes

1) Full-length *tom-1A*

Full-length *tom-1A* cDNA was amplified from *jaIs1052* strain (Gracheva et al., 2006) using the primers **GTAGCATGCGCTGGGGTATTGCAAAAAGAG** and **GTCGCATGCCTAGAAGTTGTACCACTTC** and TOPO-cloned, creating pAB29. pUNC-17::TOM-1A from pAB29 was cloned into pAB30 using SphI restriction sites and the resulting plasmid was named pAB32.

2) TOM-1A SNARE

The *tom-1A* SNARE domain (aa 1059-1124) was amplified from pAB29 using primers **GCGGATCCATGCAAATGGATAGAGCACAAGC** and **CGTGGCCACTAGAAGTTGTACCACTTC** and TOPO-cloned, creating pAB37. The *tom-1A* SNARE domain was then subcloned into pAB36 containing *pUNC-17* using BamHI/MscI restriction sites, creating pAB40.

3) TOM-1A Δ*SNARE*

The *tom-1A* Δ*SNARE* domain (aa 1-1045) includes the WD40 repeats and the downstream 57 amino acid linker, based on conserved sequence alignments

(Hattendorf et al., 2007) amplified from pAB29 using primers

AGAGTCATCCCTCAGAACAG and

GTCTAGGATCCATGCATCGGATTCACTCCAGAACTATTC, TOPO-cloned creating pAB47. *tom-1A* Δ*SNARE* was subcloned into pAB36 containing *pUNC-17* using BamH restriction sites, creating pAB48.

4) TOM-1A (1-989) lacking the linker and SNARE domain

TOM-1A(1-989) was amplified from pAB29 using primers

AGAGTCATCCCTCAGAACAG and

TATGCGGCCGCTGACTCGCCTGTTTGCTCGGCAATTTC and topo-cloned, creating pAB46. The *tom-1A* Δ*linker* was subcloned into pAB36 containing pUNC17 using BamHI/NotI restriction sites, creating pAB49.

5) TOM-1A SNARE:FLAG

The NsiI restriction site (underlined) was introduced by site-directed mutagenesis using primers **GTGGTACAACTTC<u>ATGCAT</u>TAGTGGCCAAAGGAC** and

GTCCTTTGGCCACTA<u>ATGCAT</u>GAAGTTGTACCAC using pAB40 as a template, creating pAB43. The FLAG oligos with NsiI sticky ends and 5`-phosphorylated were made as separate oligonucleotides,

P<u>T</u>GATTACAAGGATGACGACGATAAGCTT<u>ATGCA</u> and

<u>T</u>AAGCTTATCGTCGTCATCCTTGTAATC<u>ATGCA</u>, annealed and ligated into the NsiI site of pAB43, creating pAB50.

6) TOM-1A ΔSNARE:FLAG

The NsiI restriction site was included in the primer

GTCTAGGATCCATGCATCGGATTCACTCCAGAACTATTC to bypass the site-directed

mutagenesis step. Annealed FLAG oligonucleotides were ligated into pAB48 NsiI restriction site, creating pAB58.

Real-time PCR

Quantitative real-time PCR was performed as described previously (Gracheva et al., 2006). Briefly, *C. elegans* total RNA was isolated using a Trizol reagent as described by the manufacturer (Invitrogen, Carlsbad, California, United States). mRNA was reverse transcribed using the SuperScript III First Strand Synthesis Kit with oligo-dT primers (Invitrogen Carlsbad, California, United States). Real-time PCR was preformed using the following target specific primers: for *tom-1A* N-terminal (Forward-TCATCGTACGGTATCATTGC and Reverse- AGCTTCCAGACTGATTGGAG) which targeted exon 12, for the SNARE domain (Forward-GCCATGGCTTTACAGAACTT and Reverse- TCTCGAGGATAAACTCATTGC) which targeted exon22/23, and for *act-1* (Forward-GCTGGACGTGATCTTACTGATTACC and Reverse-GTAGCAGAGCTTCTCCTTGATGTC). SYBR green (Biorad) was used for amplicon detection and quantitation using the MJ Research Opticon2 real-time thermocycler (Bio-Rad, Hercules, California, United States). Relative mRNA levels were quantified using the method detailed by (Horz et al., 2004). Actin was used as a reference for calibration (Zheng et al., 2011). The levels for both *tom-1* and the SNARE domain are reported as the fold difference relative to the calibrator, *tom-1 (nu468).*

Biochemistry

1) Liquid Culture

L1 stage worms were harvested from 6 freshly-starved 100 mm agarose plates and added, along with concentrated HB101 bacteria, to 500 ml S medium supplemented with 5 ml 10,000 U/ml penicillin (Cellgro), 10 mg/ml streptomycin (Cellgro) and 10,000 U/ml nystatin (Sigma) in a 2.8 L fernbach flask. After 3 days of growth at 20°C, adult worms were harvested through a 35 μM nitex filter. Worms left in the filter were washed once with M9, 1X lysis buffer (50 mM HEPES pH 7.4, 1 mM EGTA, 1 mM $MgCl_2$, 100 mM KCl, 10% glycerol, 0.05% NP-40) and 1X lysis buffer containing a complete Mini, EDTA-free protease inhibitor cocktail tablet (Roche; 1 tablet/12 mls). Worms were spun down at 800 g for 2 minutes between washes. A 1:1 mix of worms:lysis buffer was slowly pipetted into liquid nitrogen then ground to a fine powder in a mortal and pestle.

2) Extract Preparation

Thawed ground worm powder was sonicated using a Branson sonication tip for 3 minutes (15 seconds on, 45 seconds off) at 30% amplitude and for 30 seconds at 40% amplitude. Samples were cooled in an ice bath for 2 minutes in between each minute of sonication. Sonicated samples were centrifuged in a Sorvall Ultra80 centrifuge, using a TH-641 rotor, for 11.5K RPM for 10 minutes, and then the supernatant was centrifuged at 29K RPM for 20 minutes. The supernatant was frozen in liquid nitrogen in 1 ml aliquots and stored at -80°C.

3) Immunoprecipitation

100 μl of FLAG antibody-conjugated agarose beads (Sigma F2426) were washed twice with 1 ml PBST, once with 1 ml PBS, twice with 1 ml 0.1 M glycine and twice

with 1 ml ice cold lysis buffer with 0.1 mM DTT. Beads were centrifuged at 4°C at 4K RPM for 2 minutes between washes. Beads were rotated for 2 hours at 4°C with 1ml of clarified extract. Beads were briefly rinsed twice then washed three times, by rotating for 5 minutes at 4°C, with 1 ml 0.1 mM DTT lysis buffer. Beads were incubated with 9μl of 600 μg/ml FLAG peptide at 4°C for 1 hour in Protein LoBind tubes (Epindorf). Supernatant was transferred to fresh tubes and mixed with equal volume 2X Laemmli SB and stored at -20°C.

4) Western blotting

Samples were analyzed by 12% SDS-PAGE (0.1% SDS). The nitrocellulose membrane was blocked at RT in 5% milk/TBST for 1 hour then incubated with HRP-conjugated 1° anti-FLAG antibody (Sigma A8592) at a 1:500 dilution in TBST overnight at 4°C. Membrane was washed four times for 10 minutes with TBST shaking at RT then incubated with 2 ml HRP substrate (Amersham) for 5 minutes prior to exposure to film.

Immunohistochemistry

Immunohistochemistry was performed on dissected split-open worms, as previously described (Richmond et al., 1999a) after fixation with 4% paraformaldehyde in PBS for 30 minutes. Preps were then washed 3x with TBST for 10 minutes, before blocking with 5% BSA for 1 hour. Mouse antibodies against FLAG (Sigma) were used at a final dilution of 1:100 in PBS and 0.5% Triton X-100 with 5% BSA overnight. Anti-mouse tetramethylrhodamine isothiocyanate-conjugated

secondary antibody (Jackson ImmunoResearch, West Grove, PA) was used at a 1:500 dilution for 1 hour. Images were obtained with a 60x objective on an Olympus Optical FV- 500 laser-scanning confocal microscope.

Electrophysiology

Electrophysiological methods were as previously described (Richmond et al., 1999a) with the following modifications: Ventral body wall muscle cells were recorded in the whole-cell voltage-clamp mode (holding potential -60 mV) using an EPC-10 patch-clamp amplifier and digitized at 1 kHz. The extracellular solution consisted of (in mM): NaCl 150; KCl 5; $CaCl_2$ 5; $MgCl_2$ 4, glucose 10; sucrose 5; HEPES 15 (pH 7.4, ~340mOsm). The patch pipette was filled with (in mM): KCl 120; KOH 20; $MgCl_2$ 4; (*N*-tris[Hydroxymethyl] methyl-2-aminoethane-sulfonic acid) 5; $CaCl_2$ 0.25; Na^2ATP 4; sucrose 36; EGTA 5 (pH 7.2, ~315mOsm). Evoked responses were stimulated with a 2ms depolarizing pulse delivered via a pipette placed on the anterior ventral nerve cord. Data were acquired using Pulse software (HEKA, Southboro, Massachusetts, US) and subsequently analyzed and graphed using Pulsefit (HEKA), Mini Analysis (Synaptosoft Inc., Decatur, Georgia, US) and Igor Pro (Wavemetrics, Lake Oswego, Oregon, US).

2.4 Results

The relationship between TOM-1A expression levels and inhibitory synaptic function

C. elegans tom-1 mutants exhibit an enhanced NMJ evoked response duration, resulting in an increased charge integral that reflects increased priming (Gracheva

et al., 2006). Re-introduction of full-length TOM-1A in cholinergic motor neurons reverses the *tom-1* mutant phenotype, producing inhibition of transmission relative to the wild type (Gracheva et al., 2006; McEwen et al., 2006). This inhibitory effect was due to over-expression of TOM-1, a consequence of the standard method used to create transgenic lines in *C. elegans*, which frequently results in the formation of a multicopy DNA array with high expression levels. Therefore, to compare transgenic lines expressing different TOM-1A domain constructs, we first assessed the relationship between TOM-1A expression levels and the synaptic response at the NMJ. TOM-1A mRNA levels were quantified by real-time PCR (qRT-PCR), normalized to *tom-1 (nu468)* and plotted against evoked charge integrals (Figure 1). As expected, a ~6 fold increase in TOM-1A mRNA levels greatly reduced the charge integral (72%) relative to *tom-1*(*nu468*). A further increase in TOM-1A mRNA levels to ~11 fold produced a similar reduction of the evoked response (80%), suggesting that the extent of inhibition was maximal within this range of over-expression (>6 fold).

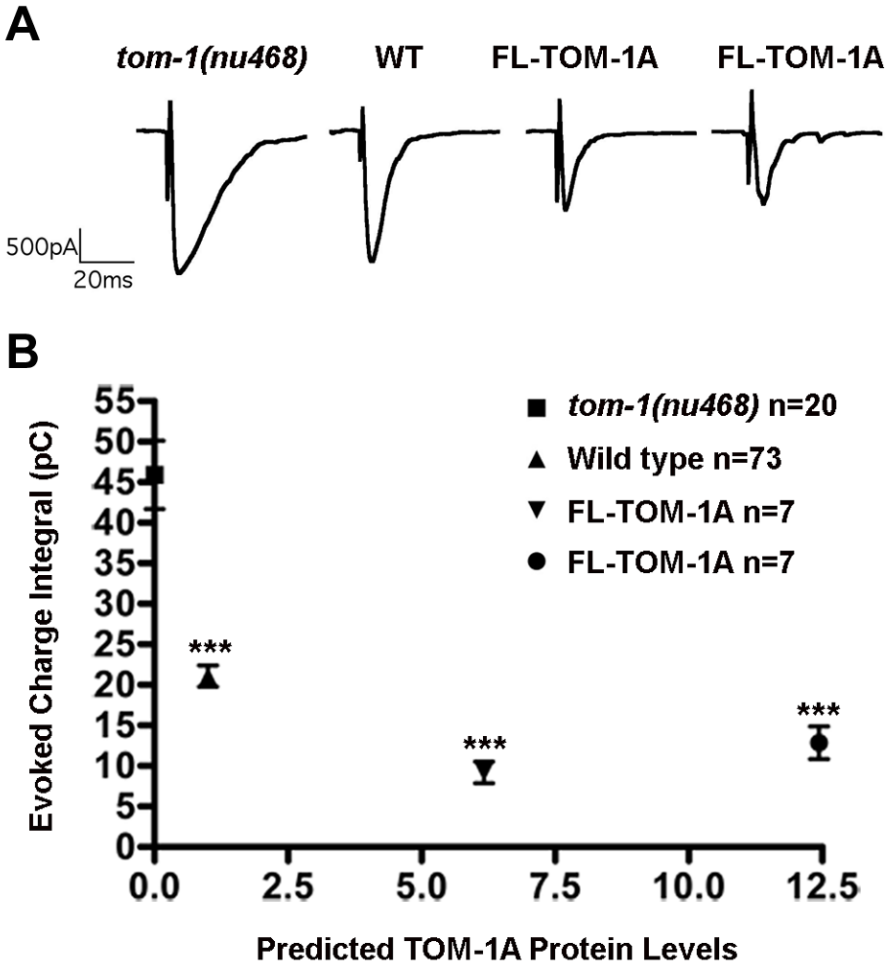

Figure 1. Inverse-relationship between predicted full-length TOM-1A expression levels and synaptic function. A. Representative evoked post-synaptic responses from the NMJ of *tom-1(nu468),* wild type and two TOM-1A integrated lines, SY1229 and SY1242, expressed in the *tom-1(nu468)* mutant background respectively. **B.** Average charge integral for evoked responses of *tom-1(nu468)* (n=20), wild type (n=73) and *tom-1(nu468)* over-expressing TOM-1A integrated lines SY1242 (~6 fold mRNA levels) (n=7) and SY1229 (~12 fold mRNA levels) (n=7) plotted against predicted TOM-1A expression levels based on quantitative real-time RT-PCR (qRT-PCR) normalized to *C. elegans* actin (*act-1*) transcript levels. Data plotted as mean ± SEM (significance values relative to *tom-1(nu468),* ✱✱✱ $p \leq 0.0001$, Mann Whitney T-test). Representative evoked NMJ traces are displayed above each strain.

Neither TOM-1A SNARE nor ΔSNARE are sufficient for TOM-1A synaptic function

To assess the ability of the SNARE and ΔSNARE domains to rescue the *tom-1* mutant phenotype, we created integrated transgenic lines of either SNARE or ΔSNARE truncated TOM-1A constructs in the *tom-1(nu468)* mutant background, expressed under the cholinergic motor neuron promoter, *Punc-17* (Figure 2A). By qRT-PCR, TOM-1A SNARE was expressed 23 -fold higher than *tom-1 (nu468)*, and TOM-1A ΔSNARE at ~17 fold. For full-length TOM-1A, these mRNA levels would be expected to produce maximal synaptic inhibition (Table 1).

Table I. ΔΔCt-values for TOM-1A transgenic lines. Transgene mRNA levels were determined by qRT-PCR using primers specific for TOM-1A N-terminal (starting at bp1840) and the SNARE domain in the *tom-1(nu468)* mutant background. ΔΔC(t) values were normalized to *tom-1(nu468)* using *act-1* transcript levels as a calibrator.

Strain	Transgenic Line	ΔΔC(t)-values for TOM-1A primers	ΔΔC(t)-values for SNARE primers
SY1230	t*om-1;* p*17*:SNARE	0.72	22.6
SY1232	t*om-1;*p*17:*SNARE-FLAG	0.58	98
SY1231	t*om-1;* p*17*:ΔSNARE	16.56	1.89
SY1233	t*om-1;* p*17:*ΔSNARE-FLAG	14.52	0.59
SY1242	t*om-1;* p*17:*TOM-1A	5.03	7.31
SY1229	t*om-1;* p*17:*TOM-1A	14.03	10.85

We then measured cholinergic evoked responses from the NMJs of each of the transgenic lines (Figure 2B). Unlike full-length TOM-1A over-expression, neither TOM-1A SNARE nor TOM-1A ΔSNARE over-expression significantly reduced the evoked amplitude relative to *tom-1(nu468)* (Figure 2C). Similarly, the enhanced charge integral and the decay kinetics of the *tom-1(nu648)* mutants were not significantly rescued by over-expression of either TOM-1A SNARE or TOM-1A ΔSNARE, unlike full-length TOM-1A (Figures 2D and2E).

The linker between the tomosyn N terminus and the SNARE domain has been postulated to act as an intramolecular switch, its interaction with the N terminus freeing the C terminus to inhibit SNARE complex formation (Yamamoto et al., 2009). To test the possibility that the linker interaction with the TOM-1A N terminus prevents the N terminus from inhibiting release, we examined evoked release in *tom-1(nu468)* mutants expressing a truncated TOM-1A N-terminal construct cleaved at amino acid 989, which removes both the linker and the SNARE domain (TOM-1A(1-989). Evoked responses from integrants expressing TOM-1A(1-989) also failed to rescue the increased charge integral of *tom-1(nu468)* mutants (charge integral of TOM-1A(1-989) 40.7 ± 3.1 pC, n=4 Vs 48.2 ± 6.1 pC, n=12 for *tom-1(nu468),* p=0.86), remaining significantly enhanced relative to the wild type (26.5 ± 2.0 pC, n=12, p=0.017, data not shown). This result suggests that the failure of TOM-1A ΔSNARE to inhibit release was not due to interactions with the downstream linker.

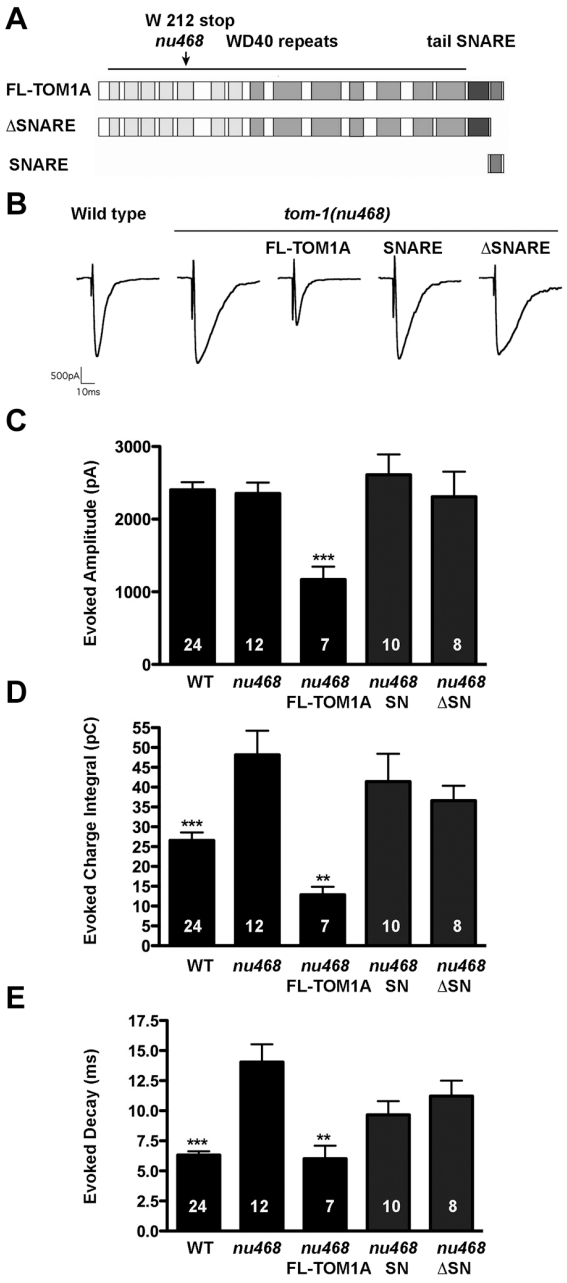

Figure 2. SNARE and ΔSNARE domains of TOM-1A fail to rescue *tom-1(nu468)* mutants. **A.** Schematic showing full-length TOM-1A (SY1242) and the SNARE (SY1230) and ΔSNARE (SY1231) truncated constructs used to generate the integrated transgenics. The position of the early stop at amino acid W212 for *tom-1(nu46*8) is indicated by the arrow **B.** Representative traces of evoked post-synaptic responses and plots of evoked amplitude (✱✱✱, p=0.006) **(C),** evoked charge integral (✱✱,p=0.0014, ✱✱✱, p=0.007) **(D)** and evoked half-time decay ((✱✱,p=0.001, ✱✱✱, p<0.0001) **(E).** All data are expressed as mean ± SEM. The Mann Whitney T-test was used to determine significance values relative to *tom-1(nu468)*. The sample size (n) is indicated as a number in each bar.

Both the TOM-1A SNARE and ΔSNARE truncated constructs are stably expressed and localized to nerve cord synapses

To determine whether the lack of rescue by TOM-1A SNARE and ΔSNARE constructs was due to either poor expression or mislocalization, we generated C-terminal FLAG-tagged versions of both the SNARE and ΔSNARE constructs. The mRNA levels of the FLAG-tagged constructs determined by quantitative RT-PCR were ~26 fold for SNARE:FLAG and ~8-fold for ΔSNARE:FLAG relative to *tom-1 (nu468)* (Table 1). Protein extraction and Western blotting of the transgenic worms expressing FLAG-tagged SNARE or ΔSNARE constructs confirmed that proteins of the predicted size (~7kDa and ~110 kDa respectively) were generated (Figure 3A). We next examined the subcellular localization of the truncated TOM1-A proteins in the cholinergic neurons of *C. elegans* by immunostaining with anti-FLAG antibodies. Staining was imaged along the ventral nerve cord anterior to the vulva, where all electrophysiological recordings were performed (Figure 3B). The expression pattern of both SNARE:FLAG and ΔSNARE:FLAG was diffusely distributed along the nerve cord in keeping with previous observations of full-length TOM-1A tagged with GFP (McEwen et al., 2006). Despite their normal expression pattern, both SNARE:FLAG and ΔSNARE:FLAG failed to rescue the *tom-1(nu468)* phenotype, recapitulating the results observed in the untagged lines (Figure 4). These data indicate that the inability of either the TOM1-A SNARE or ΔSNARE domain to restore TOM-1 function was not due to misexpression.

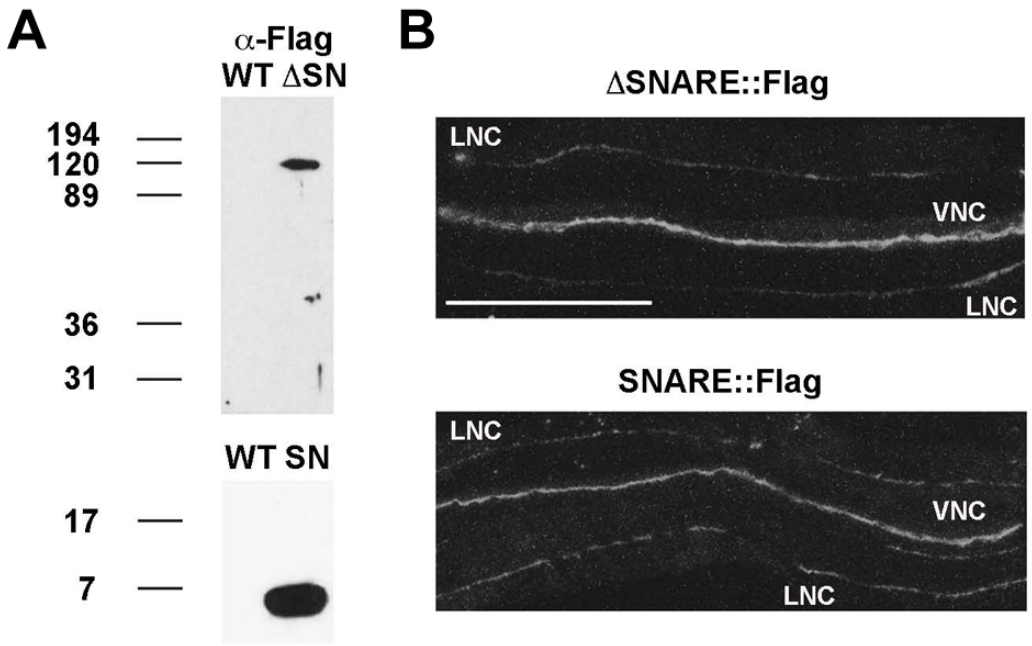

Figure 3. Both TOM1-A SNARE and ΔSNARE are stably expressed and localized at synapses. **A.** The FLAG tagged SNARE and ΔSNARE constructs are of the predicted size on Westerns. **B**. Representative confocal images of SNARE::FLAG and ΔSNARE::FLAG expression in the ventral nerve cord (VNC) anterior to the vulva, the region used for electrophysiological recording. Staining in the lateral nerve cord (LNC) was also observed. Scale bar is 50 μm.

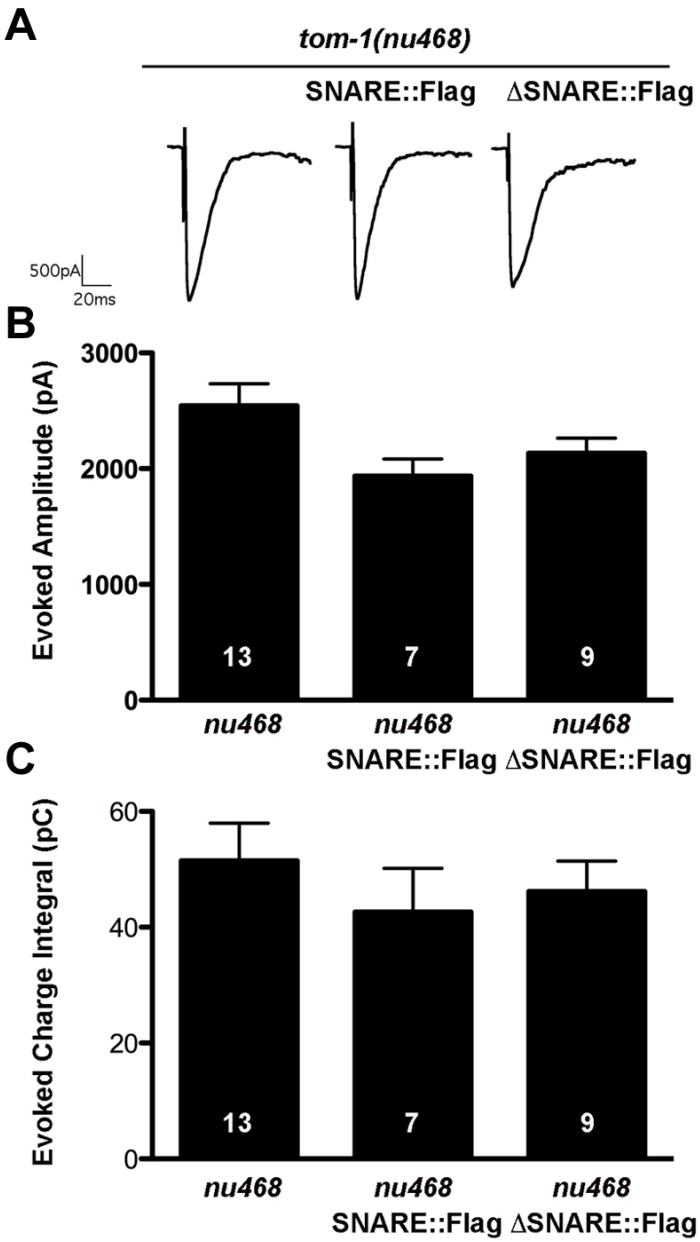

Figure 4. Flag-tagged TOM-1A SNARE and ΔSNARE transgenics phenocopy untagged lines. A. Representative evoked response traces for SNARE::FLAG (SY1232) and ΔSNARE::FLAG (SY1233) expressing lines. **B.** Plots of average evoked amplitude and **(C)** evoked charge integral. All data are expressed as mean ± SEM, the sample size (n) is indicated as a number in each bar. Mann Whitney T-tests showed values were not significantly different.

Over-expression of TOM-1A SNARE or ΔSNARE fails to inhibit synaptic release in wild-type worms

In cultured neurons, in which endogenous tomosyn is present, expression of either tomosyn SNARE or tomosyn ΔSNARE has been reported to inhibit synaptic transmission (Sakisaka et al., 2008; Yamamoto et al., 2009). To address whether *C. elegans* TOM-1A SNARE or ΔSNARE expression has an inhibitory effect in the presence of endogenous TOM-1, we crossed the truncated lines into the wild-type background. Evoked synaptic responses were not inhibited by either TOM-1A SNARE or ΔSNARE, whereas full-length TOM-1A over-expression caused a significant decrease in evoked charge integral (Figure. 5).

Co-expression of SNARE and ΔSNARE constructs fails to reconstitute TOM-1A function

To address whether co-expression of the TOM-1A SNARE and TOM-1A ΔSNARE constructs could reconstitute TOM-1A function, we co-expressed both constructs (SNARE/ΔSNARE) in the *tom-1(nu468)* background. Unlike full-length TOM-1A, co-expression of TOM-1A SNARE/ΔSNARE failed to rescue the enhanced evoked response of the *tom-1(nu468)* mutant (Figure 6A-C). Similarly, co-expression of TOM-1A SNARE/ΔSNARE failed to recapitulate the inhibitory effect of full-length TOM-1A over-expression in the wild-type background (Figure 6 D-F).

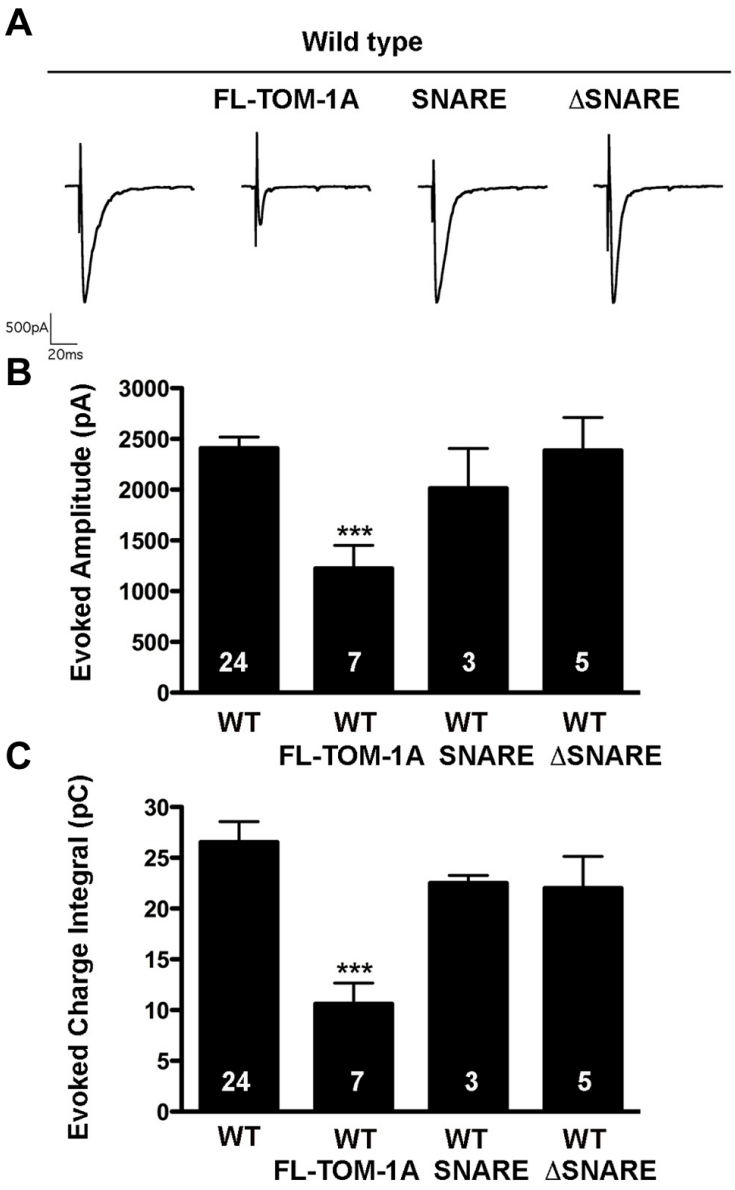

Figure 5. Over-expression of TOM1-A SNARE or ΔSNARE constructs do not inhibit synaptic release in the wild-type background. A. Representative evoked traces for full-length TOM-1A (SY1237), SNARE (SY1234) and ΔSNARE (SY1235) expressing transgenes in the wild-type background. **(B)** Average evoked amplitude and **(C)** Average charge integral were only significantly reduced by full-length TOM-1A relative to wild type (***, p=0.0005, and p=0.0007 for B and C, respectively). All data are expressed as mean ± SEM, the sample size (n) is indicated as a number in each bar, significance values obtained with the Mann Whitney T-test.

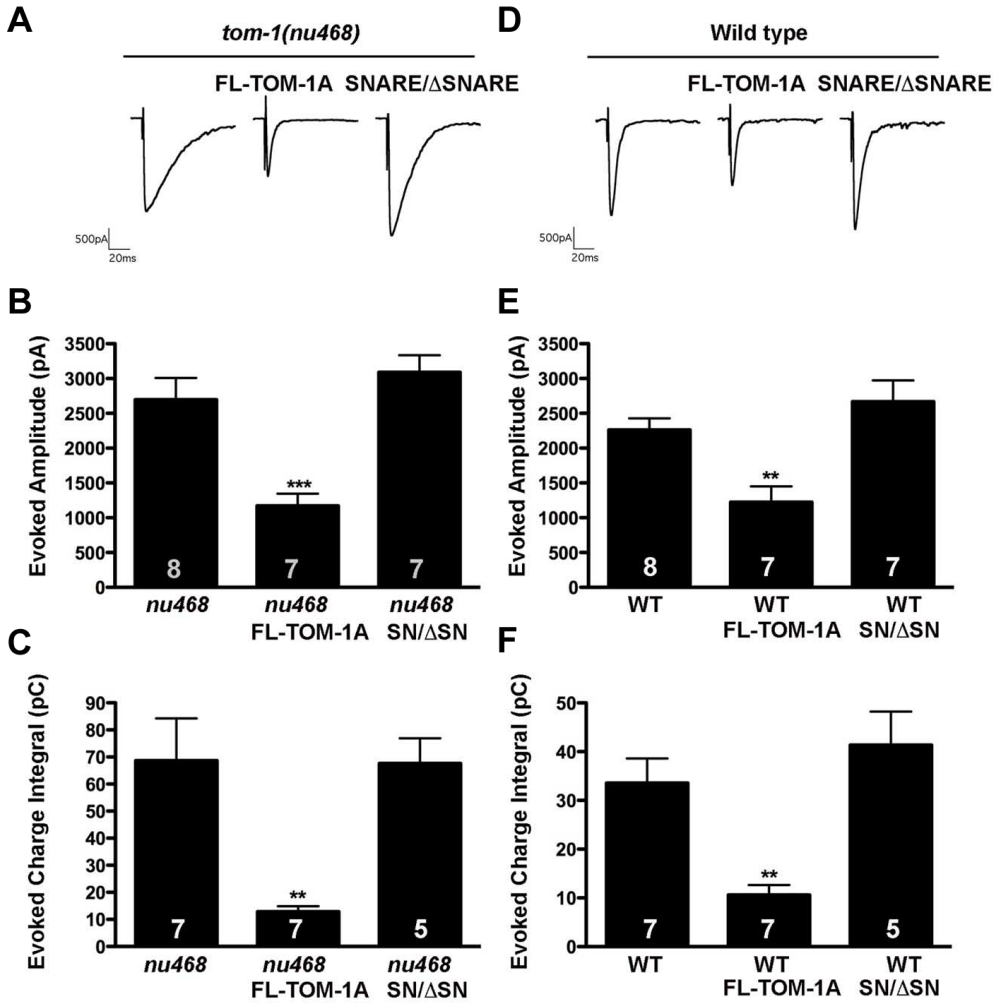

Figure 6. Co-expression of SNARE and ΔSNARE constructs failed to reconstitute TOM-1A function. A. Representative evoked response traces for *tom-1(nu468)*, and with full-length TOM-1A over-expression (SY1242) or co-expression of SNARE and ΔSNARE (SY1239), **(B)** average evoked amplitudes (∗∗∗, p=0.0006) and **(C)** average evoked charge integrals (∗∗, p=0.0021). **(D)** Representative evoked response traces for wild type alone, and with TOM-1A over-expression (SY1237) or co-expression of SNARE and ΔSNARE (SY1240), **(E)** average evoked amplitudes (∗∗, p=0.0033) and **(F)** evoked charge integrals (∗∗, p=0.0037). All data are expressed as mean ± SEM, the sample size (n) is indicated as a number in each bar, significance values obtained with the Mann Whitney T-test.

2.5 Discussion

Although the inhibitory role of tomosyn in exocytosis is well established, the molecular events underlying this negative regulation remain to be fully elucidated (Ashery et al., 2009). To further our understanding of tomosyn function, we examined the inhibitory capacity of the two conserved tomosyn domains *in vivo*. Our results indicate that the integrity of *C. elegans* TOM-1 is critical for its inhibitory function, as neither TOM-1A SNARE nor ΔSNARE were able to restore TOM-1 function, when expressed separately or together in *tom-1* mutants.

Although biochemical evidence strongly implicates the tomosyn SNARE domain in the regulation of SNARE complex formation (Hatsuzawa et al., 2003; Pobbati et al., 2004; Sakisaka et al., 2008), the inhibitory capacity of this domain depends on the experimental context (Hatsuzawa et al., 2003; Yizhar et al., 2007; Yamamoto et al., 2009). Whereas the tomosyn SNARE domain expressed in cultured SCG neurons (Sakisaka et al., 2008) or applied to inverted PC12 cell plasma membrane sheets (Hatsuzawa et al., 2003) inhibits secretion, evoked release is unaffected in both chromaffin cells (Yizhar et al., 2007) and, as shown here, in *C. elegans* motor neurons. What experimental variable might account for these different outcomes? Since tomosyn SNARE-dependent synaptic inhibition in SGC cells has only been assayed in wild-type neurons, it is possible that the SNARE domain may inhibit release by altering intramolecular or intermolecular interactions of endogenous tomosyn. However, the inability of the tomosyn SNARE domain to inhibit release when endogenous tomosyn was present in wild type *C. elegans* as well as chromaffin cells argues against this possibility. Alternatively, the

ability of the SNARE domain to impact SCG neuron and PC12 ghost cell secretion may reflect the achievement of higher expression levels by microinjection or direct application in these cells. While we cannot rule out this explanation, the lack of an inhibitory effect of SNARE over-expression in either chromaffin cells or *C. elegans* neurons, at levels effective for full-length tomosyn, argues against the physiological relevance of the observed inhibition in SCG and PC12 ghost cells. It is also possible that the molecular events underlying the inhibitory capacity of the tomosyn SNARE domain are differentially tuned in the neurons of vertebrates and *C. elegans*. The vertebrate tomosyn SNARE domain has been shown to readily form tomosyn SNARE complexes in cell free assays and to compete with synaptobrevin in the assembly of SNARE complexes (Hatsuzawa et al., 2003; Pobbati et al., 2004). We know from *in vitro* assays that the *C. elegans* TOM-1 SNARE domain is much less efficient than the SNARE domain of C. *elegans* synaptobrevin (SNB-1) in promoting the assembly of recombinant SNARE complexes (Gracheva et al., 2006). Moreover, the *C. elegans* SNAP-25 homolog (RIC-4) is much less efficient than vertebrate SNAP-25 in facilitating both TOM-1 and SNB-1-containing SNARE complex formation *in vitro*. Substituting vertebrate SNAP-25 for RIC-4 greatly enhances levels of both *C. elegans* TOM-1 and SNB-1 containing SNARE complexes *in vitro* (Gracheva et al., 2006). Thus, we postulate that *in vivo*, *C. elegans* TOM-1 SNARE may be much less effective in inhibiting fusogenic SNARE complex formation relative to the vertebrate tomosyn SNARE domain in SCG cells. For this explanation to fit the current data, it would suggest that there must also be differences in the ability of the vertebrate tomosyn

SNARE domain to impact dense core granule secretion in chromaffin cells relative to SCG synapses.

In contrast to the SNARE domain, expression of the tomosyn N-terminal domain inhibits release from both chromaffin (Yizhar et al., 2007) and SCG cells (Yamamoto et al.; Sakisaka et al., 2008; Yamamoto et al., 2009), as does full-length tomosyn lacking SNARE-syntaxin interactions in PC12 cells (Constable et al., 2005). Yet, TOM-1 lacking the SNARE domain fails to rescue the *C. elegans tom-1* mutant phenotype. A recent analysis of rat tomosyn mutants indicates that tomosyn promotes the formation of SNARE complex oligomers, providing a possible second mechanism by which tomosyn may limit the assembly of fusogenic SNARE complexes through the sequestration of SNARE proteins (Sakisaka et al., 2008). Although the precise mechanism underlying SNARE complex oligomerization is unknown, the tomosyn N-terminal domain recapitulates this effect in cell free assays (Sakisaka et al., 2008). Since the isolation of native SNARE complexes from *C. elegans* has yet to be achieved, we are unable to address whether *tom-1* mutants show a similar reduction in SNARE complex oligomerization. Regardless, the inability of TOM-1A ΔSNARE over-expression to rescue *tom-1* mutants or inhibit release in wild type *C. elegans* suggests that, in this *in vivo* context, expression of full-length TOM-1 is required for functionality.

How might linkage of the two TOM-1 domains within the full-length protein contribute to the ability of TOM-1 to negatively regulate synaptic transmission? Recently, evidence for a third tomosyn inhibitory mechanism has emerged, which

involves a calcium-dependent interaction between the rat tomosyn N terminus and the vesicle-associated calcium-sensor, synaptotagmin (Yamamoto et al.). The binding of tomosyn to synaptotagmin interferes with the *in vitro* membrane-bending ability of synaptotagmin, a function implicated in the vesicle fusion process (Martens et al., 2007; Hui et al., 2009). Furthermore, injection of the synaptotagmin cytoplasmic domain represses the ability of the tomosyn N-terminal domain to inhibit release from cultured SCG neurons, suggesting the interaction between the tomosyn N-terminal domain and endogenous synaptotagmin underlies this inhibitory effect. Interestingly, synaptotagmin binding to full-length tomosyn also enhances the ability of the tomosyn SNARE domain to form tomosyn SNARE complexes (Yamamoto et al.). These data imply that the tomosyn N-terminal interaction with synaptotagmin may favorably position the C-terminal tomosyn SNARE domain to initiate tomosyn SNARE complex assembly. This result suggests that the integrity of tomosyn could facilitate simultaneous interference with synaptotagmin function and SNARE complex assembly, via the linked N- and C-terminal domains, respectively. In this model, the spatial proximity of the two tomosyn domains, would be an important requirement for the dual inhibition and may explain why the integrity of TOM-1 is essential for inhibitory function at *C. elegans* synapses.

In conclusion, we have conducted the first *in vivo* analysis of TOM-1 structure-function in a *tom-1* mutant background. Based on our results we conclude that the physical link between the N- and C-terminal domains is critically important for the normal function of TOM-1. This result differs from previous studies in

cultured mammalian cells, in which over-expression of the SNARE domain produced variable results and the N terminus inhibited secretion. It remains to be seen whether expression of either the tomosyn SNARE or delta-SNARE domains in the recently available mouse tomosyn mutants restores tomosyn function *in vivo* (Yamamoto et al., 2009).

Specific contributions:

Conducted all qRT-PCR and immunohistochemistry experiments. Assisted in writing the manuscript.

III. Differential roles for Snapin and Synaptotagmin in the synaptic vesicle cycle.

Szi-Chieh Yu, Susan M. Klosterman, Ashley A. Martin, Elena O. Gracheva, and Janet E. Richmond. PLOS ONE 2013.

[1]Biological Sciences, University of Illinois at Chicago, Chicago, Illinois, USA

[2]Biological and Biomedical Sciences, Yale University, New Haven, Connecticut, USA

* Corresponding author: jer@uic.edu

3.1 Abstract

Evoked synaptic transmission is dependent on interactions between the calcium sensor Synaptotagmin I and the SNARE complex, comprised of Syntaxin, SNAP-25, and Synaptobrevin. Recent evidence suggests that Snapin may be an important intermediate in this process, through simultaneous interactions of Snapin dimers with SNAP-25 and Synaptotagmin. In support of this model, cultured neurons derived from embryonically lethal Snapin null mutant mice exhibit desynchronized release and a reduced readily releasable vesicle pool. Based on evidence that a dimerization-defective Snapin mutation specifically disrupts priming, Snapin is hypothesized to stabilize primed vesicles by structurally coupling Synaptotagmin and SNAP-25. To explore this model *in vivo* we examined synaptic transmission in viable, adult *C. elegans* Snapin (*snpn-1*) mutants. The kinetics of synaptic transmission were unaffected at *snpn-1* mutant neuromuscular junctions

(NMJs), but the number of docked, fusion competent vesicles was significantly reduced. However, analyses of *snt-1* and *snt-1;snpn-1* double mutants suggest that the docking role of SNPN-1 is independent of Synaptotagmin. Based on these results we propose that the primary role of Snapin in *C. elegans* is to promote vesicle priming, consistent with the stabilization of SNARE complex formation through established interactions with SNAP-25 upstream of the actions of Synaptotagmin in calcium-sensing and endocytosis.

3.2 Introduction

Neurotransmitter release is dependent on the assembly of SNARE (soluble *N*-ethylmaleimide sensitive factor adaptor protein receptor) complexes formed between the plasma membrane associated proteins, Syntaxin and SNAP-25 (synaptosomal-associated protein 25 kDa) and the vesicle-associated protein Synaptobrevin (VAMP-2) (Trimble et al., 1988; Sollner et al., 1993b; Fasshauer et al., 1998; Sutton et al., 1998b). The zippering together of the coiled-coil SNARE motifs of these three proteins is thought to bring the vesicle membrane into close apposition with the plasma membrane, developing a fusion competent state in a process known as priming (Jahn et al., 2003; Matos et al., 2003). Based on clostridial toxin disruption as well as knockout studies, all three SNARE proteins are considered to be essential components of this minimal membrane fusion machinery (Augustine et al., 1996; Schiavo et al., 2000; Schoch et al., 2001).

In addition to the SNAREs, the integral synaptic vesicle protein Synaptotagmin-1 plays a prominent role as a Ca^{2+} sensor (Brose et al., 1992),

triggering the synchronous fusion of primed vesicles in response to action potential induced Ca^{2+} entry through voltage-gated Ca^{2+} channels (Geppert et al., 1994). Two Ca^{2+} binding domains within the cytoplasmic region of Synaptotagmin, called C2A and C2B are critical for this function and exhibit increased affinity for both the SNARE complex and membrane lipids upon calcium-binding, which together promote the exocytic event (Davletov and Sudhof, 1993). The speed and accuracy of the Synaptotagmin/SNARE complex interaction is an important determinant of exocytic response kinetics (Fernandez-Chacon et al., 2001; Striegel et al., 2012). Recent studies have suggested that the highly conserved protein, Snapin, may also contribute to the timing and efficacy of this process (Pan et al., 2009).

Snapin was first identified as a SNAP-25 interacting protein in a yeast two hybrid screen of human brain cDNA, and was subsequently shown to bind Synaptotagmin-1 (Ilardi et al., 1999). By interacting with both the SNARE complex and Synaptotagmin-1, Snapin dimers are postulated to promote the Synaptotagmin-1/SNARE complex interaction. Phosphorylation of Snapin by protein kinase A (PKA) enhances the association of Snapin and Synaptotagmin-1 with the SNARE complex thus, Snapin is also a potential effector of PKA-dependent synaptic facilitation (Chheda et al., 2001; Thakur et al., 2004; Tian et al., 2005).

Although Snapin and Synaptotagmin-1 are predicted to act in the same pathway on the basis of biochemical interactions, analysis of vertebrate Synaptotagmin-1, and Snapin mutant cultured neurons reveal different phenotypes. Specifically, neurons derived from Snapin mutants have reduced synaptic event

frequency (Pan et al., 2009) whereas studies of Synaptotagmin-1 mutants often report increased endogenous rates (Broadie et al., 1994; Littleton et al., 1994; Pang et al., 2006), although not in autaptic cultures (Geppert et al., 1994), possibly reflecting differences in synaptic behavior with different culture conditions (Xu et al., 2009). Furthermore, in some studies Synaptotagmin-1 has also been implicated in endocytosis, possibly by binding to the heterooligomeric AP-2 protein complex, which recruits clathrin and results in the formation of clathrin-coated vesicles (Zhang et al., 1994; Jorgensen et al., 1995; Poskanzer et al., 2003; Yao et al., 2012). An endocytic role for Snapin is less clear, although cultured Snapin neurons have fewer vesicles, which could reflect a vesicle recycling defect (Pan et al., 2009). However, cell culture experiments such as these are not always able to fully recapitulate protein function in the intact nervous system. Neither the role of Snapin nor its functional interplay with Synaptotagmin has been examined *in vivo. C. elegans* offers an excellent model system in which to assess the consequences of mutating Snapin (*snpn-1),* Synaptotagmin (*snt-1)*, as well as double mutants, at the behavioral, electrophysiological, and ultrastructural levels within an intact organism.

3.3 Materials and Methods

Genetics

Nematodes were maintained on agar plates seeded with OP50 bacteria. Strains used were N2 Bristol, *snpn-1(tm1892)* 2x outcrossed, NM204 *snt-1(md290)*, SY1297 *snt-1(md290)snpn-1(tm1892)*, GH19 *glo-2(zu455)*, ZM1462 *nuIs94[Pacr-*

2::SNB-1::GFP], SY1368 *snpn-1(tm1892)*;*nuIs94[Pacr-2::SNB-1::GFP],* SY1361 *snt-1(md290)*;*[Pacr-2::SNB-1::GFP},* SY1449 *snpn-1(tm1982); jaIs1092*(integrated P*unc-17::snpn-1*; 6x outcrossed), SY1498 *jaEx1058[Psnpn-1::GFP-snpn-1::snpn-1utr(pSY1); Prab-3::mCherry::unc-54utr(pGH8)]; snpn-1(tm1892)*.

Standard conventional cloning protocols were used to generate the SNPN-1 over-expression vector for cholinergic rescue *[Punc-17::snpn-1]*. Genomic DNA for the *C. elegans snapin* gene, *snpn-1* was amplified from adult hermaphrodites using the following primers, primer 1: 5'-ACGGATCCATGTCGTCAACTGCTGGAGGCGAAGTG and primer 2: 5'-CAGGATCCGAAAATAGACAAACAGCTGCCG. The primers each contain a BamHI restriction site that was used to ligate this product into a vector containing the *Punc-17 promoter*.

The multisite gateway three-fragment vector construction protocol (Invitrogen cat. 12537-023) was used to generate the SNPN-1 expression vector, *jaEx1058[Psnpn-1::GFP-snpn-1::snpn-1utr]*. Primer 3: 5'-AAAACGTAATTGGCTGCCGATTTTGAG and primer 4: 5'-GAAAAATGAAGGAAGTTGGCTTCAGAG were used to amplify a region spanning six hundred and seventy five base pairs upstream of the *snpn-1* start codon, the *snpn-1* gene, and its 3'UTR from adult hermaphrodite genomic DNA using the HotStarTaq Plus Master Mix kit (Qiagen, cat. 203643). The PCR product was then cloned into pCRII-Blunt-TOPO vector using the Zero Blunt TOPO PCR Cloning Kit. From this PCR product the *snpn-1* promoter and the *snpn-1* coding region plus 3'UTR were

separately amplified using gateway primers (primer 5: 5'-GGGGACAACTTTGTATAGAAAAGTTGCCAAAACGTAATTGGCTGCCGATT and primer 6: 5'- GGGGACTGCTTTTTTGTACAAACTTGTCATTTTAGCTGTAAGAAAGAAGA for the *snpn-1* promoter, and primer 7: 5'-GGGGACAGCTTTCTTGTACAAAGTGGCCATGTCGTCAACTGCTGGAGGCG, primer 8: 5'-GGGGACAACTTTGTATAATAAAGTTGTGAAAAATGAAGGAAGTTGGCTTC) for the *snpn-1* coding region and 3'UTR). The *snpn-1* promoter region was then cloned into the pDONR221 P4-P1r vector. The GFP sequence without a stop codon was cloned into the pDONR221 vector and the genomic *snpn-1* sequence along with 848 base pairs of downstream sequence after the stop codon was cloned into pDONR221 P2r-P3. A ligation reaction was then performed so that all three sequences in the donor vectors were in the destination vector, pDEST R4-R3 Vector II producing an N-terminally GFP-tagged SNPN-1 under the *snpn-1* promoter.

Quantitative RT-PCR

Total mRNA was isolated from 8 plates of the worms for each strain using TRIzol (Invitrogen) extraction. Genomic DNA was removed using the TURBO-DNAFree Kit (Ambion). Reverse transcription was done from purified mRNA using the SuperScript III First-Strand Synthesis System (Invitrogen) with oligo(dT) primers. qRT-PCR was performed using fluorescent detection and quantification of SYBR green-labeled PCR product using an MJResearch Opticon2 real-time thermocycler. The cycle threshold [C(t)] value for Snapin was normalized to that of a dynamin (*dyn-1*) control using the equation: $\Delta C(t)\text{sample} = C(t)snpn\text{-}1 - C(t)dyn\text{-}$

1. Normalized C(t) values for the *snpn-1* mutant (tm1892) samples were then referenced to the wild type (calibrator) to determine the relative amount of *snpn-1* mRNA using the equation: $\Delta\Delta C(t)_{sample} = \Delta C(t)_{sample} - \Delta C(t)_{calibrator}$. Primers for RT-PCR were: primer 9: 5'-CTGTGGACTTGCTCCCCTAC and primer 10: 5'-TTTTGTGAGACGTTCGAGGA.

Behavioral assay

Behavioral analysis was conducted on N2 and the *snpn-1(tm1892)*, *snt-1(md290)*, and *snt-1(md290);snpn-1(tm1892)* mutants. Thrashing behavior for individual worms placed in M9 medium was measured per minute over a 3 minute period. Head tap assays were performed on worms acclimated for 1 minute on seeded agar plates. A worm pick was used to gently tap the worm on the head, and the total number of elicited body bends was counted. A body bend is described as the movement in which the head of the worm completes a full sinusoid.

Electrophysiology

The dissection and electrophysiological methods were as previously described (Richmond et al., 1999b; Richmond, 2009). Briefly, animals were immobilized with Histoacryl Blue glue, and a lateral cuticle incision was made with a glass needle, exposing the ventral medial body wall muscles. Body wall muscle recordings were made in the whole-cell voltage-clamp configuration (holding potential, -60 mV) using an EPC-10 patch-clamp amplifier and digitized at 1 kHz. The 5mM Ca^{2+} extracellular solution consisted of 150 mM NaCl, 5 mM KCl, 5 mM $CaCl_2$, 4 mM $MgCl_2$, 10 mM glucose, 5 mM sucrose, and 15 mM HEPES (pH 7.3, ~340 mOsm), Ca^{2+}

was replaced with NaCl in the 1mM Ca^{2+}extracellular solution. The patch pipette was filled with 120 mM KCl, 20 mM KOH, 4 mM $MgCl_2$, 5 mM (N-tris[Hydroxymethyl] methyl-2-aminoethane-sulfonic acid), 0.25 mM $CaCl_2$, 4 mM Na^2ATP, 36 mM sucrose, and 5 mM EGTA (pH 7.2, ~315 mOsm). Data were acquired using Pulse software (HEKA, Southboro, Massachusetts, United States) run on a Dell computer. Subsequent analysis and graphing was performed using Pulsefit (HEKA), Mini analysis (Synaptosoft Inc., Decatur, Georgia, United States) and Igor Pro (Wavemetrics, Lake Oswego, Oregon, United States).

Confocal imaging and analysis

Puncta/10μm for each strain expressing SNB-1::GFP was determined as described previously (Kim *et al* 2007). In brief, young adults for each genotype were mounted on 2% agarose pads and immobilized using 10% sodium azide (Sigma) in M9 buffer. Images were obtained with a 60x objective on an Olympus Optical FV-500 laser scanning confocal microscope. Synapses along the dorsal nerve cord were analyzed using the 'Punctaanalyser' program in Matlab (Kim et al., 2008).

Electron microscopy

High-pressure freezing and freeze substitution. N2, *snpn-1(tm1892), snt-1(md290)* and *snt-1(md290)snpn-1(tm1892)* young adult hermaphrodites for each strain were prepared for high-pressure freezing as described previously (Rostaing et al., 2004). Briefly, 10–15 animals were loaded in a specimen chamber filled with *Escherichia coli* and immobilized by high-pressure freezing at -180°C under high pressure in a Bal-Tec HPM010 and moved to liquid nitrogen.

Freeze substitution was performed in a Reichert AFS machine (Leica, Oberkochen, Germany) as described previously for morphological analysis, using tannic acid (0.1%) and 0.5% gluteraldehyde fixative introduced over 96 hours, followed by 2% osmium oxide (OsO4) (Weimer et al., 2006). Fixed specimens were then embedded in Araldite 502 over 48 h period at 65°C. Serial sections were cut at a thickness of 40 nm, collected on formvar-covered, carbon-coated copper grids (EMS, FCF2010-Cu), and counterstained in 2.5% aqueous uranyl acetate for 4 min, followed by Reynolds lead citrate for 2 min. Images were obtained on a Jeol JEM-1220 (Tokyo, Japan) transmission electron microscope operating at 80 kV. Micrographs were collected using a Gatan digital camera (Pleasanton, CA) at a magnification of 100x.

Morphometric analysis of ventral nerve cord serial sections was scored blind. Images were quantified using NIH ImageJ software. A synapse was defined as a set of serial sections containing a presynaptic specialization and two flanking sections from both sides without presynaptic specialization.

Statistical analysis

All graphed data were plotted as mean and S.E.M, and significance was assessed using the Mann-Whitney test. Statistically significant values were: not significant $p > 0.05$, * $p \leq 0.05$, ** $p \leq 0.01$, *** $p \leq 0.001$.

3.4 Results

snpn-1 mutants exhibit locomotory defects

The single *C. elegans* Snapin homolog (*snpn-1*) encodes a 122 amino acid protein that is 29% identical (59% similar) to mouse Snapin. We obtained a deletion mutant, *snpn-1(tm1892)*, which eliminates 520 genomic base pairs, spanning the upstream regulatory sequence, the start codon, the first exon and intron, and half of the second exon of the three exon *snpn-1* coding region (Fig. 1A). Based on the extent of the *snpn-1* deletion and the complete absence of a detectable transcript following qRT-PCR (data not shown), this mutant is thought to be a molecular null (Hermann et al., 2012). Unlike mouse Snapin mutants which die shortly after birth, *C. elegans snpn-1(tm1892)* mutants are viable and fertile, allowing us to assess the behavioral consequences in freely moving adult *snpn-1* nulls. A gentle tap to the head produces a reliable backing response in wild-type worms that can be scored as number of body bend reversals. As shown in Figure 1B, *snpn-1(tm1892)* mutants produced significantly fewer body bend reversals in response to a head tap when compared to wild-type worms ($p=0.0008$). Similarly, the thrashing response of *snpn-1(tm1892)* mutants elicited by placing worms in M9 medium, was significantly depressed when compared to the wild type after 3 minutes ($p<0.0001$) (Fig. 1C). Given that the interaction between Snapin and Synaptotagmin suggests a functional link between these two proteins, we next assessed the behavioral consequences of eliminating SNPN-1 on the behavior of *C. elegans snt-1* mutants. Where as the head tap response and thrashing measurements of *snt-1(md290)* null mutants were more severely impacted in

comparison to *snpn-1* mutants (Fig. 1B,C), the *snt-1;snpn-1* double mutants showed no further reduction, with the exception of the third minute of thrashing (P=0.016) suggesting that any additive functions of SNT-1 and SNPN-1 are marginal and require prolonged activity.

The behavioral defects in *snpn-1* mutants are indicative of altered neuromuscular function. To assess whether SNPN-1 acts pre or post-synaptically at neuromuscular junctions (NMJs) we first generated an extrachromasomal GFP-tagged *snpn-1* transgene under its own promoter. GFP::SNPN-1 expression was broadly expressed in the nervous system based on colocalization with mCherry driven by the *C. elegans rab-3* promoter which is panneuronally expressed (Fig. 1D), but absent from body wall muscles suggesting that SNPN-1 plays a presynaptic role.

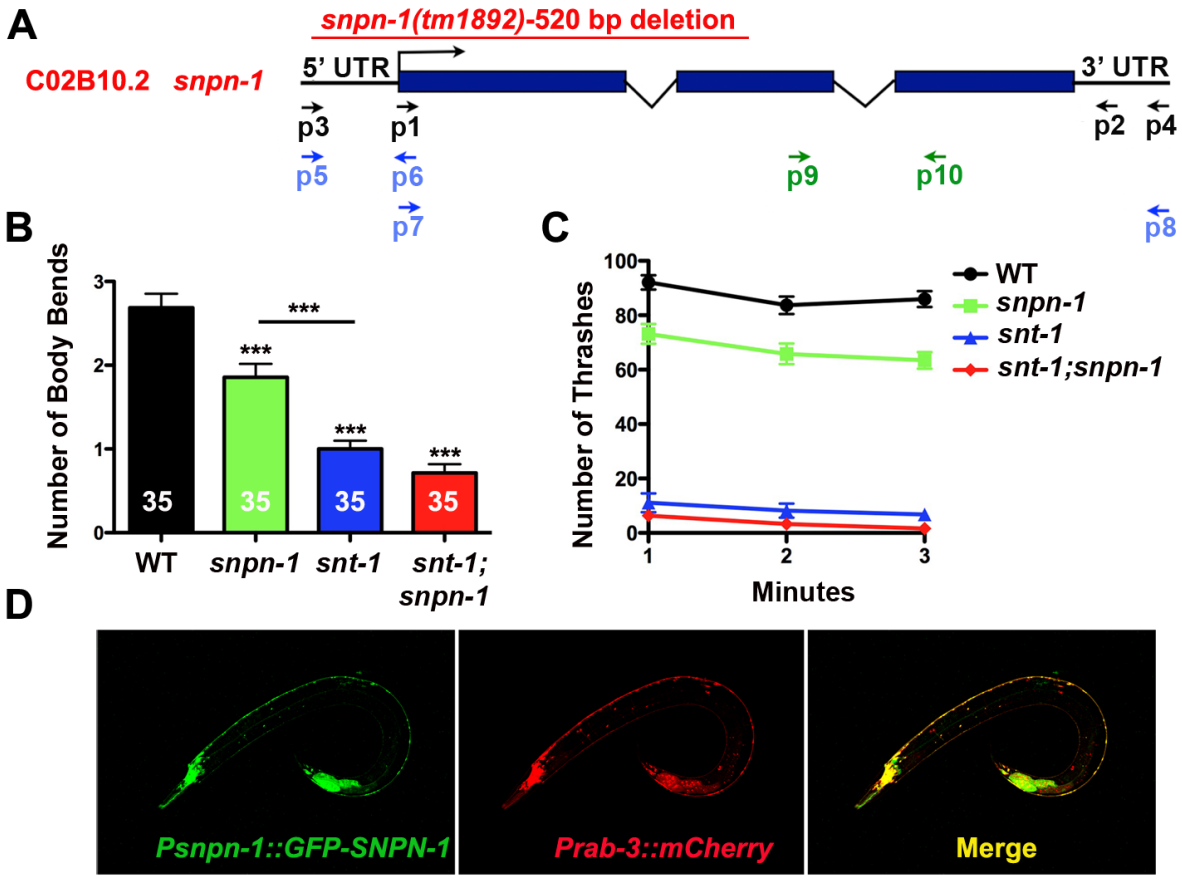

Figure 1. Neuronally expressed *C. elegans* Snapin and Synaptotagmin regulate locomotory behavior. (A) The Snapin (*snpn-1*) gene structure and location of the *snpn-1(tm1892)* deletion. **(B)** The mean ± SEM number of body bend reversals triggered by a single head tap were significantly reduced in *snpn-1(tm1892)*, *snt-1(md290)* and the double mutants. **(C)** The mean ± SEM values for thrashing responses of *snpn-1* mutants placed in solution show a modest decrease compared to *snt-1* and *snt-1;snpn-1* doubles mutants. It should be noted that subtle differences between *snt-1* single and double mutants would be difficult to discern in this assay, given the already very low thrashing rates observed in *snt-1* mutants. Significance values for all mutants are ≤ 0.0001 relative to wild-type. **(D)** Expression of GFP::SNPN-1 under the *snpn-1* promoter co-localized with mCherry driven by the pannueronal *pRab-3* promoter throughout the *C. elegans* nervous system.

snpn-1 mutants exhibit an evoked synaptic defect

To directly assay for alterations in synaptic transmission, recordings were made from the cholinergic NMJs of dissected worms. These *in situ* recordings, initially performed in the presence of 5mM Ca^{2+} Ringer, revealed a trend toward reduced evoked junctional current (EJC) amplitudes and charge integrals in *snpn-1* mutants, although these decreases did not reach significance (p=0.0635 and p=0.174, respectively) (Fig. 2A-C). The frequency of endogenous synaptic events in *snpn-1* mutants was also within the wild type range (p=0.953) (Fig. 2E). Consistent with their more severe behavioral deficits, *snt-1* mutants on the other hand, showed a significant reduction in both EJC amplitude (p=0.0014) and charge integral (p=0.0019), as well as endogenous event frequency in 5mM Ca^{2+} Ringer (p=0.0007) (Fig. 2A-C,E). Both EJCs and endogenous synaptic events in the *snt-1;snpn-1* double mutants were no more severe than *snt-1* alone, showing that in the *snt-1* background, loss of SNPN-1 has no additional effect on these release parameters (Fig. 2A-C,E).

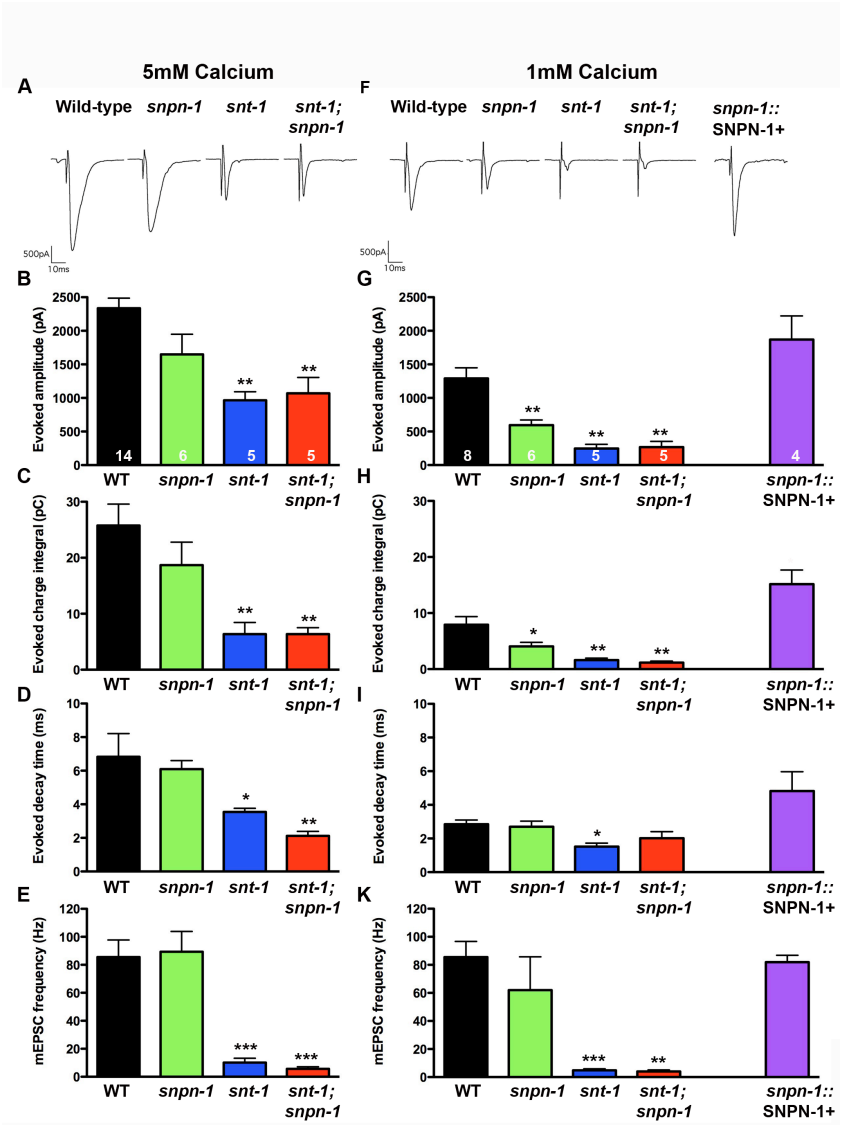

Figure 2. Electrophysiological analysis of *snpn-1* and *snt-1* mutants. (A) Representative evoked post-synaptic responses from voltage-clamped body wall muscles following nerve cord stimulation in acutely dissected worms in $5Ca^{2+}$ and **(F)** and $1Ca^{2+}$ extracellular saline. Plots of the average evoked amplitude **(B,G)**, evoked charge integral **(C,H)** evoked decay **(D,I)** and endogenous mini frequency **(E,K)** demonstrate that both *snpn-1* and *snt-1* mutants have release defects that are more severe in *snt-1* mutant. The significant synaptic defects of *snpn-1* mutants observed under low $0.5Ca^{2+}$ conditions are fully rescued by expressing *SNPN-1* under the cholinergic *Punc-17* promoter **(F-K).** In all parameters plotted, *snpn1;snt-1* double mutants do not exhibit additivity.

Given the established role of Synaptotagmin as a calcium-sensor for synaptic vesicle exocytosis, and the proposed functional interaction between SNT-1 and SNPN-1, we next examined EJCs in *snpn-1* and *snt-1* mutants in reduced (1mM) Ca^{2+} Ringer, where changes in the Ca^{2+}-sensitivity of release are more apparent. Under these recording conditions, EJC amplitude and charge integral of *snpn-1* mutants were significantly reduced when compared to wild-type (p=0.0027 and p=0.02, respectively), although the reduction was less severe than those of *snt-1* mutants (p=0.0016 and p=0.0016) (Fig. 2F-H). A similar trend towards fewer endogenous minis was also observed in 1mM Ca^{2+} Ringer (*snt-1* p=0.0007), although this was not significant for *snpn-1* mutants (p=0.414) (Fig. 2K). As seen in 5mM Ca^{2+} Ringer, evoked and endogenous synaptic events of *snt-1;snpn-1* doubles were no more reduced than *snt-1* alone.

Unlike mouse cultured neurons from Snapin mutants, we saw no evidence of asynchronous release in *C. elegans snpn-1* mutants or slower EJC decay kinetics in either 5mM or 1mM Ca^{2+} (Fig. 2D,I). However, *snt-1* mutants, showed faster decay kinetics that reached significance in all but the low calcium double mutant. This effect could be due to more efficient acetylcholine (ACh) clearance from the cleft resulting from greatly reduced ACh release levels. Alternatively, the faster decay kinetics of *snt-1* mutants may reflect a shorter release phase, associated with the release properties of the remaining unidentified calcium-sensors in the absence of SNT-1.

SNPN-1 acts presynaptically to regulate release

To determine whether the synaptic defect of *snpn-1* mutants is due to loss of neuronal SNPN-1, we integrated a non-tagged genomic *snpn-1* transgene driven by the cholinergic neuron specific promoter, *Punc-17* into the genome of *snpn-1* mutants and assessed rescue of the cholinergic EJC in 1mM Ca^{2+} Ringer. As shown (Fig. 2F-H), *Punc-17::snpn-1* rescued the evoked response to wild-type levels (EJC amplitude p=0.21 relative to wild-type, EJC charge integral slightly exceeding wild-type (p=0.028)) (Fig. 2F-H), indicating that the synaptic defect is specific to the *snpn-1* gene deletion and not a background mutation, and that SNPN-1 is required presynaptically for normal synaptic transmission.

Snapin is also known to be a component of BLOC-1 (biogenesis of lysosome-related organelle complex) (Hermann et al., 2012). To address the possibility that the synaptic phenotype of *snpn-1* mutants represents disruption of BLOC-1, we recorded the NMJ evoked responses from a mutant of the BLOC-1 protein, Pallidin(*glo-2*), in 1mM external calcium (Hermann et al., 2012). Unlike *snpn-1* mutants, *glo-2(zu455)* mutants exhibited wild-type response amplitudes (wild-type 1291 +/-159 pA, n=8, *glo-2* 1285+/-135 pA, n=5, p=0.94) suggesting that the *snpn-1* synaptic phenotype is not due to disruption of BLOC-1 function.

SNPN-1 does not affect synapse number in C. elegans

Cultured hippocampal neurons from Snapin mutant mice have significantly fewer synapses (Pan et al., 2009). If this phenotype is conserved, it could explain the behavioral and electrophysiological defects observed in *C. elegans snpn-1* mutants. .

To test whether *snpn-1* mutants have altered synaptic density, we crossed a transgenic line expressing GFP-tagged Synaptobrevin under the cholinergic neuronal promoter *Pacr-2* into the *snpn-1* mutant background. GFP puncta along the dorsal nerve cord, where individual cholinergic synapses can be readily discerned, were imaged and scored to provide a measure of synaptic density (Fig. 3). Neither the density ($p=0.51$) nor average fluorescence intensity ($p=0.061$) of puncta was altered in *snpn-1* mutants when compared to the wild type, indicating that the observed locomotory and electrophysiological defects were not the result of altered synaptic number (Fig. 3B,C). Similarly, *snt-1* mutants showed normal synaptic density ($p=0.57$) and puncta intensity ($p=0.22$) (Fig. 3B,C).

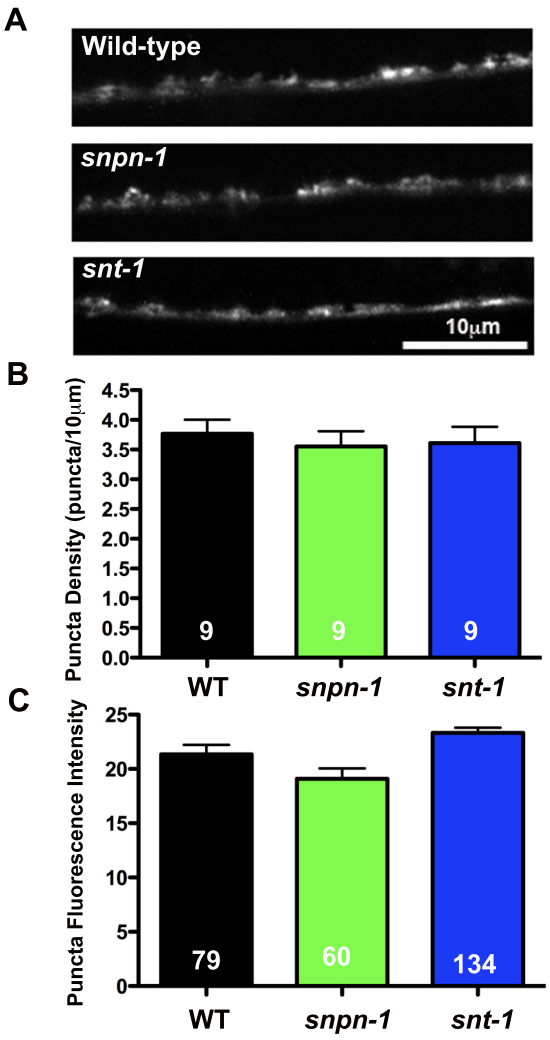

Figure 3. The functional defects of *snpn-1* and *snt-1* mutants are not associated with reduced synaptic density. **(A)** Representative confocal images of dorsal cord synaptic puncta visualized using the GFP tagged synaptic vesicle protein, Synaptobrevin (SNB-1::GFP). **(B-C)** Quantification of average synaptic vesicle density and SNB-1::GFP puncta fluorescence show no significant differences between the *snpn-1* and *snt-1* mutants relative to Wild-type.

SNPN-1 functions in synaptic vesicle docking

To determine which step of the vesicle cycle is impacted in *snpn-1* mutants and to examine the degree of functional overlap between SNPN-1 and SNT-1, we prepared *snpn-1, snt-1* and *snt-1;snpn-1* double mutants for EM analysis using high-pressure freeze fixation (HPF) and freeze substitution. 40nm serial sections were collected anterior to the vulva to obtain electron micrographs of NMJs in the region where electrophysiological recordings were made (Fig. 4A). Morphometric analyses of NMJ profiles with a visible presynaptic density were then performed. The total number of synaptic vesicles per synaptic profile was normal in *snpn-1* mutants relative to wild-type NMJs ($p=0.28$), whereas the vesicle density of *snt-1* mutants was significantly reduced ($p<0.0001$), a phenotype that has previously been linked to an endocytic defect associated with loss of SNT-1 (Fig. 4B) (Jorgensen et al., 1995). The presence of large irregular cisternae in *snt-1* mutants provided further evidence of abnormal endocytosis ($p<0.0001$) (Fig. 4A,C). The lack of cisternae ($p=0.77$ relative to wild-type) and normal vesicle density in *snpn-1* mutants suggests that SNPN-1 does not play a direct role in vesicle recycling, nor does it impact the function of SNT-1 in this process. Consistent with this conclusion *snt-1; snpn-1* double mutants have similar vesicle numbers and cisternae to the *snt-1* single mutants (Fig. 4C).

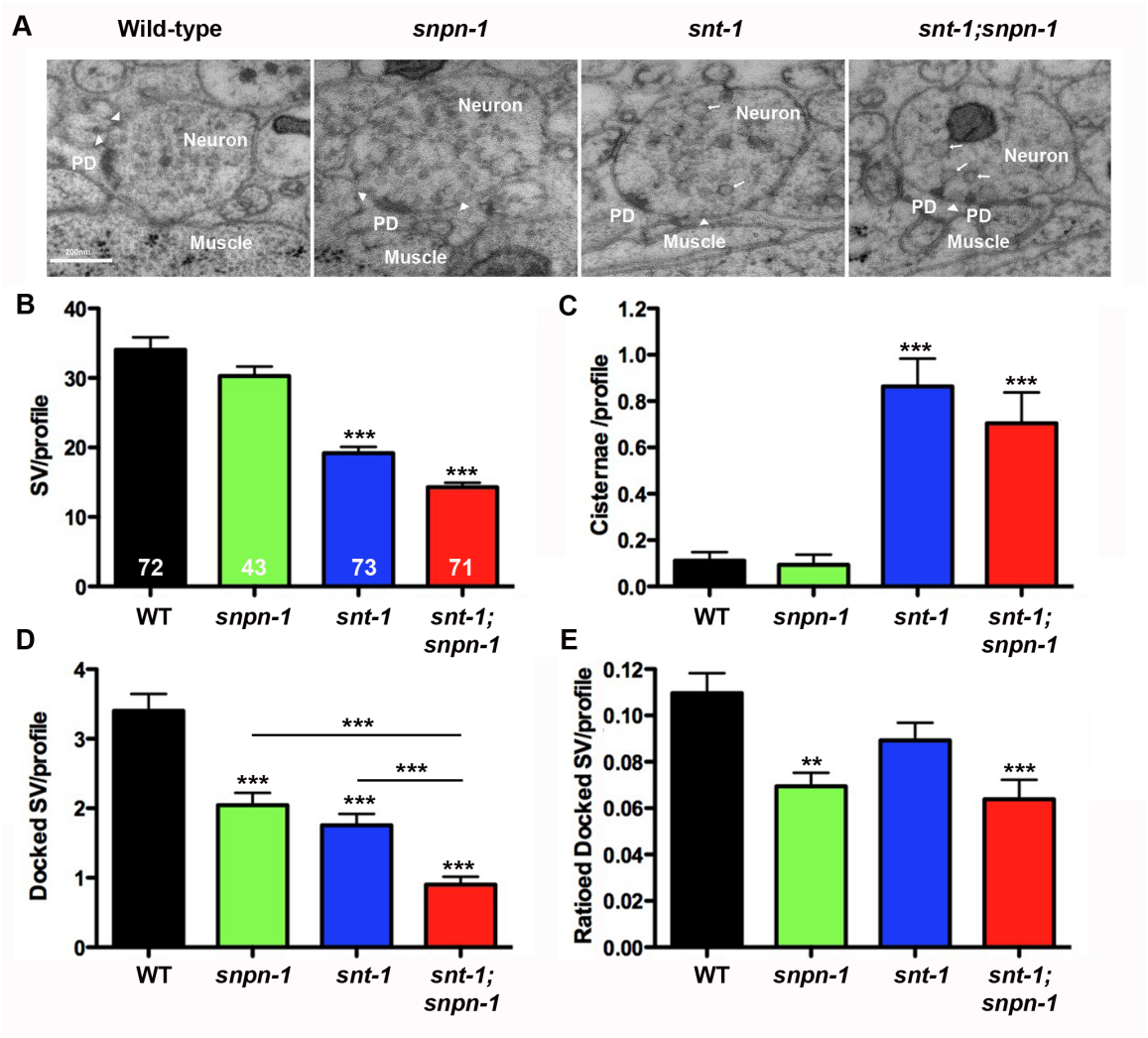

Figure 4. The different ultrastructural phenotypes of *snpn-1* and *snt-1* mutants are additive suggesting independent roles in the synaptic vesicle cycle. (A) Representative micrographs of neuromuscular junctions (NMJs) from 40nm sections of specimens prepared by high-pressure freeze fixation (HPS). The neuronal presynaptic density in each synaptic profile is labeled PD, examples of docked synaptic vesicles (SV) are indicated with an arrowhead and cisternae are indicated by an arrow. The plotted data show that the average number of synaptic vesicles per synaptic profile is reduced in *snt-1* but not *snpn-1* mutants **(B)** and that *snt-1*, but not *snpn-1* mutants exhibit high numbers of cisternae **(C).** Both *snt-1* mutant phenotypes are indicative of an endocytic defect. Plots of the number of SVs docked at the plasma membrane show reductions in both *snpn-1* and *snt-1* mutants **(D),** however, when the docking defect is plotted as a ratio of SVs in each profile, the docking defect only persists in *snpn-1* mutants.

Although synaptic vesicle density was unaffected in *snpn-1* mutants, the number of vesicles that are morphologically docked on the plasma membrane was significantly reduced (p=0.0005) (Fig. 4D). *snt-1* mutants also showed a reduction in absolute number of docked vesicles (p<0.0001) (Fig. 4D), however in the case of *snt-1*, this docking defect appeared to be a consequence of reduced vesicle density, based on the fact that the fraction of docked vesicles plotted as a function of total vesicles per profile in *snt-1* mutants was not significantly reduced compared to wild-type (p=0.17) (Fig. 4E). The fact that the 50% reduction in absolute docked vesicles in *snt-1* mutants was less pronounced than the 75% reduction in EJC charge integral suggests that SNT-1 has additional functions beyond endocytosis, consistent with the well-documented role of *snt-1* as a calcium sensor promoting vesicle fusion. In contrast, the vesicle-docking defect of *snpn-1* mutants was not due to reduced vesicle density, and therefore implicates SNPN-1 in vesicle docking (p=0.0016 for the fraction of docked vesicles relative to wild-type). Furthermore, the additivity of absolute docking defects observed in the *snt-1;snpn-1* double mutants (p<0.0001 relative to *snpn-1* and p=0.0001 relative to *snt-1*), suggests that the SNPN-1 docking function is independent of SNT-1 (Fig. 4D).

There is an apparent disparity between the additivity of the docking defect in the *snt-1;snpn-1* double mutant relative to the single *snt-1* mutant (p=0.0001) (Fig 4D), and the lack of additivity of the EJC deficit in the double mutant when compared to the *snt-1* mutant alone (EJC amplitude p=1.0, charge integral p=0.55) (Fig 2G,H). To address this issue, the distribution of docked vesicles relative to the presynaptic density (Fig 5A), the presumptive Ca^{2+} entry and release site of the NMJ,

was examined in the *snpn-1* and *snt-1* single and double mutants. This analysis demonstrated that the number of vesicles docked near the presynaptic density was reduced to similar levels in *snt-1* and *snt-1;snpn-1* double mutants (Fig. 5C,D), both of which were more severe than *snpn-1* alone (Fig. 5B). Thus, the similar extent of the electrophysiological deficits observed in *snt-1* single and *snt-1;snpn-1* double mutants may be a reflection of the similar degree to which releasable docked vesicles adjacent to the presynaptic density are reduced.

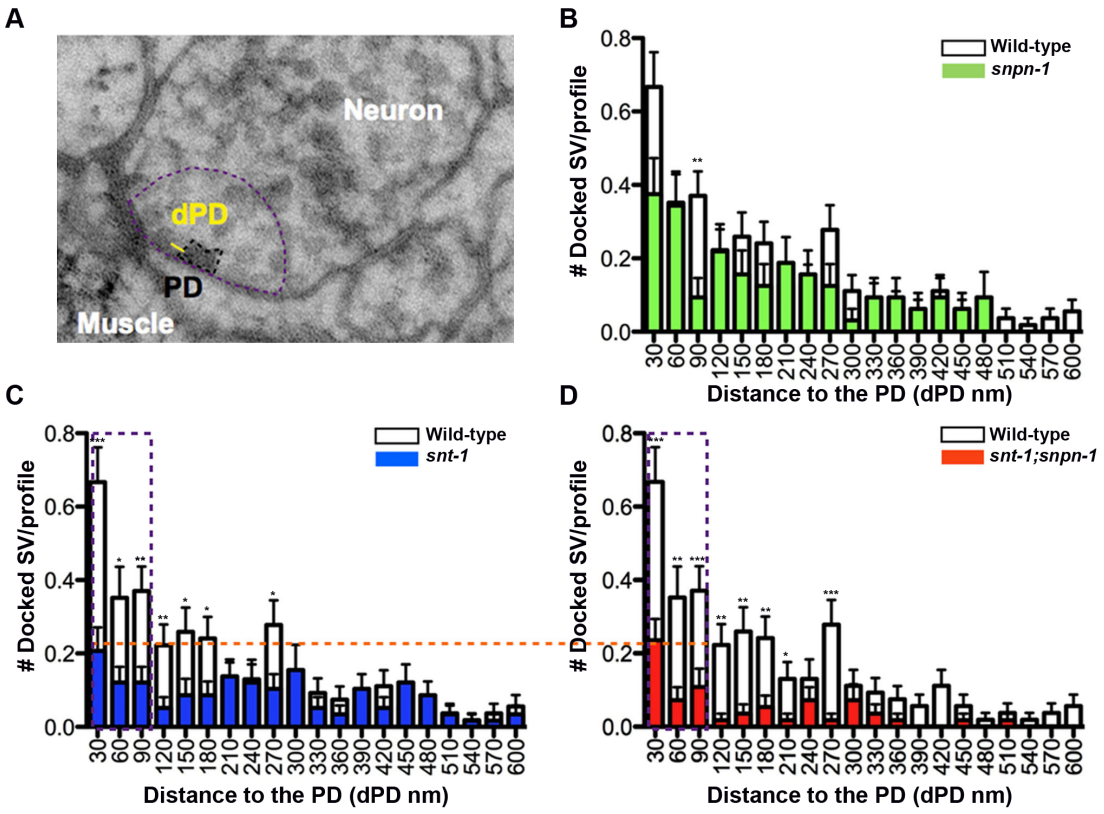

Figure 5. PD proximal vesicle docking deficits in *snt-1* and *snt-1;snpn-1* mutants correlate with their release defects. (A) The distance from docked synaptic vesicle (SV) membrane to the closest PD referred to as dPD, is used to plot the distribution of docked vesicles relative to the PD, in graphs **(B-D)**. The extent of the vesicle docking defect (highlighted by the horizontal dashed line) within 90 nm of the PD (depicted as a vertical rectangular box on graphs) is similar in *snt-1* **(C)** and *snt-1;snpn-1* double mutants **(D)**. All statistically significant values for dPD, plotted as mean and SEM for mutants when compared to the wild type are shown.

3.5 Discussion

In situ recordings and ultrastructural data from the NMJs of *snpn-1* mutant worms demonstrate a role for Snapin in synaptic vesicle docking and exocytosis. Specifically, *snpn-1* mutants exhibit reduced vesicle docking and a concomitant drop in evoked release amplitude, more evident in low calcium recording conditions. Cortical neurons cultured from mouse Snapin mutants also exhibit a synaptic vesicle docking defect at the EM level, however this defect is associated with a corresponding reduction in total vesicle number within these synapses which is not observed at *C. elegans snpn-1* mutants (Pan et al., 2009). Thus, the ratio of docked vesicles in mouse Snapin mutants is not impacted, suggesting that docking in mouse Snapin mutants is likely a secondary consequence of vesicle depletion.

Under the HPF fixation conditions used to prepare *C. elegans* NMJs for EM analysis, morphological vesicle docking has previously been shown to require both the priming factor UNC-13(Munc13) and the plasma membrane SNARE, UNC-64(Syntaxin), indicating that morphological docking is a correlate of vesicle priming (Weimer et al., 2006; Gracheva et al., 2007; Hammarlund et al., 2007). A small residual docked but unprimed pool near the presynaptic density in these mutants requires interactions between vesicle-associated Rab-3(RAB-3) with integral components of the presynaptic density, Rim(UNC-10) and Liprin(SYD-2), which promote vesicle docking near release sites (Gracheva et al., 2007; Gracheva et al., 2008; Stigloher et al., 2011). Given that vertebrate Rab-3 and Rim interact with Munc13 in a trimeric complex (Dulubova et al., 2005), these two processes (Rab-3/Rim dependent docking and UNC-13/SNARE-dependent priming) are thought to

act in concert to maintain a superprimed vesicle pool close to the presynaptic density, the presumptive release site at which voltage gated Ca^{2+} channels are enriched. The existence of a Rab3-dependent superprimed vesicle pool was first established on the basis of recordings from mouse hippocampal neurons from Rab3 quadruple knockouts (Schluter et al., 2006). These mutants exhibit a deficit in fusion events due to loss of a subpopulation of vesicles with higher release probabilities postulated to be proximal to Ca^{2+} entry points. Consistent with this interpretation, *C. elegans Rab-3*, *unc-10*(Rim) and *syd-2*(Liprin) mutants all exhibit a more pronounced reduction in evoked release under low Ca^{2+} recording conditions corresponding to loss of proximally docked vesicles (Gracheva et al., 2008; Stigloher et al., 2011). The observation that SNPN-1 also promotes vesicle docking near presynaptic densities could explain the increased severity of the release deficit observed in *C. elegans snpn-1* mutants under low Ca^{2+} conditions which normally favor fusion of proximal, superprimed vesicles. Given that Snapin is an established SNAP-25 binding partner, the docking defect that we observe in *C. elegans* Snapin mutants is most consistent with previous evidence implicating the Snapin/SNAP-25 interaction in the stabilization of assembled SNARE complexes, promoting priming (Ilardi et al., 1999; Pan et al., 2009).

The degree to which Snapin regulates release appears to be species specific. In both *C. elegans snpn-1* mutants and a *Drosophila* Snapin RNAi line (Dickman et al., 2012), the evoked release defects associated with loss of Snapin are mild. In contrast, cortical neurons derived from Snapin knockout mice, exhibit severe evoked release defects, which are still evident at synapses from heterozygotes (Pan

et al., 2009). Similarly, there are no defects in synaptic development or density in either *C. elegans* or *Drosophila* following loss of Snapin, while Snapin-null mice, die as neonates (Tian et al., 2005) and exhibit reduced brain cell density, as well as reduced cell viability and synaptic density in cultured cortical neurons (Pan et al., 2009; Zhou et al., 2012). These mammalian neuronal growth and survival defects are associated with loss of BDNF/TrkB retrograde signaling through disruption of a Snapin/Dynein interaction (Zhou et al., 2012), and may exacerbate synaptic function in cultured mouse Snapin mutant synapses to a greater extent than that observed *in situ* at fly and worm NMJs.

Biochemical evidence indicates that dimerized vertebrate Snapin can interact simultaneously with SNAP-25 and Synaptotagmin (Pan et al., 2009), promoting the interaction between the calcium sensor and the SNARE complex to enhance the efficacy of release of the primed vesicle pool. Consistent with this model, cultured neurons derived from Snapin mutant mice exhibit severe defects in both the frequency of endogenous release and the amplitude of evoked synaptic transmission, attributable to a reduced primed vesicle pool based on sucrose responses (Pan et al., 2009). A similar reduction in the readily releasable pool has been observed in chromaffin cells derived from Snapin knockout mice, suggesting Snapin also promotes dense core vesicle priming (Tian et al., 2005). Furthermore, a point mutation in vertebrate Snapin that reduces Snapin dimerization and weakens binding to both SNAP-25 and Synaptotagmin, fails to restore the vesicle priming defect of neurons from Snapin null mice (Pan et al., 2009). While our results are consistent with a priming function for Snapin in *C. elegans*, we see no evidence that

this function requires the simultaneous binding of Snapin to SNAP-25 and Synaptotagmin. Specifically, our analyses of *snt-1* and *snt-1;snpn-1* double mutants suggest that the docking defect in *C. elegans* Snapin mutants persists in the absence of Synaptotagmin. Thus in *C. elegans*, the function of Snapin in synaptic vesicle docking/priming appears to be Synaptotagmin-independent and most likely reflects disruption of Snapin interactions with SNAP-25, resulting in the destabilization of SNARE complexes. A similar conclusion was reached for the role of *Drosophila* Snapin in synaptic homeostasis, a process that exhibits genetic interactions between Snapin and SNAP-25, but is independent of Synaptotagmin (Dickman et al., 2012). It remains a possibility that the priming role of mouse Snapin is also independent of Synaptotagmin, the failure of the dimerization defective Snapin mutant to rescue release amplitude reflecting the observed disruption of the SNAP-25 interaction independent of the simultaneous disruption of Synaptotagmin binding.

C. elegans snt-1 mutants exhibit evidence of an endocytic defect, consistent with an established interaction of this protein with the AP-2 complex, required for clathrin-mediated endocytosis (Zhang et al., 1994; Jorgensen et al., 1995; Poskanzer et al., 2003; Yao et al., 2012). Specifically, *snt-1* mutants accumulate abnormal levels of cisternae and show synaptic vesicle depletion (Jorgensen et al., 1995). This reduction in vesicle replenishment correlates with the pronounced reduction in endogenous mini frequency in *C. elegans snt-1* mutants, suggesting that vesicle depletion compromises endogenous release in addition to evoked release. This observation contrasts with the increase in mini frequency observed at Synaptotagmin mutant larval NMJs in *Drosophila* and in most mouse cultures,

changes that have been attributed to loss of a fusion clamp normally provided by Synaptotagmin (Broadie et al., 1994; Littleton et al., 1994; Pang et al., 2006). Possibly, the fusion clamp effect observed in these systems is masked in adult *C. elegans* as a result of a lifetime of vesicle depletion coupled with the worms very high endogenous release rate at NMJs, that may emphasize the endocytic defect rather than loss of a fusion clamp. In contrast to *snt-1* mutants, *C. elegans snpn-1* mutants show no evidence of a vesicle recycling defect, based on similar vesicle density and number of cisternae to wild-type. This again supports the conclusion of this study that the impact of Snapin on synaptic transmission in *C. elegans* appears to be independent of Synaptotagmin function.

3.6 Acknowledgements

Anna Burdina and Hetal Patel for development of reagents. Mei Zhen and Taizo Kawana for in house Matlab software (Punctaanalyzer). Greg Herman and Daniel Saxton for *snpn-1* primer design and Marc Hammarlund for plasmids. . Some strains were provided by the CGC, which is funded by NIH Office of Research Infrastructure Programs (P40 OD010440).

Specific contributions:

Generated transgenic rescuing line, performed the SNB-1::GFP genetics, imaging, and analysis. Assisted in writing the manuscript.

IV. VPS-39 promotes fusion competent vesicles in *C. elegans*

Susan M. Klosterman, Szi-Chieh Yu, Anna O Burdina, and Janet Richmond

4.1 Introduction

In neurons, neurotransmitter-filled synaptic vesicles must fuse with the presynaptic membrane to release their contents onto target cells. Synaptic transmission is critically dependent on the core SNARE fusion machinery composed of three SNARE proteins: Synaptobrevin, Syntaxin, and SNAP-25 (Littleton et al., 1998). Additionally, a number of regulatory proteins interact with the SNAREs in the steps leading up to membrane fusion, including the priming factors (M)UNC-13, (M)UNC-18, Complexin, Snapin, and the calcium sensor Synaptotagmin.

In contrast to the permissive roles of many SNARE interacting proteins, accumulating evidence suggests that the Syntaxin and SNAP-25 binding partner, Tomosyn, negatively regulates synaptic transmission. Tomosyn, a synaptically enriched protein lacking a membrane anchor, contains a C-terminal SNARE motif homologous to that of Synaptobrevin (Fujita et al., 1998; Masuda et al., 1998). Consequently, Tomosyn can form a non-fusogenic ternary complex with Syntaxin and SNAP-25 thereby limiting vesicle priming (Hatsuzawa et al., 2003). The tomosyn SNARE complex has a similar alpha helicity, heat-stability and crystal structure, to that of the fusogenic SNARE complex formed between Syntaxin, SNAP-25 and Synaptobrevin, and both complexes are disassembled by N-ethylmaleidmide-sensitive factor (NSF) (Pobbati et al., 2004). Recent evidence indicates that the inhibitory function of Tomosyn requires both the C terminal

SNARE binding domain and the large N terminal region. The specific role of the N terminus which contains two 14 WD repeats capable of forming two protein interacting ß propellers is unknown. In an effort to identify novel interactors of this domain we preformed a yeast-two hybrid screen in which three independent clones of VPS-39, a member of the homotypic fusion and vacuole protein sorting (HOPS) complex were isolated.

The HOPS complex is comprised of six functionally conserved proteins belonging to the vacuolar protein sorting (Vps) family (Wurmser et al., 2000) first identified on the basis of yeast mutations exhibiting defective vacuolar morphologies (Raymond et al., 1992). Vps39 binds to the other members of the HOPS complex (Vps18, 11, 16, 33 and 41) via an interaction with the C terminus of Vps11 (Plemel et al.). Importantly, the HOPS complex is known to interact with both the yeast syntaxin homolog (Vam3) (Sato et al., 2000), as well as mammalian Syntaxin1A (Kim et al., 2006), implicating the complex in vesicle fusion. Yeast Vps39 also binds the yeast, Rab-7 homolog, Ypt7 and can promote guanine nucleotide exchange (Wurmser et al., 2000; Chotard et al., 2010). Functional studies suggest that through these interactions, the HOPS complex regulates several fusion events including vacuole docking and SNARE-mediated vacuole fusion in yeast (Eitzen et al., 2000; Price et al., 2000; Sato et al., 2000; Wurmser et al., 2000). Similarly, over-expression of the human Vps39 homolog (hVam6) results in extensive clustering and fusion of lysosomes and late endosomes, which is also observed with a constitutively active form of Rab7 (Caplan et al., 2001).

Furthermore, the mammalian HOPS complex members (Vps18 and Vps16)

are enriched in neurons and their over-expression produces increased asynchronous synaptic discharges in neuronal cultures, suggesting the HOPS complex may also regulate synaptic transmission. While the precise role of the HOPS complex in neurons is unknown, the fact that this complex binds to Syntaxin, Munc18 and promotes release has given rise to the hypothesis that it may regulate an inhibitor of vesicle fusion (Kim et al., 2006).

Given this evidence for a neuronal function of the HOPS complex, and our observation that *C. elegans* tomosyn (TOM-1) binds the HOPS complex, component VPS-39, we set out to determine if VPS-39 plays a functional role in synaptic transmission. To address this question we obtained a putative null mutant of *C. elegans vps-39*, and performed a detailed characterization of this strain.

4.2 Materials and Methods

Genetics/Strains

All strains were maintained at 15-20 ‘C on NGM agar plates seeded with OP50 bacteria using standard methods (Brenner, 1974). The genotypes used in this paper are as follows: Bristol N2, *vps-39 (tm2253)* loss of function allele which was out-crossed and balanced with pF25B3.3::GFP due to maternal-effect embryonic lethality (SY1245) and VPS-39 over-expression lines: Pvps-39::vps-39::mCherry::unc-54 3’UTR, *vps-39 (tm2253)* (jaEx1056, SY1455), Prab-3::vps-39::mCherry::unc-54 3’UTR, *vps-39 (tm2253)* (jaIs1096, SY1517) and Prab-3::vps-39::unc-54 3’UTR, vps-39 (*tm2253*) (jaIs1099, SY1540). Both expression lines contain str-1::GFP as the co-injection marker. The reference strain used for

coelomocyte analysis was KG1640 (unc-129::CTNS-1a-RFP, unc-129::nlp-21-Venus, ttx-3::RFP). The stain was then crossed into the balanced loss-of-function allele and the mCherry over-expression line to generate SY1409 and SY1524, respectively. EG1985 oxIs34[openSYX, Pmyo-2:GFP];unc-64(js115) was used and then crossed into a balanced vps-39 mutant background and the mCherry over-expression line to generate SY1549 and SY1550 respectively. SY1540 was also crossed into *unc-13* (e51) to generate SY1557.

Molecular Biology

Molecular biology was performed using standard techniques. All expression constructs were generated using the MultiSite Gateway Three-Fragment Vector Construction Kit (Invitrogen) using the High Fidelity Phusion Polymerase (Finnzymes) for amplification. 1.6kb upstream of VPS-39 was amplified and cloned into pDONR P4-P1R (Invitrogen) using the primers below (red base pairs indicate the homologous recombination sites compatible with the gateway vector):

GGGGACAACTTTGTATAGAAAAGTTGCGCTTTCTTCAGCACAGGGTTCTTC and

GGGGACTGCTTTTTTGTACAAACTTGCCATTTTGCTTTGGTGGGTCGAAG

Genomic vps-39 was amplified without the stop codon and cloned into pDONR 221 using:

GGGGACAAGTTTGTACAAAAAAGCAGGCTCGATGTACGATGCATACACGCCTTGC

and **GGGGACCACTTTGTACAAGAAAGCTGGGTCATTTCTGTTTCCTCCTTGAGAATC**

After the final recombination into pDEST R4-R3 Vector II, all constructs were injected at 10ng/ml with STR-1::GFP as a co-injection marker. Stable extra-

chromosomal transgenic lines were integrated using TMP mutagenesis and then out-crossed a minimum of four times.

Yeast media, strains and plasmids

Reagents for the screen were based on the Matchmaker Gal4 Two-Hybrid System 3 (Clontech Laboratories, Inc). Media was purchased from Clontech and prepared according to the manufacturer. *Saccharomyces cerevisiae* strain used was AH109, genotype MATa, trp1-901, leu2-3, 112, ura3-52, his3-200, gal4D, gal80D, LYS2::GAL1-UAS-GAL1TATA-HIS3, GAL2-UAS-GAL2-TATA-ADE2, URA3 : : MEL1-UAS-MEL1-TATA-lacZ (James et al., 1996) (A. Holtz, unpublished). Plasmid pGBKT7 containing the DNA-binding domain was used as a bait vector; pGADT7 containing the DNA-activation domain was used as a prey vector for the targeted yeast two-hybrid assay, and the pGADGH vector was used for cDNA library construction.

***C. elegans* cDNA library amplification**

A *C. elegans* cDNA library was kindly provided by Dr. Maureen Barr (University of Wisconsin, Madison). This library was created from a *him-5(e1490)* population of worms (50% males) and was directionally cloned into the pGAD-GH vector at the EcoRI and XhoI sites. The complexity of the library was estimated to be approximately 7.3x10e^{7}. The library was titered and amplified according to the Matchmaker Gal4 Two-Hybrid System 3 User Manual (Clontech). Briefly, the titer was determined to be 4.2x10e^{9}, and the library was amplified by plating on 300 LB/Amp plates at a high density to obtain 3x of independent clones in the library (6x10e^{6}). The cell mass was washed off the 300 LB/Amp plates, and the library DNA

was Maxi-prepped (Qiagen). Several small and large-scale aliquots were stored at -80°C.

The N-terminus of *C. elegans* TOM-1 with 7 predicted WD40 repeats (aa 1-440) was amplified with the following pair of primers:

AB8F (ATGGATCCACCATGGCAATGGATAGAGCAAAGAAAAAGTTTGCATCAGC) and AB9R (GTGCGGCCGCTCCCAGGAGTGGTATATTCACAACAGC).

The PCR fragment was gel-purified and cloned into TOPO vector (Invitrogen), creating plasmid pAB8, digested with NotI and NcoI restriction enzymes and cloned into NotI/NcoI sites of pGBKT7 plasmid, creating pAB9. pGBKT7 plasmid contains a cMyc tag to test the expression of bait.

Microscopy

Fluorescently labeled strains were mounted on 2% agarose pads with 10% sodium azide, and imaged using an Olympus Fluoview laser-scanning confocal system (40x or 60x objective-oil immersion). For immunohistochemistry, worms were dissected to expose the nerve cord as previously described (Richmond and Jorgensen, 1999) and fixed with 4% paraformaldehyde in PBS for 30 minutes. Preps were then washed 3x with TBST for 10 minutes before blocking with 5% BSA for 1 hour. Primary antibody incubation was performed overnight at a 1:100 dilution, and secondary antibody incubation was done at a 1:500 dilution for 1 hour the following day. Images were obtained with the same system described above but using the 60x water objective. ImageJ was used to generate maximum-intensity z projections in both cases. The z projections were also analyzed using ImageJ by measuring the

fluorescence intensity for a specific region of interest. The number of discernable puncta per coelomocyte were counted manually.

Pharmacology

Acute sensitivity to trichlorfon/dylox (Chem Services) was tested by time-course dependent paralysis. Worms were placed on drug treated plates and examined every ten minutes. Dylox was used at a final concentration of 5mM on standard NGM plates seeded with OP50. Ten young adults of each strain were used per test, which was replicated a minimum of three times. Animals were considered paralyzed if they did not respond to harsh touch with a platinum wire. All pharmacological assays were performed blind.

Electrophysiology

Electrophysiological methods were preformed as previously described (Richmond, 2009). In short, animals were immobilized with Histoacryl Blue glue, and incisions anterior to the vulva were made using a glass needle to expose the ventral medial body wall muscle. Recordings were made in whole-cell voltage-clamp configuration with a holding potential of -60mV using an EPC-10 patch-clamp amplifier and digitized at 1 kHz. The 5mM Ca^{2+} extracellular solution consisted of 150 mM NaCl, 5 mM KCl, 5 mM $CaCl_2$, 4 mM $MgCl_2$, 10 mM glucose, 5 mM sucrose, and 15 mM HEPES (pH 7.3, ~340 mOsm), Ca^{2+} was replaced with NaCl in the 0.5mM Ca^{2+}extracellular solution. The patch pipette was filled with 120 mM KCl, 20 mM KOH, 4 mM $MgCl_2$, 5 mM (N-tris[Hydroxymethyl] methyl-2-aminoethane-sulfonic acid), 0.25 mM $CaCl_2$, 4 mM Na^2ATP, 36 mM sucrose, and 5 mM EGTA (pH 7.2, ~315 mOsm). Data were

acquired using Pulse software (HEKA, Southboro, Massachusetts, United States) run on a Dell computer. Subsequent analysis and graphing was performed using Pulsefit (HEKA), Mini analysis (Synaptosoft Inc., Decatur, Georgia, United States) and Igor Pro (Wavemetrics, Lake Oswego, Oregon, United States).

Electron Microscopy

Young-adult hermaphrodites were prepared by high-pressure freeze (HPF) fixation as previously described (Weimer, 2006). Briefly, 10–15 animals were loaded in a specimen chamber filled with *Escherichia coli* and immobilized by high-pressure freezing at -180°C under high pressure in a Bal-Tec HPM010 machine and stored in liquid nitrogen.

Freeze substitution was performed in a Reichert AFS machine (Leica, Oberkochen, Germany) as described previously for morphological analysis, using tannic acid (0.1%) fixative introduced over 24 hours, followed by 2% osmium oxide (OsO4). Fixed specimens were then embedded in Araldite 502 over 48 h period at 65°C. Serial sections were cut at a thickness of 40 nm, collected on formvar-covered carbon coated copper grids (EMS, FCF2010-Cu), and counterstained in 2.5% aqueous uranyl acetate for 4 min, followed by Reynolds lead citrate for 2 min. Images were obtained on a Jeol JEM-1220 (Tokyo, Japan) transmission electron microscope operating at 80 kV. Micrographs were collected using Gatan digital camera (Pleasanton, CA).

Morphometric analysis of ventral nerve cord serial sections were scored blind. Images were quantified using NIH Image software. A synapse was defined as

a set of serial sections containing a presynaptic specialization and data from two flanking sections from both sides without presynaptic specialization were also included.

Statistical analysis

All data are expressed as mean ± SEM. The Mann Whitney U-test was used to determine significance values. * indicates a p value from 0.01-0.05, **0.001-0.01, and ***<0.001.

4.3 Results

TOM-1 N-Terminus binds VPS-39

To identify novel binding partners of the TOM-1 N-terminal, we performed a yeast-two hybrid (Y2H) screen and identified three independent clones mapping to the C terminal region of *vps-39/vam6* (Figure 1A). We subsequently verified that the Y2H interaction was conserved in full-length TOM-1. VPS-39 is highly conserved among species and contains three known protein domains, a Rab binding domain (RBD), a clathrin heavy chain repeat (CHCR) and a membrane localization domain (MLD). *C. elegans* VPS-39 shares 30% identity and 50% homology to the human homolog, Vam6. VPS-39 is a conserved member of the HOPS complex known to mediate interactions between Rab7 and the SNARE complex (Figure 1B). In order to study consequences due to loss of VPS-39, a *vps-39 (tm2253)* mutant strain was obtained from the CGC. This allele contains a 1045bp deletion and a 4bp insertion spanning exons 7-9 indicated by the bar (Figure 1C). When homozygous, this mutation

causes a maternal-effect embryonic lethality phenotype, and was therefore was balanced with a GFP marker in order to maintain the strain.

VPS-39 is expressed in many tissues and is required in early development

In order to determine the expression pattern of VPS-39 an mCherry tagged full-length transgene driven by 1.6kb of upstream sequence was generated. A transgenic line expressing this construct revealed expression of VPS-39 in many tissues types including neurons, muscles, and coelomocytes (Figure 2A). *vps-39* homozygous mutants survived, grew to adulthood, but laid nonviable eggs.

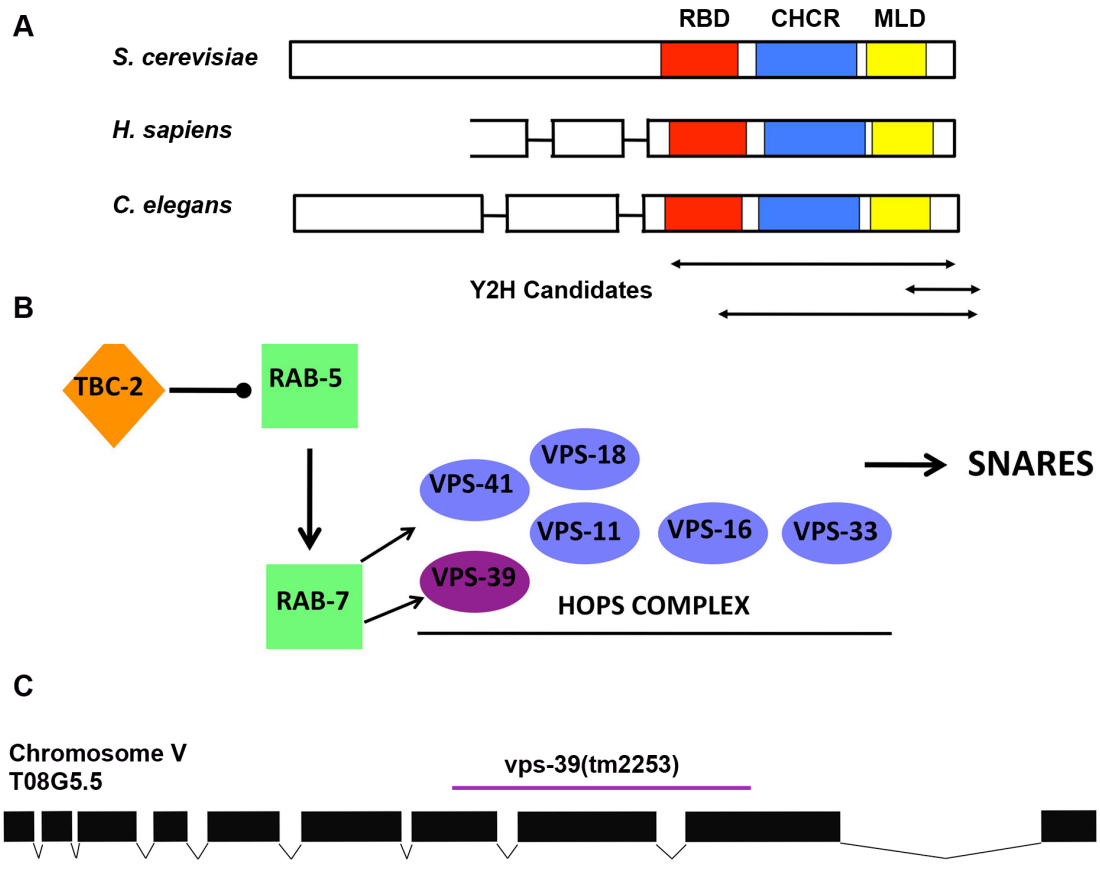

Figure 1. VPS-39 is a member of the HOPS complex. (A) VPS-39 is well conserved among species and contains three motifs: a Rab binding domain (RBD), Clathrin heavy chain repeat domain (CHCR), and a membrane localization domain (MLD). Three independent Y2H candidates of the VPS-39 C-terminus were identified using the *C. elegans* TOM-1 N-terminal as bait. **(B)** VPS-39 is a member of the HOPS complex that is activated by RAB-5 and RAB-7 and inhibited by TBC-2. **(C)** *vps-39* gene structure consisting of 10 exons. The *tm2253* allele impacts exons 7-9 and consists of a 1045bp deletion and a 4bp insertion.

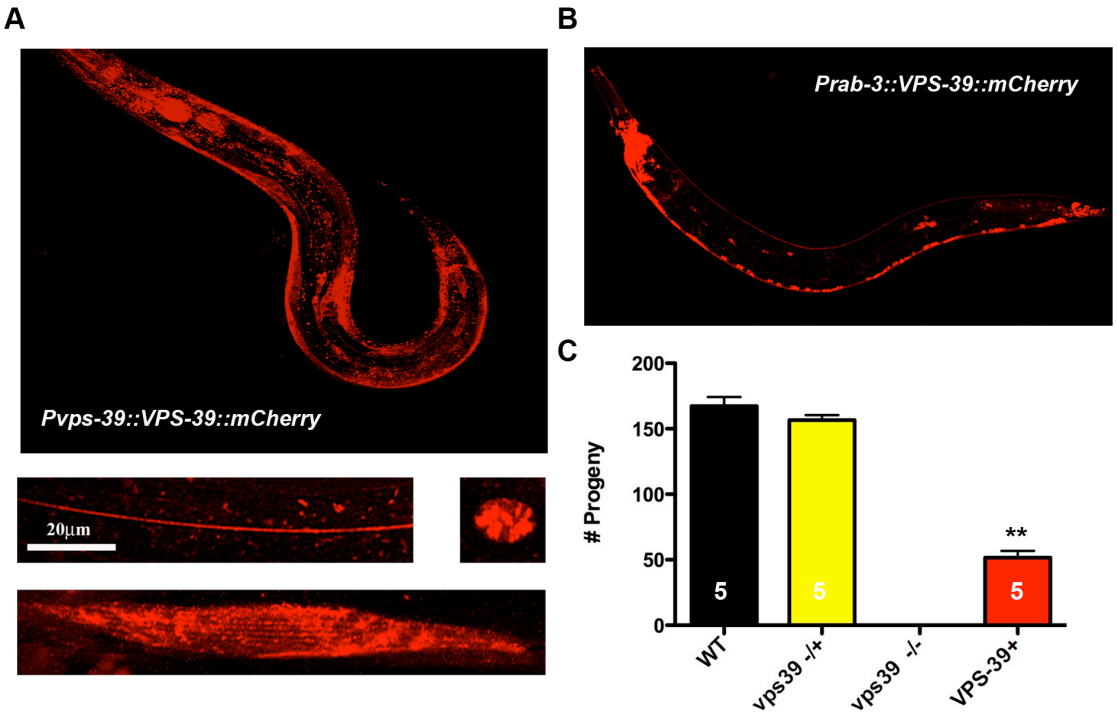

Figure 2. VPS-39 expression and rescue of embryonic lethality. **(A)** *VPS-39::mCherry* driven by 1.6kb of upstream sequence is expressed in many tissues. Enlarged images of a VPS-39::mCherry labeled neuron, coelomocyte, and body wall muscle are shown. **(B)** Expression of an integrated pRab-3::VPS-39::mCherry which was used for all rescue experiments. **(C)** Quantification indicating the # of viable progeny after 4 days, sample size indicated in each bar. A partial rescue of the *vps-39* mutant phenotype is observed by expressing VPS-39 only in neurons.

Expression of VPS-39 in neurons using the pan-neuronal *rab-3* promoter (Figure 2B) partially rescues of the embryonic lethality of *vps-39 (tm2253)* (Figure 2C).

VPS-39 is required for GFP processing in the coelomocytes

TBC-2, an upstream inhibitor of HOPS complex function (Figure 1B) has been reported to impact endosomal processing in coelomocytes resulting in an accumulation of abnormally large GFP labeled vesicles (Chotard et al., 2010). VPS-39 is also expressed in coelomocytes and would be predicted to display the opposite phenotype to *tbc-2* mutants. We therefore examined the distribution of neuronally derived GFP secreted from NLP-21::GFP peptide containing vesicles as depicted in Figure 3A. As expected coelomocytes in *vps-39* mutants exhibited an altered morphological expression pattern consisting of a significantly increased number of abnormally small GFP puncta when compared to wild-type (Figures 3B and 3C). This phenotype was not rescued by expression VPS-39 in neurons, indicating the requirement for VPS-39 in coelomocytes is independent of neuronal function (Figures 3B and 3C). The overall GFP fluorescence intensity per coelomocytes has previously been used as an indirect assay of peptide release. As shown in Figure 3D, the average GFP fluorescence intensity was not significantly altered in the *vps-39* mutants suggesting that peptide release is unaffected. However, given the coelomocyte processing defects caused by loss of VPS-39, conclusions based on GFP intensity under these circumstances may be inappropriate.

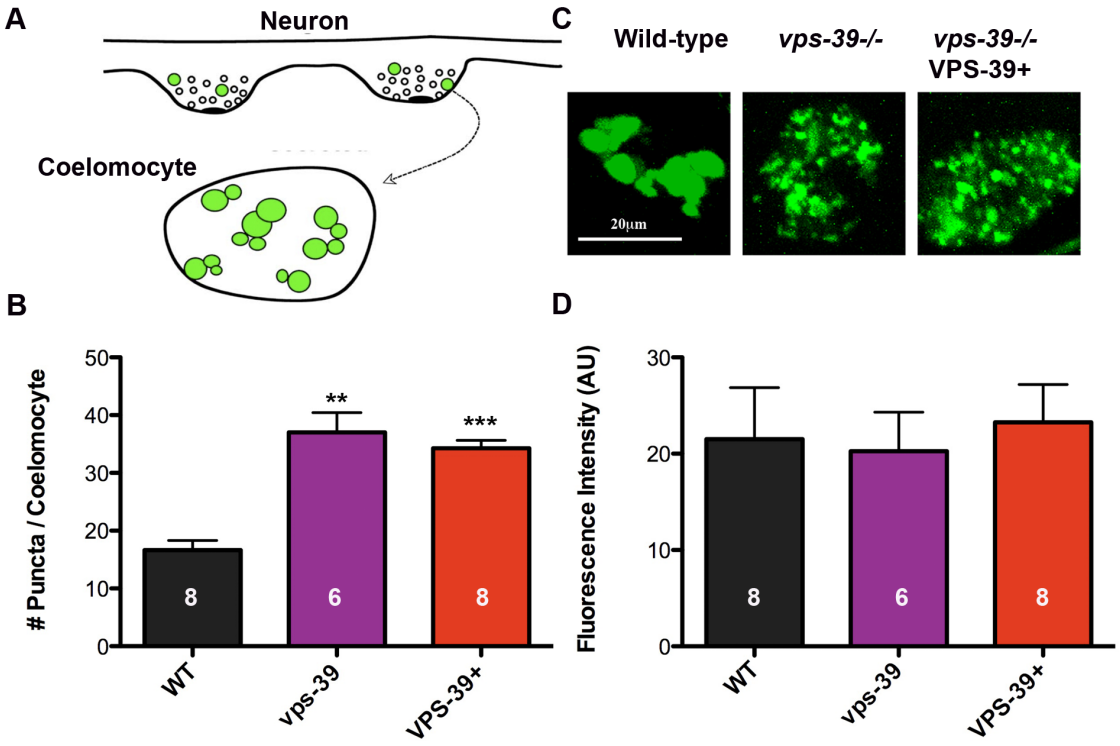

Figure 3. VPS-39 is required for coelomocyte processing. **(A)** Schematic of the assay in which GFP is secreted from neurons into the pseudocoelom and then undergoes endocytosis by the coelomocytes. **(B)** Loss of VPS-39 significantly increases the number of puncta/coelomoctye, which cannot be rescued by neuronal expression. **(C)** Representative images of GFP uptake in coelomocytes. **(D)** There is no significant difference in the GFP fluorescence intensity in *vps-39* mutants.

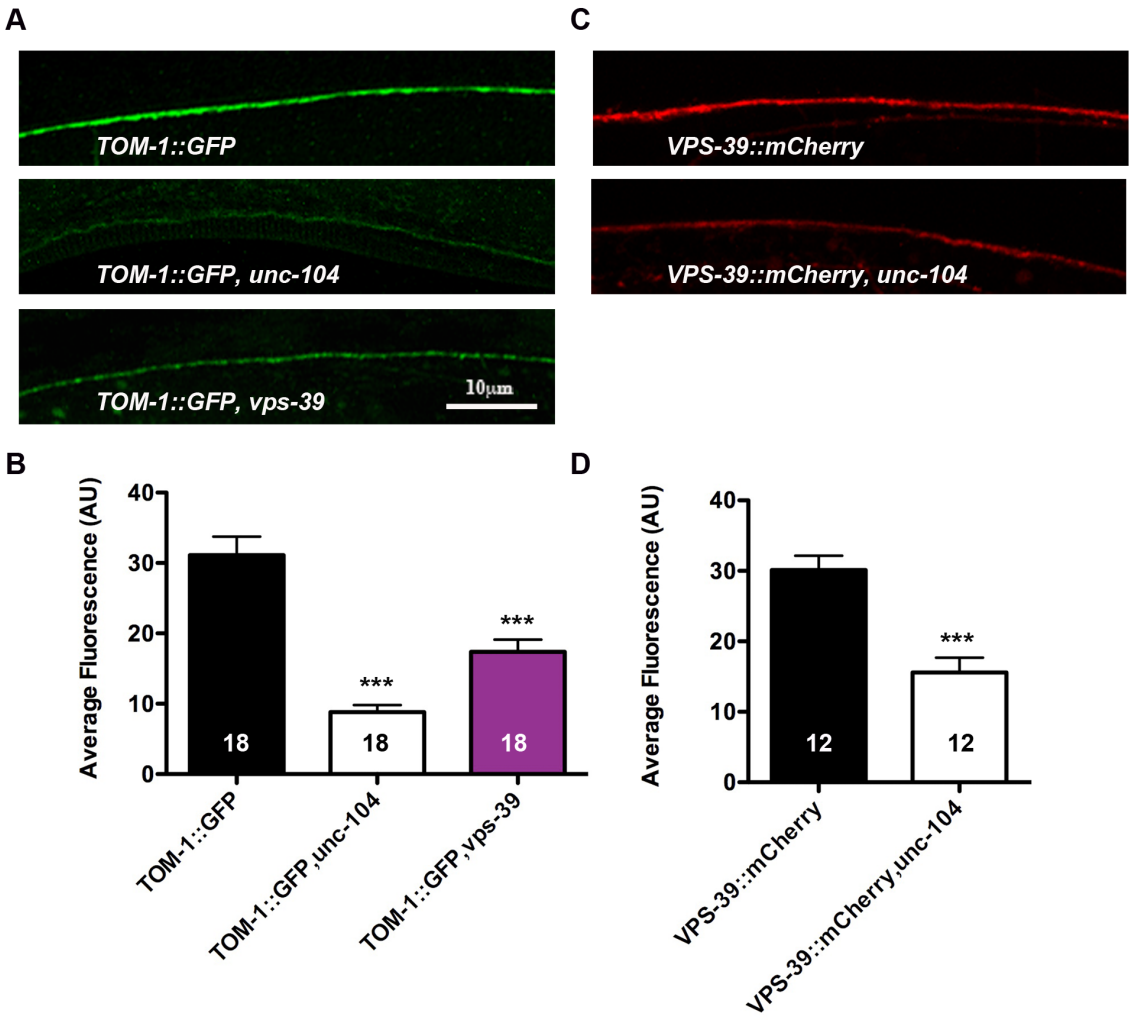

Figure 4. Expression of *TOM-1::GFP* and *VPS-39::mCherry*. (A) Representative images from the dorsal nerve cord (DNC) showing a reduction in *TOM-1::GFP* expression in the *unc-104* and *vps-39* mutant backgrounds. **(B)** Quantification indicates a significant reduction in both *unc-104* and *vps-39* mutants. Number of measurements is indicated in each bar (3/worm) **(C)** Representative images from the DNC of VPS-39::mCherry also showing a reduction in an *unc-104* mutant. **(D)** Quantificaiton also indicates a significant reduction in VPS-39::mChery expression in the *unc-104* mutant.

VPS-39 affects TOM-1 expression and both appear to be vesicle-associated

Given the Y2H data linking TOM-1 and VPS-39, we next examined whether this interaction was required for protein stabilization by crossing an integrated TOM-1::GFP transgene into the *vps-39* mutant background. TOM-1::GFP expression in the *vps-39* mutant background was reduced by approximately 50% (Figure 4A). Efforts to generate the reciprocal in which an integrated VPS-39::mCherry transgene was expressed in a *tom-1* mutant background resulted in synthetic lethality precluding analysis. However, the synaptic enrichment of both VPS-39::mCherry and TOM-1::GFP was shown to require Kinesin (UNC-104)-dependent transport, suggesting that both proteins associate with transport vesicles (Figure 4). Specifically, we observe an accumulation of VPS-39 and TOM-1 in the motor neuron cell bodies in *unc-104* mutants, and a corresponding decrease in labeling at distal synapses. In contrast, TOM-1::GFP fails to accumulate in the cell bodies of *vps-39* mutants (Supplemental Figure 1). Together these results are consistent with a physical interaction between VPS-39 and TOM-1, although efforts to pull-down VPS-39 using tagged TOM-1 and vice versa were unsuccessful, possibly reflecting a weak interaction or consequences of the considerable challenges of performing biochemistry in *C. elegans*.

VPS-39 functions in neurons to promote cholinergic synaptic transmission

Given that VPS-39 is expressed in neurons, regulates TOM-1 levels, and has an essential role in early viability we next assayed synaptic function in intact worms. The acetylcholinesterase inhibitor, trichlorfon (dylox), can be used as an indirect measure of acetylcholine release at the NMJ, as time dependent ACh accumulation in

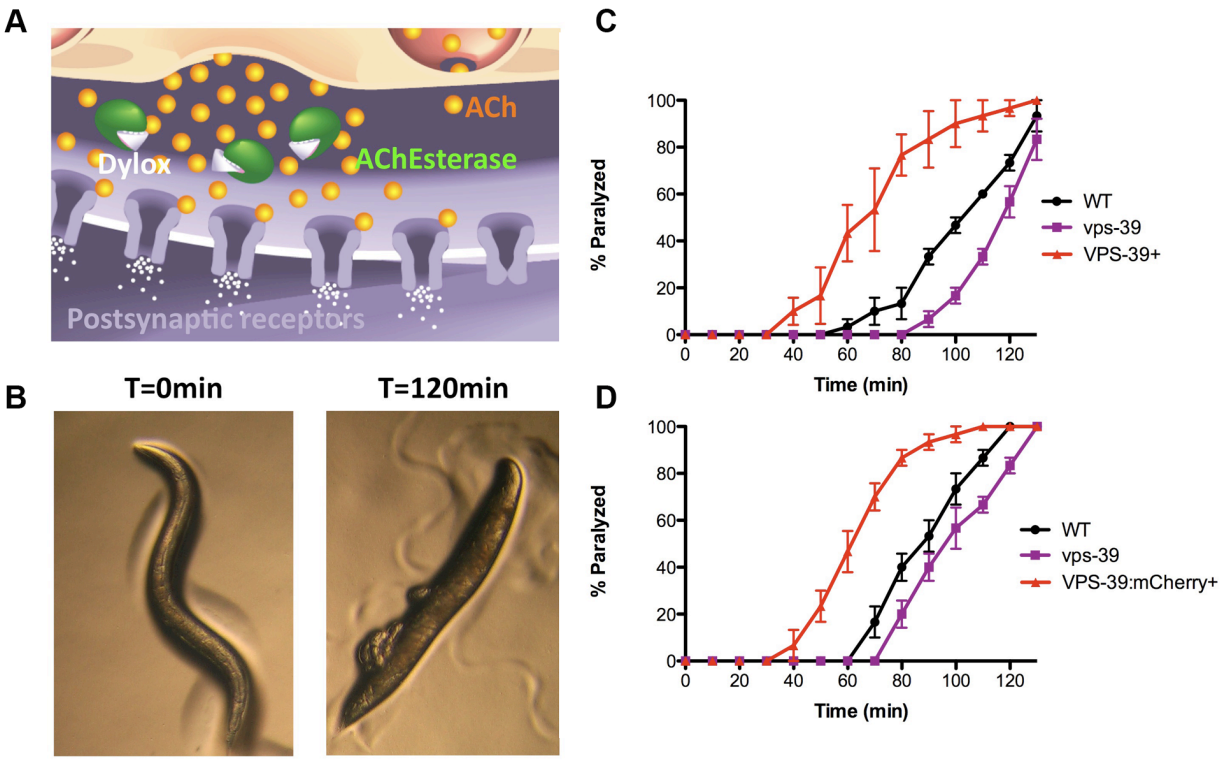

Figure 5. VPS-39 is involved in ACh release at the NMJ. (A) Schematic of the assay in which the AChEsterase is blocked by dylox. This leads to a buildup of ACh in the cleft and can be used as a measure of release. **(B)** A worm initially exposed to 5mM dylox (T=0min) has deep body bends and a worm after 120 minutes of exposure is completely straight and paralyzed due to ACh accumulation in the synaptic cleft. **(C)** Dylox sensitivities showing a resistance in *vps-39* mutants which can be reversed by expressing VPS-39 in neurons. **(D)** Same as **(C)** but an independent VPS-39 expressing line containing an mCherry tag was used. Each experiment was repeated three times, each time using 10 worms per strain.

the synaptic cleft leads to hypercontracted body-wall muscles resulting in complete paralysis (Figures 5A and 5B). Therefore, it will take longer for mutants defective in ACh release to paralyze. In contrast to the dylox hypersensitivity of *tom-1* mutants, using this assay we observed a dylox resistant phenotype in *vps-39* mutants consistent with reduced ACh release (Figures 5C and 5D). This resistance to dylox can be reversed by expression of VPS-39 in neurons using two separate integrated transgenic lines, one containing an mCherry tag (Figures 5C and 5D). The use of two independent integrated VPS-39 transgenes indicates that the rescue is not due to a positional effect of the gene insertion and confirms the functionality of the VPS-39::mCherry construct used in subsequent experiments.

Neuronal architecture and postsynaptic density is unaffected in vps-39 mutants

Dylox resistance in *vps-39* mutants could be due to defects in synaptogenesis. To address this possibility we first examined the expression of the post synaptic nicotinic receptor ACR-16::GFP. The receptor fluorescence intensity was unaltered suggesting that synaptogenesis was not impacted (Figures 6A and 6B). Consistent with this interpretation, cholinergic neuronal architecture was normal as measured by the integrity and axon targeting of the nerve cord (Figures 6C-E). These results, in conjunction with neuronal rescue of the *vps-39* mutant suggest that VPS-39 functions presynaptically to regulate ACh release.

VPS-39 regulates evoked synaptic transmission

To determine the precise nature of the presynaptic defect in *vps-39* mutants, voltage clamped recordings from body wall muscles of dissected worms in response to

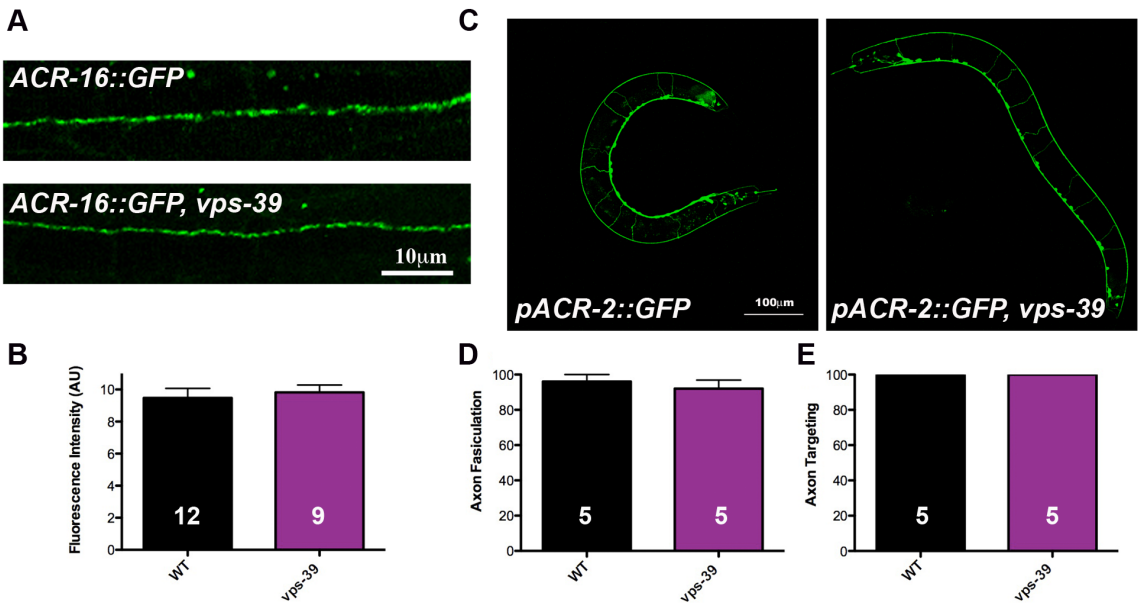

Figure 6. VPS-39 is not required for synaptic development. **(A)** Representative images of ACR-16::GFP staining in a *vps-39* mutant background. **(B)** No significant difference in expression was observed in the *vps-39* mutant. Number of measurements indicated in each bar (3 measurements/worm) **(C)** Representative images of *pACR-2::GFP* in a *vps-39* mutant background. **(D-E)** No significant difference in axon fasciculation or axon targeting was observed, sample size (# of worms examined) indicated in bars.

nerve stimulation were obtained. The evoked response from the NMJ of *vps-39* mutants was significantly reduced as evidenced by a smaller, more rapidly decaying EPSC leading to a pronounced reduction in total charge integral (Figures 7A-D). Under normal extracellular calcium recording conditions (5mM), expression of VPS-39 in neurons restored the evoked response back to wild-type levels (Figures 7A-D).

To determine whether *vps-39* mutants impact the calcium sensitivity of release we examined evoked responses under low calcium conditions (0.5mM) (Figures 7E-F). In 0.5mM calcium we observed a similar defect in evoked release leading to a 57% reduction in the charge integral in *vps-39* mutants, which was identical to the reduction observed in 5mM calcium (57%). This defect was again rescued by neuronal expression of VPS-39. These results indicate that the synaptic transmission defects are not attributable the calcium dependence of release.

VPS-39 functions to dock/prime synaptic vesicles at the ultra-structural level

Reduced evoked release could result from changes in synaptic vesicle biogenesis. To examine synaptic ultrastructure, worms were prepared by high-pressure freeze fixation and cholinergic NMJs from ultra-thin sections (40nm) were subsequently imaged. Cholinergic NMJs from *vps-39* mutants as well as the rescuing VPS-39 transgenic line displayed wild-type numbers of synaptic vesicles (WT=30.97+/-1.64 vesicles/profile n=66 profiles, *vps-39* mutant 27.7+/-0.93 n=54 profiles, VPS-39+ 27.9+/-1.01 n=56). This result indicates that changes in vesicle density does not account for the release defect.

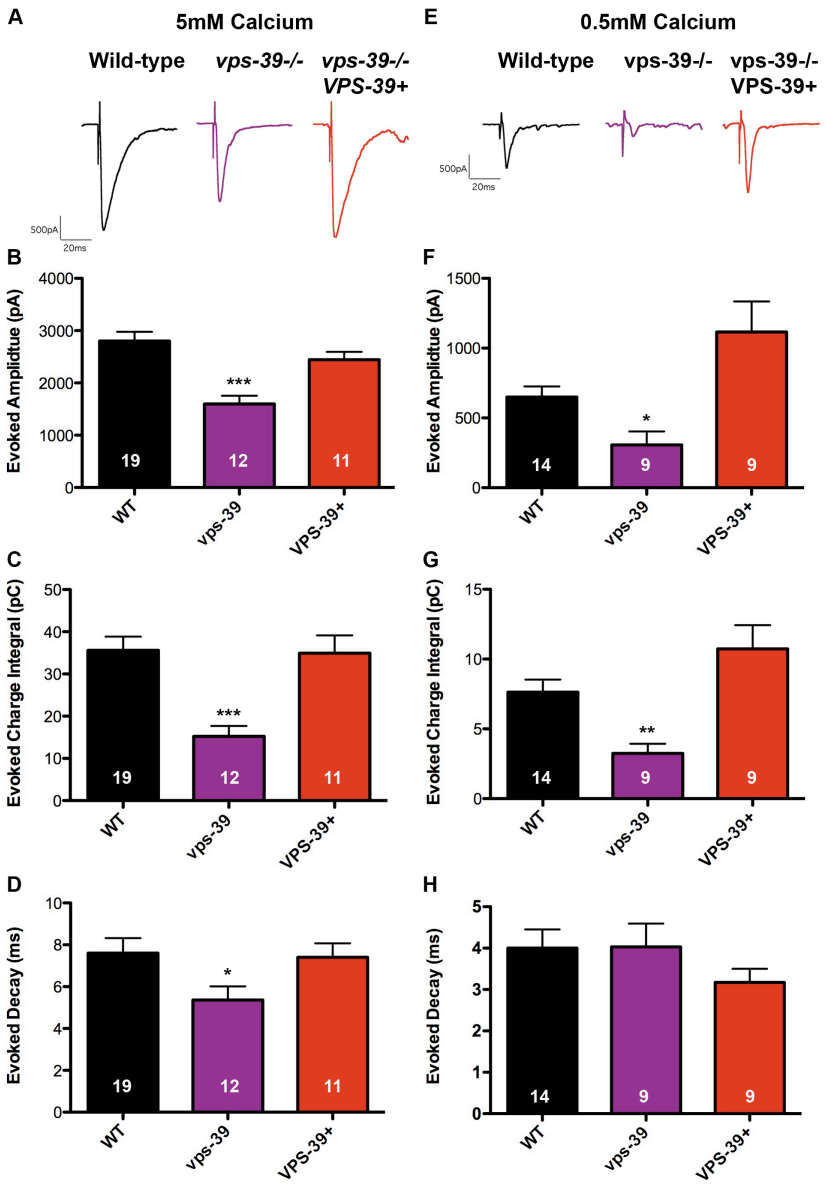

Figure 7. VPS-39 functions to promote evoked NMJ responses. (A) Representative evoked traces at 5mM calcium. **(B)** Evoked amplitude, **(C)** evoked charge integral and **(D)** evoked decay at 5mM calcium all display a significant reduction in *vps-39* mutants, which is rescued to wild-type levels upon VPS-39 expression in neurons. **(E)** Representative evoked traces at 0.5mM calcium. **(F)** Evoked amplitude and **(G)** evoked charge integral are also significantly reduced in the *vps-39* mutant at 0.5 calcium and restored back to wild-type levels upon expression of VPS-39. **(H)** There are no significant differences in evoked decay for any of the strains at 0.5 mM calcium. Sample size indicated in each bar.

Previous studies have established that the number of morphologically docked vesicles in the presynaptic terminal correlates with the number of primed, fusion competent vesicles. To determine whether VPS-39 regulates synaptic vesicle docking/priming, we examined the docked vesicle number in *vps-39* mutants (Figure 8). When the numbers of docked vesicles are examined, *vps-39* mutants exhibit a significant reduction in synaptic vesicles contacting the presynaptic membrane (Figure 8B). The docked synaptic vesicle distribution relative to the presynaptic density (PD) is reduced throughout the terminal in *vps-39* mutants suggesting that *vps-39* mutants have fewer primed vesicles. Consistent with this interpretation, the VPS-39 expression in the mutant background restores the proximal docked vesicle pool (< 90 nm from the PD) and functionally rescues release.

vps-39 mutants do not phenocopy tom-1 mutants

In contrast to *vps-39* mutants, *tom-1* mutants exhibit enhanced release, which has been attributed to an increase in the docked/primed vesicle pool. Therefore the *vps-39* mutant phenotype does not reflect the 50% decrease of TOM-1::GFP expression. However, *tom-1* heterozygotes exhibit wild-type aldicarb sensitivity and EJCs, suggesting a 50% decrease in TOM-1 is not deleterious to release. Based on these data, we hypothesize that VPS-39 regulates additional components of the release machinery, the obvious candidates being *C. elegans* homologs of Munc18 (UNC-18) and Syntaxin (UNC-64), both of which are known to bind to the HOPS complex and exhibit vesicle docking defects by HPF EM in *C. elegans* (Weimer et al., 2003; Hammarlund et al., 2007).

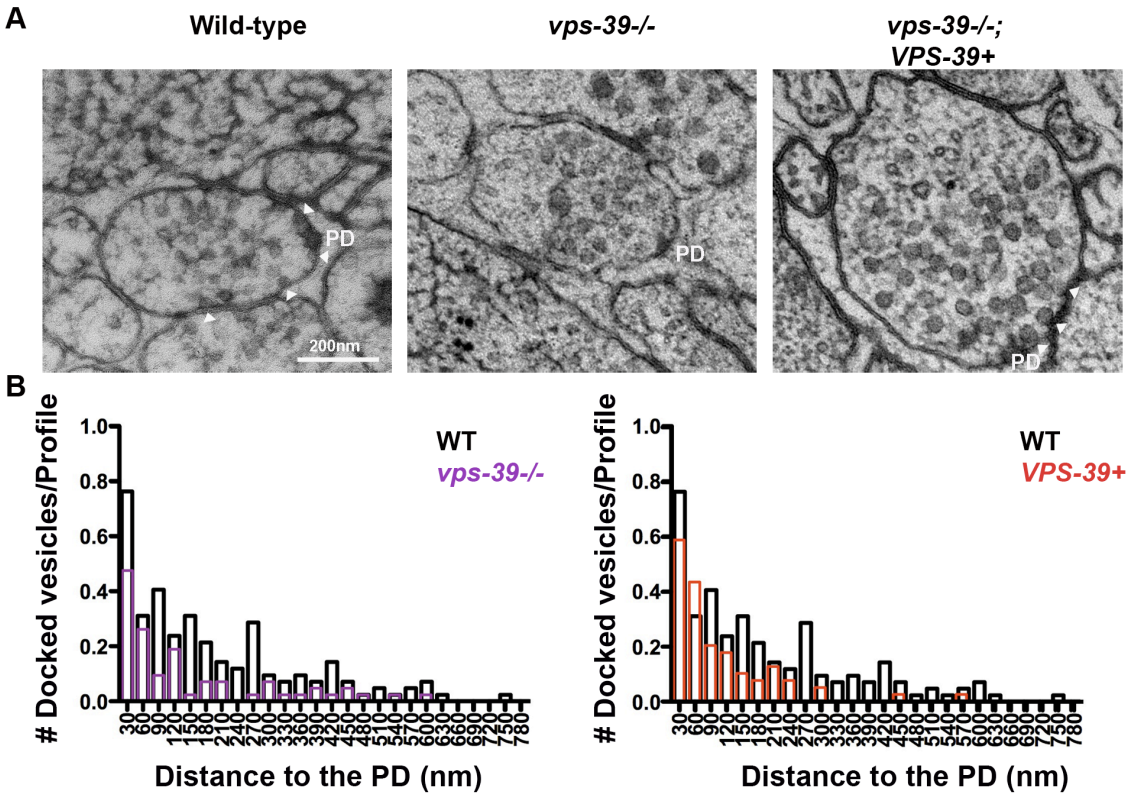

Figure 8. VPS-39 is required for vesicle docking/priming. (A) Representative electron micrographs. **(B)** Distribution of docked vesicles with respect to the PD showing *vps-39* mutants (purple) have a reduced number. VPS-39 expression profiles (red) display increased docking near the PD. n=38 profiles for WT, n=42 for *vps-39* mutant, and n=29 for VPS-39+.

VPS-39/HOPS functions to open UNC-18/Syntaxin dimers

Vesicle priming is dependent on interactions between the SNARE binding domains of Synatxin, SNAP-25 and Synaptobrevin. Syntaxin adopts a default "closed" conformation in which the SNARE binding motif is occluded. Efficient trafficking of "closed" Syntaxin to synaptic terminals is dependent on the chaperone function of Munc18. The molecular events that trigger the closed to open Syntaxin transition are unknown. Several lines of evidence implicate VPS-39 and the HOPS complex in this process: 1) HOPS proteins, Vps16 and Vps18 bind to both Munc18 and Syntaxin. 2) Over-expression of hVPS18 in cultured neurons promotes spontaneous release (Kim et al., 2006). 3) *vps-39/vam6* loss of function mutants in yeast, mouse and now shown in *C. elegans,* all exhibit vesicle fusion defects (Kramer and Ungermann, 2011). 4) Over-expression of hVam6 leads to enhanced lysosomal and endosomal fusion (Caplan et al., 2001). Based on this evidence, we hypothesized that VPS-39 regulates *C. elegans* homologs of Munc18 (UNC-18) and Syntaxin (UNC-64) to promote vesicle priming.

If VPS-39 is required to open Syntaxin, we predict that constitutively open Syntaxin should by-pass the requirement for VPS-39. To test this hypothesis we generated *vps-39* mutants expressing a constitutively open form of *C. elegans* Syntaxin (UNC-64(LE-AA) (Richmond et al., 2001). Expression of open Syntaxin enhanced the dylox sensitivity of *vps-39* mutants beyond that of wild-type worms, although not to the same extent observed in open Syntaxin alone suggesting that open Synatxin partially bypasses the requirement for VPS-39 (Figure 9A). Consistent with this behavioral data, open Syntaxin rescued the evoked release

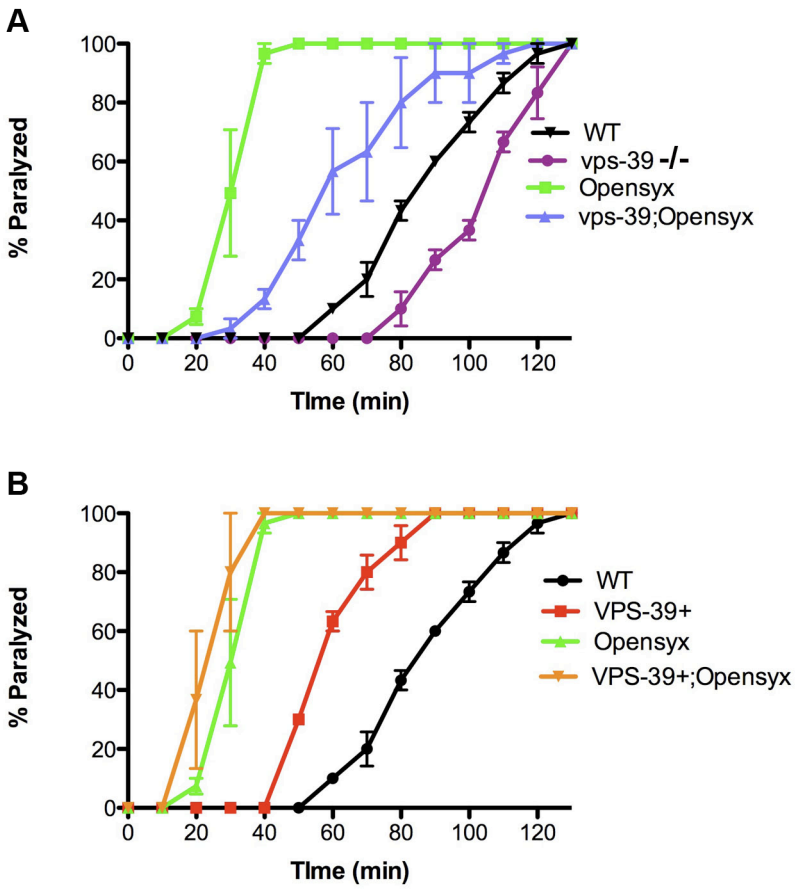

Figure 9. Open Syntaxin partially rescues the dylox resistance of *vps-39* mutants. (A) Dylox sensitivities of *vps-39* mutant with and without open Syntaxin. **(B)** Dylox sensitivities of VPS-39 neuronal expression with and without open Syntaxin. Each experiment was repeated three times, each time using 10 worms/strain.

amplitude of *vps-39* mutants to wild-type levels (Figures 10A and 10B). The faster decay kinetics of *vps-39* mutants were also restored to wild-type levels, where as open Syntaxin alone significantly prolonged the evoked response relative to wild-type. Together these observations suggest that open Syntaxin partially rescues the *vps-39* synaptic phenotype (Figures 10C and 10D).

The enhanced release in the open Syntaxin strain is due to the prolonged duration of the evoked response, which correlates with an increase in the number of morphologically docked vesicles distal to the PD (Hammarlund et al., 2007). Therefore, we hypothesize that the delayed release due to open Syntaxin reflects the time required for calcium entering at the PD to reach distally primed vesicles plus the larger diffusion time for released ACh to activate receptors localized at the post-synaptic density. To test this model, we recorded EJCs in low calcium, conditions which should reduce calcium entry, limiting the fusion of vesicles to those closest to the PD. Consistent with this interpretation, the EJC duration of open Syntaxin expressing worms in low calcium saline, was no longer increased when compared to wild-type (Figures 10E and 10H). Furthermore, in low calcium open Syntaxin failed to rescue *vps-39* mutants (Figures 10E-H). These data imply that open Syntaxin ameliorates the release defect of *vps-39* mutants by restoring vesicle docking/priming in an untargeted fashion.

Our EM (Figure 8) analysis suggests that VPS-39 rescues the docked vesicle pool proximal to the PD in *vps-39* mutants. As expected release at both high and low

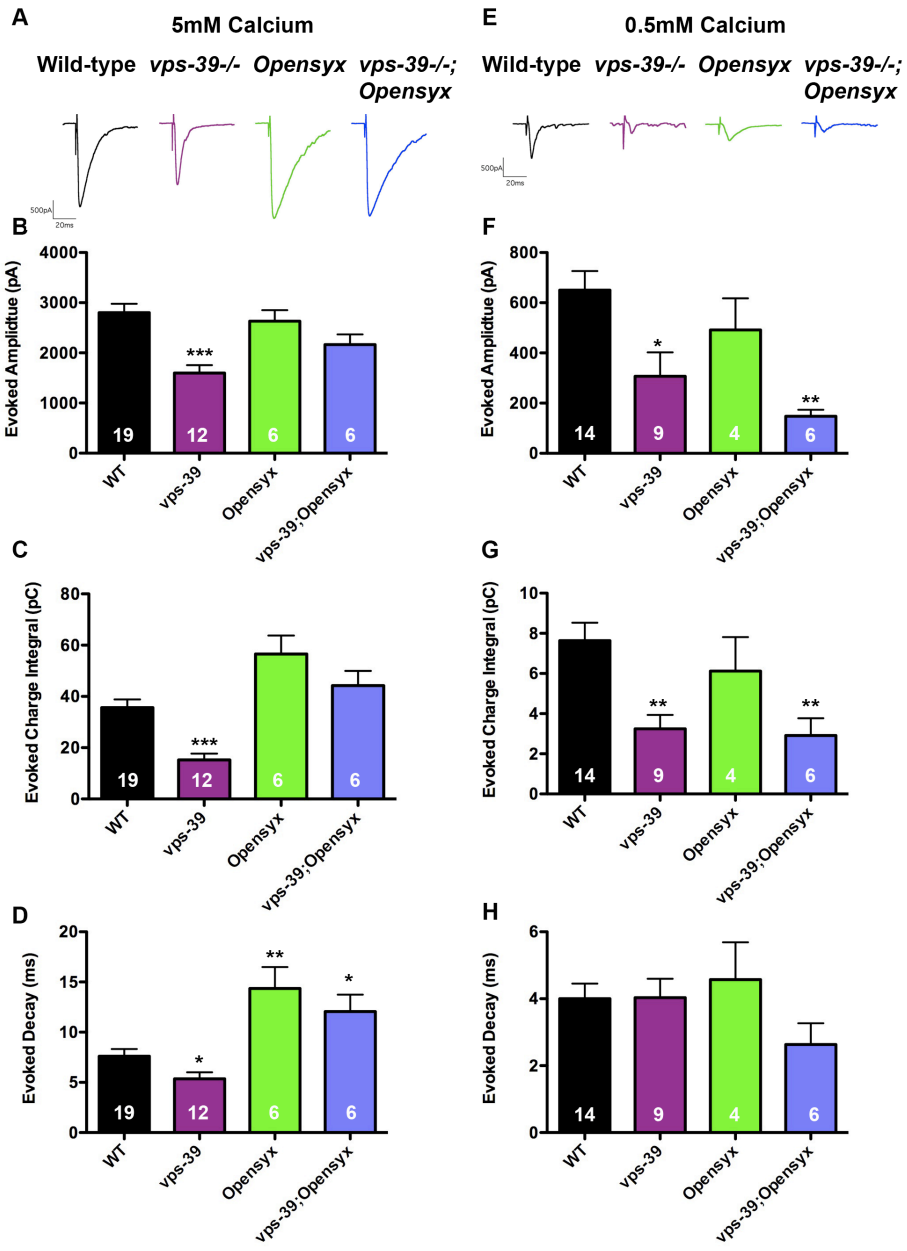

Figure 10. Open Syntaxin partially rescues the *vps-39* mutant evoked defect. **(A)** Representative evoked NMJ traces of *vps-39* mutant with and without open Syntaxin at 5mM calcium. **(B)** Evoked amplitude, **(C)** evoked charge integral and **(D)** evoked decay defects observed in the *vps-39* mutant are all significantly rescued to wild-type levels at 5mM calcium. **(E)** Representative evoked NMJ traces for the same strains in 0.5 mM calcium. **(F)** Evoked amplitude and **(G)** evoked charge integral *vps-39* mutant defects are not rescued in 0.5mM calcium. **(H)** None of the evoked decays are significantly different from each other.

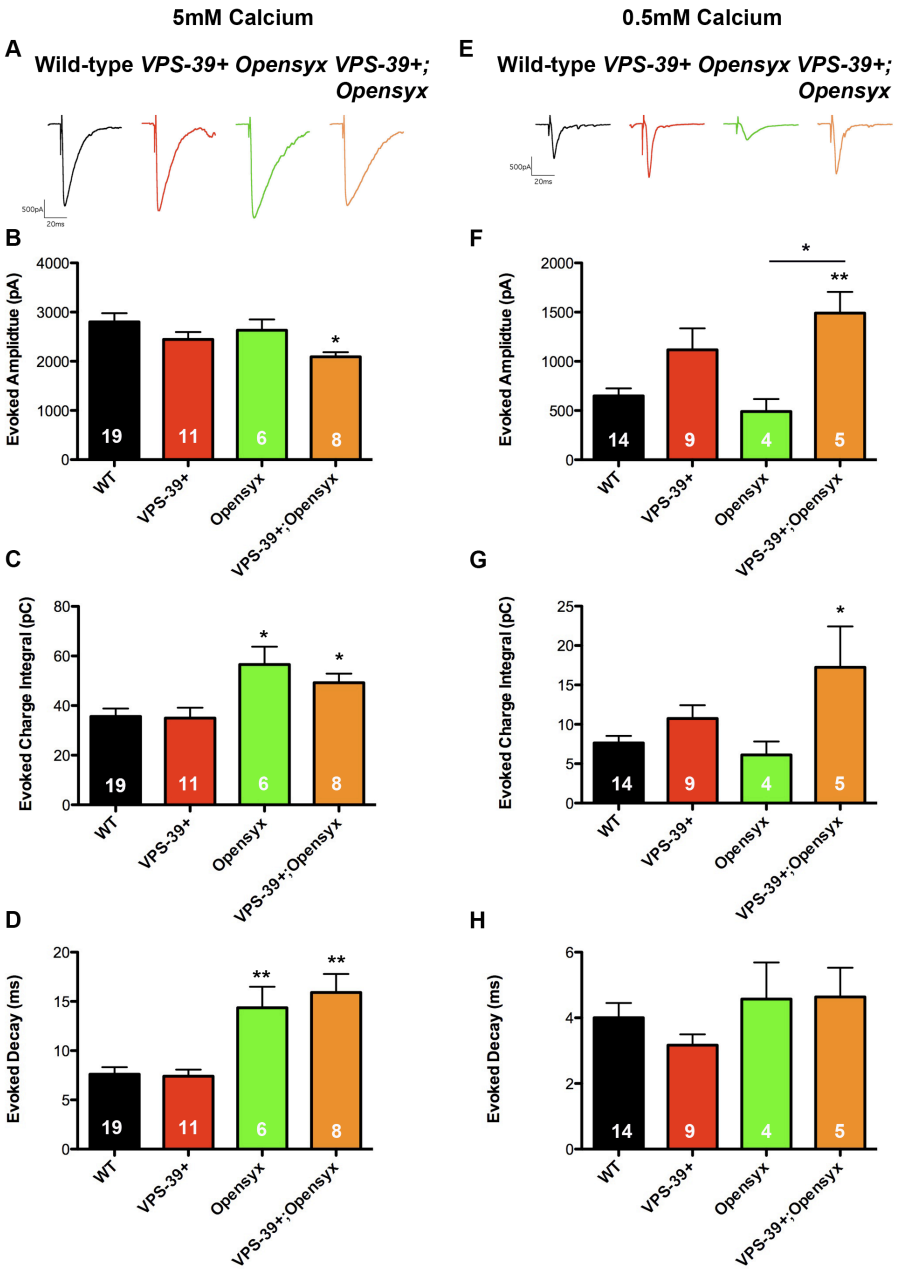

Figure 11. VPS-39/open Syntaxin co expression enhances release at low calcium. (A) Representative traces of VPS-39 expression with and without open Syntaxin at 5mM calcium. **(B)** Evoked amplidue, **(C)** evoked charge integral, and **(D)** evoked decay are indicative of a prolonged response whenever open Syntaxin is present at 5 mM calcium. **(E)** Representative traces of VPS-39 expression with and without open Syntaxin at 0.5mM calcium. **(F)** Evoked amplitude, **(G)** evoked charge integral, and **(H)** evoked decay at 0.5mM calcium. VPS-39+ can significantly enhance the evoked amplitude of open Syntaxin at 0.5mM calcium **(F).**

calcium levels were also restored in these worms (Figures 7 and 10). Furthermore VPS-39 compensated for the open Syntaxin release defects observed in low calcium (Figures 11E-H), consistent with the hypothesis that VPS-39 promotes fusion competent vesicles proximal to the PD.

The PD localized priming factor, UNC-13 interacts with the N-terminus of open Syntaxin and is thought to promote SNARE complex assembly by binding to Syntaxin after it has transitioned to the open state. Consistent with this model, previous studies have shown that priming defective *unc-13* mutants are partially rescued by expression of open Syntaxin (Richmond et al., 2001). If VPS-39 functions upstream of UNC-13 to trigger the opening of Syntaxin, as our data imply, we predict that VPS-39 overexpression will not rescue *unc-13* mutants. Consistent with this model, VPS-39 overexpression failed to rescue the evoked synaptic response of *unc-13* mutants (Figures 12A and 12B).

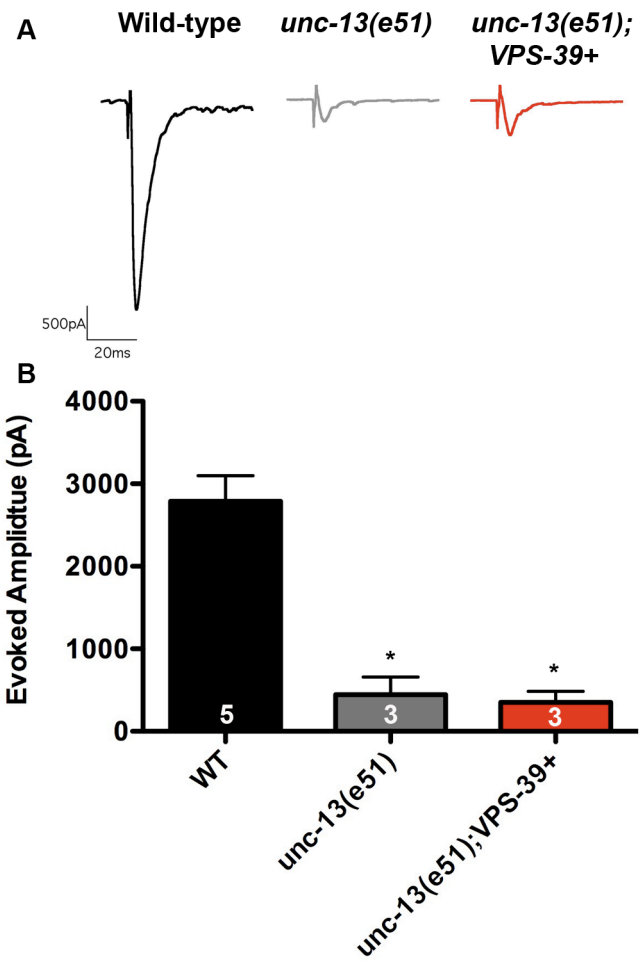

Figure 12. Expression of VPS-39 in neurons does not rescue *unc-13* mutants. **(A)** Representative traces of *unc-13* mutant with and without VPS-39 expression. **(B)** Evoked amplitudes of the *unc-13* mutant alone and in the *unc-13* mutant expressing VPS-39 are significantly reduced when compared to wild-type. Sample size indicated in each bar.

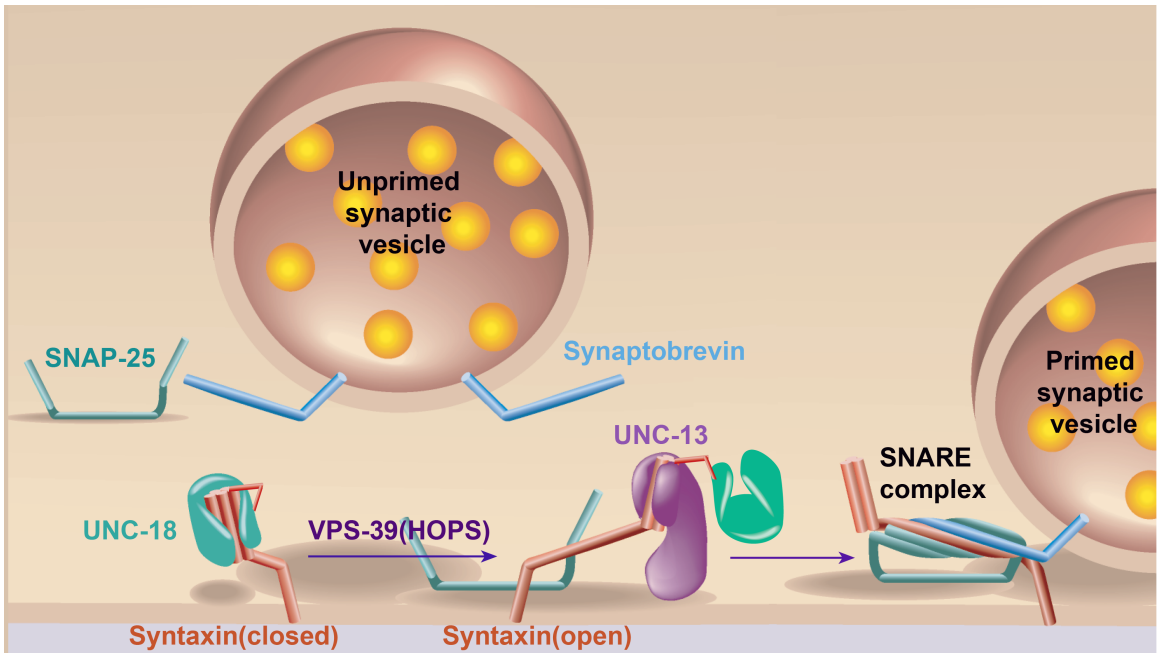

Figure 13. Model of VPS-39 function. VPS-39, likely in conjunction with the HOPS complex, functions to convert the UNC-18/Syntaxin dimer from the closed conformation to the open state. Once this opening has occurred, it can then be stabilized by UNC-13, which is enriched at the presynaptic density.

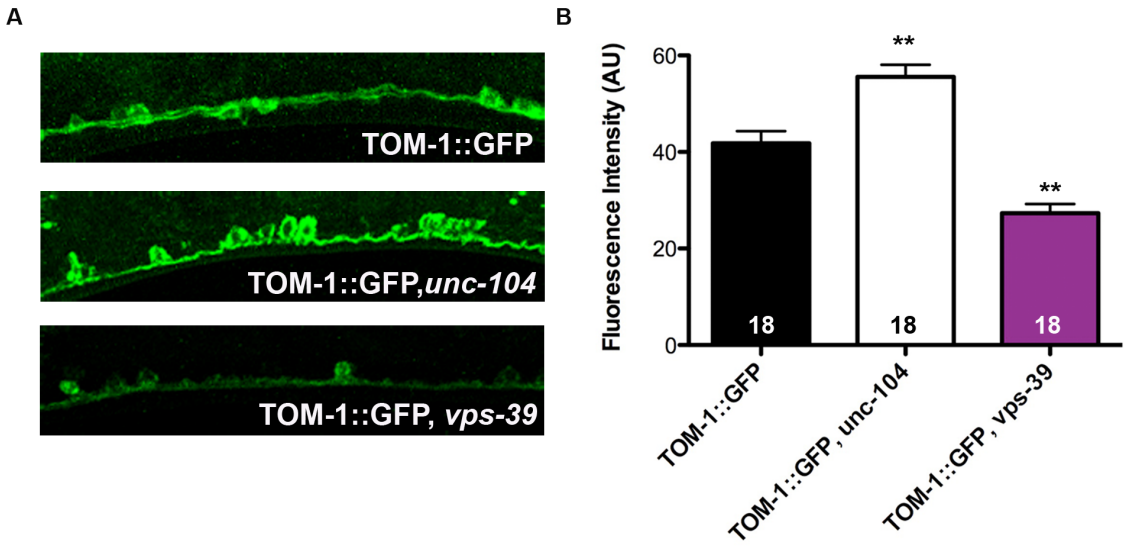

Supplementary Figure 1. TOM-1::GFP accumulates in cell bodies of *unc-104* but not *vps-39* mutants. A) Representative images of TOM-1::GFP along the ventral nerve cord in the *unc-104* and *vps-39* mutant background. B) Background subtracted quantification of cell body fluorescence intensity showing a significant increase in *unc-104* mutants and a significant decrease in *vps-39* mutants. Number of measurements is indicated in each bar, 3 measurements/worm.

4.4 Discussion

VPS-39 was identified as a potential TOM-1 binding partner in a yeast two-hybrid assay. Both TOM-1 and VPS-39 have been linked to the regulation of SNARE complexes and vesicle fusion. However, the synaptic consequences of genetically ablating *vps-39* have never been examined. Therefore, we performed a detailed characterization of VPS-39 function in the genetic model organism *C. elegans*. Analysis of a putative *vps-39* mutant revealed a defect in synaptic transmission based on pharmacological and electrophysiological data, which correlated with a decrease in the docked SV pool.

The phenotypes associated with loss of VPS-39 include a reduction in homotypic fusion of vesicles within ceolomocytes, neuronal-dependent embryonic lethality and cholinergic release defects. Consistent with this result, *C. elegans* mutants lacking TBC-2, a GAP known to indirectly regulate VPS-39 through inactivation of two sequential RAB proteins (RAB-5 and RAB-7, Figure 1B), exhibit enhanced fusion. Consequently, *tbc-2* mutants have abnormally large ceolomocyte vesicles, due to increased homotypic fusion and also exhibit large intestinal endosomes (Chotard et al., 2010). Furthermore, *rab-5(RNAi)*, the *rab-7(ok511)* deletion mutant, *vps-39(RNAi),* and *vps-41(RNAi*) all strongly suppress the enlarged endosomal vesicle phenotype observed in *tbc-2(tm2241*) mutant intestines (Chotard et al., 2010). All of these observations support the notion that TBC-2 inhibits fusion while RAB-5, RAB-7, and the HOPS complex components VPS-39, and VPS-41 promote fusion in *C. elegans*.

Although the present data implicate VPS-39 in synaptic transmission, it is unclear whether VPS-39 function requires the other HOPS complex members. However, *C. elegans* mutants impacting the HOPS complex components, VPS-16 and VPS-33, exhibit the same maternal embryonic lethality as that observed in *vps-39* mutants, indicating there is a conserved phenotype. To fully substantiate that these HOPS complex members also regulate synaptic transmission will require a detailed characterization of balanced versions of the loss-of-function mutants, which is beyond the scope of the present study.

These data support a generalized fusion role for the VPS-39-dependent pathway, in multiple tissues, consistent with its ubiquitous expression pattern in *C. elegans.* Furthermore, this function appears to be highly conserved based on the following observations from other organisms. In yeast, deletion of Vps-39 results in a cytoplasmic accumulation of vesicles which fail to fuse with the vacuole (Raymond et al., 1992). Zebrafish that lack the Vps39 homolog (*lbk*) display an enhancement in the number of vesicles in their retinal pigment epithelium, indicative of a fusion defect of endocytic vesicles (Schonthaler et al., 2008). In contrast, when the human homolog, Vam6p, is over-expressed it induces abnormal clustering and fusion of lysosomes. This latter observation suggests that hVam6p may function as a tethering/docking factor (Caplan et al., 2001).

Although we cannot discriminate between direct actions of VPS-39 on synaptic function versus indirect actions through endosomal or lysosomal sorting, based on our analysis of *C. elegans* VPS-39 we propose the following mechanism of

action. VPS-39, likely in conjunction with the HOPS complex, promotes a Syntaxin conformational change that is then stabilized by UNC-13, allowing SNARE complex formation to proceed (Figure 13). This model is based on the following experimental evidence. We have ruled out developmental changes or altered calcium sensitivity as the underlying causes of the presynaptic defect in *vps-39* mutants. Our ultrastructural data instead place VPS-39 function in the docking/priming process of the synaptic vesicle cycle, a stage that is dependent on the Syntaxin binding protein, UNC-13. Evidence suggests that UNC-13 is required to maintain Syntaxin in an open configuration compatible with SNARE complex formation at the PD, where UNC-13 is enriched (Betz et al., 1997; Dulubova et al., 1999; Richmond et al., 2001). The fact that constitutively open Syntaxin rescues both *unc-13* and *vps-39* mutants places both proteins at this stage of the pathway. However, VPS-39 overexpression fails to rescue *unc-13* mutants suggesting the HOPS complex acts upstream of UNC-13. Based on these data and previous biochemical evidence (Kim et al., 2006), we propose that VPS-39 promotes the transition of UNC-18/closed syntaxin to the open synatxin configuration, that can then be stabilized by UNC-13.

This study was initially based on yeast-2 hybrid data suggesting VPS-39 is a putative TOM-1 binding partner, an observation supported by the reduction in TOM-1::GFP seen in *vps-39* mutants. Given that TOM-1 is a negative regulator of vesicle priming, the observation that *vps-39* mutants have less neurotransmitter release was initially counterintuitive, as *tom-1* loss-of-function mutants have enhanced release. However, our subsequent analyses clearly support a role for VPS-

39 at a stage of vesicle priming that is upstream of TOM-1 function. What then is the reason for the reduced *TOM-1::GFP* expression in *vps-39* mutants? One possibility is that the VPS-39 interaction is required for the kinesin-dependent transport of TOM-1 to the synapse, given that we have shown both proteins are retained in the cell soma in an *unc-104* (Kinesin) mutant. However, in *vps-39* mutants we do not observe an accumulation of TOM-1::GFP in the cell bodies, suggesting that TOM-1 levels are globally reduced in the absence of VPS-39. An alternative explanation for the reduction in TOM-1::GFP expression is that in *vps-39* mutants the TOM-1 binding domain of Syntaxin is occluded, preventing the membrane association of TOM-1. Under these conditions TOM-1 may be degraded through the proteasome complex, which is known to regulate tomosyn levels (Williams et al., 2011).

4.5 Acknowledgements

We would like to thank; Marc Hammarlund for kindly providing Gateway donor vectors, Denis Touroutine for an expression vector, and the *C. elegans* knockout consortium for strains.

Specific Contributions:

Cloned and generated all the transgenic animals, performed and analyzed all confocal imaging, conducted all Dylox testing, and wrote the manuscript.

REFERENCES

Ashery U, Bielopolski N, Barak B, Yizhar O (2009) Friends and foes in synaptic transmission: the role of tomosyn in vesicle priming. Trends Neurosci 32:275-282.

Augustine GJ, Burns ME, DeBello WM, Pettit DL, Schweizer FE (1996) Exocytosis: proteins and perturbations. Annu Rev Pharmacol Toxicol 36:659-701.

Baba T, Sakisaka T, Mochida S, Takai Y (2005) PKA-catalyzed phosphorylation of tomosyn and its implication in Ca2+-dependent exocytosis of neurotransmitter. J Cell Biol 170:1113-1125.

Bai J, Tucker WC, Chapman ER (2004a) PIP2 increases the speed of response of synaptotagmin and steers its membrane-penetration activity toward the plasma membrane. Nat Struct Mol Biol 11:36-44.

Bai J, Wang CT, Richards DA, Jackson MB, Chapman ER (2004b) Fusion pore dynamics are regulated by synaptotagmin*t-SNARE interactions. Neuron 41:929-942.

Bennett MK, Calakos N, Scheller RH (1992) Syntaxin: a synaptic protein implicated in docking of synaptic vesicles at presynaptic active zones. Science 257:255-259.

Betz A, Okamoto M, Benseler F, Brose N (1997) Direct interaction of the rat unc-13 homologue Munc13-1 with the N terminus of syntaxin. J Biol Chem 272:2520-2526.

Brenner S (1974) The genetics of Caenorhabditis elegans. Genetics 77:71-94.

Broadie K, Bellen HJ, DiAntonio A, Littleton JT, Schwarz TL (1994) Absence of synaptotagmin disrupts excitation-secretion coupling during synaptic transmission. Proc Natl Acad Sci U S A 91:10727-10731.

Brose N, Petrenko AG, Sudhof TC, Jahn R (1992) Synaptotagmin: a calcium sensor on the synaptic vesicle surface. Science 256:1021-1025.

Caplan S, Hartnell LM, Aguilar RC, Naslavsky N, Bonifacino JS (2001) Human Vam6p promotes lysosome clustering and fusion in vivo. J Cell Biol 154:109-122.

Chapman ER (2008) How does synaptotagmin trigger neurotransmitter release? Annu Rev Biochem 77:615-641.

Chapman ER, Hanson PI, An S, Jahn R (1995) Ca2+ regulates the interaction between synaptotagmin and syntaxin 1. J Biol Chem 270:23667-23671.

Chernomordik LV, Kozlov MM (2003) Protein-lipid interplay in fusion and fission of biological membranes. Annu Rev Biochem 72:175-207.

Chheda MG, Ashery U, Thakur P, Rettig J, Sheng ZH (2001) Phosphorylation of Snapin by PKA modulates its interaction with the SNARE complex. Nat Cell Biol 3:331-338.

Chotard L, Mishra AK, Sylvain MA, Tuck S, Lambright DG, Rocheleau CE (2010) TBC-2 regulates RAB-5/RAB-7-mediated endosomal trafficking in Caenorhabditis elegans. Mol Biol Cell 21:2285-2296.

Constable JR, Graham ME, Morgan A, Burgoyne RD (2005) Amisyn regulates exocytosis and fusion pore stability by both syntaxin-dependent and syntaxin-independent mechanisms. J Biol Chem 280:31615-31623.

Craxton M (2007) Evolutionary genomics of plant genes encoding N-terminal-TM-C2 domain proteins and the similar FAM62 genes and synaptotagmin genes of metazoans. BMC Genomics 8:259.

Davletov BA, Sudhof TC (1993) A single C2 domain from synaptotagmin I is sufficient for high affinity Ca2+/phospholipid binding. J Biol Chem 268:26386-26390.

Dickman DK, Tong A, Davis GW (2012) Snapin is critical for presynaptic homeostatic plasticity. J Neurosci 32:8716-8724.

Dulubova I, Sugita S, Hill S, Hosaka M, Fernandez I, Sudhof TC, Rizo J (1999) A conformational switch in syntaxin during exocytosis: role of munc18. EMBO J 18:4372-4382.

Dulubova I, Lou X, Lu J, Huryeva I, Alam A, Schneggenburger R, Sudhof TC, Rizo J (2005) A Munc13/RIM/Rab3 tripartite complex: from priming to plasticity? Embo J 24:2839-2850.

Eitzen G, Will E, Gallwitz D, Haas A, Wickner W (2000) Sequential action of two GTPases to promote vacuole docking and fusion. EMBO J 19:6713-6720.

Fasshauer D, Margittai M (2004) A transient N-terminal interaction of SNAP-25 and syntaxin nucleates SNARE assembly. J Biol Chem 279:7613-7621.

Fasshauer D, Sutton RB, Brunger AT, Jahn R (1998) Conserved structural features of the synaptic fusion complex: SNARE proteins reclassified as Q- and R-SNAREs. Proc Natl Acad Sci U S A 95:15781-15786.

Fasshauer D, Antonin W, Subramaniam V, Jahn R (2002) SNARE assembly and disassembly exhibit a pronounced hysteresis. Nat Struct Biol 9:144-151.

Fernandez-Chacon R, Konigstorfer A, Gerber SH, Garcia J, Matos MF, Stevens CF, Brose N, Rizo J, Rosenmund C, Sudhof TC (2001) Synaptotagmin I functions as a calcium regulator of release probability. Nature 410:41-49.

Fujita Y, Shirataki H, Sakisaka T, Asakura T, Ohya T, Kotani H, Yokoyama S, Nishioka H, Matsuura Y, Mizoguchi A, Scheller RH, Takai Y (1998) Tomosyn: a syntaxin-1-binding protein that forms a novel complex in the neurotransmitter release process. Neuron 20:905-915.

Geppert M, Bolshakov VY, Siegelbaum SA, Takei K, De Camilli P, Hammer RE, Sudhof TC (1994) The role of Rab3A in neurotransmitter release. Nature 369:493-497.

Gladycheva SE, Lam AD, Liu J, D'Andrea-Merrins M, Yizhar O, Lentz SI, Ashery U, Ernst SA, Stuenkel EL (2007) Receptor-mediated regulation of tomosyn-syntaxin 1A interactions in bovine adrenal chromaffin cells. J Biol Chem 282:22887-22899.

Gracheva EO, Hadwiger G, Nonet ML, Richmond JE (2008) Direct interactions between C. elegans RAB-3 and Rim provide a mechanism to target vesicles to the presynaptic density. Neurosci Lett 444:137-142.

Gracheva EO, Burdina AO, Touroutine D, Berthelot-Grosjean M, Parekh H, Richmond JE (2007) Tomosyn negatively regulates both synaptic

transmitter and neuropeptide release at the C. elegans neuromuscular junction. J Physiol 585:705-709.

Gracheva EO, Burdina AO, Holgado AM, Berthelot-Grosjean M, Ackley BD, Hadwiger G, Nonet ML, Weimer RM, Richmond JE (2006) Tomosyn inhibits synaptic vesicle priming in Caenorhabditis elegans. PLoS Biol 4:e261.

Hammarlund M, Palfreyman MT, Watanabe S, Olsen S, Jorgensen EM (2007) Open syntaxin docks synaptic vesicles. PLoS Biol 5:e198.

Hanson PI, Roth R, Morisaki H, Jahn R, Heuser JE (1997) Structure and conformational changes in NSF and its membrane receptor complexes visualized by quick-freeze/deep-etch electron microscopy. Cell 90:523-535.

Hatsuzawa K, Lang T, Fasshauer D, Bruns D, Jahn R (2003) The R-SNARE motif of tomosyn forms SNARE core complexes with syntaxin 1 and SNAP-25 and down-regulates exocytosis. J Biol Chem 278:31159-31166.

Hattendorf DA, Andreeva A, Gangar A, Brennwald PJ, Weis WI (2007) Structure of the yeast polarity protein Sro7 reveals a SNARE regulatory mechanism. Nature 446:567-571.

Hayashi T, McMahon H, Yamasaki S, Binz T, Hata Y, Sudhof TC, Niemann H (1994) Synaptic vesicle membrane fusion complex: action of clostridial neurotoxins on assembly. EMBO J 13:5051-5061.

Hermann GJ, Scavarda E, Weis AM, Saxton DS, Thomas LL, Salesky R, Somhegyi H, Curtin TP, Barrett A, Foster OK, Vine A, Erlich K, Kwan E, Rabbitts BM, Warren K (2012) C. elegans BLOC-1 functions in trafficking to lysosome-related gut granules. PLoS One 7:e43043.

Herrick DZ, Sterbling S, Rasch KA, Hinderliter A, Cafiso DS (2006) Position of synaptotagmin I at the membrane interface: cooperative interactions of tandem C2 domains. Biochemistry 45:9668-9674.

Horz HP, Kurtz R, Batey D, Bohannan B (2004) Monitoring microbial populations using real-time qPCR on the MJ research Opticon 2 system. Application Note 2004; 3.

Hui E, Bai J, Chapman ER (2006) Ca2+-triggered simultaneous membrane penetration of the tandem C2-domains of synaptotagmin I. Biophys J 91:1767-1777.

Hui E, Johnson CP, Yao J, Dunning FM, Chapman ER (2009) Synaptotagmin-mediated bending of the target membrane is a critical step in Ca(2+)-regulated fusion. Cell 138:709-721.

Ilardi JM, Mochida S, Sheng ZH (1999) Snapin: a SNARE-associated protein implicated in synaptic transmission. Nat Neurosci 2:119-124.

Jahn R, Lang T, Sudhof TC (2003) Membrane fusion. Cell 112:519-533.

James P, Halladay J, Craig EA (1996) Genomic libraries and a host strain designed for highly efficient two-hybrid selection in yeast. Genetics 144:1425-1436.

Jorgensen EM, Hartwieg E, Schuske K, Nonet ML, Jin Y, Horvitz HR (1995) Defective recycling of synaptic vesicles in synaptotagmin mutants of *Caenorhabditis elegans*. Nature 378:196-199.

Kim BY, Sahara Y, Yamamoto A, Kominami E, Kohsaka S, Akazawa C (2006) The interaction of mammalian Class C Vps with nSec-1/Munc18-a and syntaxin 1A regulates pre-synaptic release. Biochem Biophys Res Commun 350:691-697.

Kim JS, Lilley BN, Zhang C, Shokat KM, Sanes JR, Zhen M (2008) A chemical-genetic strategy reveals distinct temporal requirements for SAD-1 kinase in neuronal polarization and synapse formation. Neural Dev 3:23.

Koh TW, Bellen HJ (2003) Synaptotagmin I, a Ca2+ sensor for neurotransmitter release. Trends Neurosci 26:413-422.

Kramer L, Ungermann C (2011) HOPS drives vacuole fusion by binding the vacuolar SNARE complex and the Vam7 PX domain via two distinct sites. Molecular biology of the cell 22:2601-2611.

Littleton JT, Stern M, Perin M, Bellen HJ (1994) Calcium dependence of neurotransmitter release and rate of spontaneous vesicle fusions are altered in Drosophila synaptotagmin mutants. Proc Natl Acad Sci U S A 91:10888-10892.

Littleton JT, Chapman ER, Kreber R, Garment MB, Carlson SD, Ganetzky B (1998) Temperature-sensitive paralytic mutations demonstrate that synaptic exocytosis requires SNARE complex assembly and disassembly. Neuron 21:401-413.

Martens S, Kozlov MM, McMahon HT (2007) How synaptotagmin promotes membrane fusion. Science 316:1205-1208.

Masuda ES, Huang BC, Fisher JM, Luo Y, Scheller RH (1998) Tomosyn binds t-SNARE proteins via a VAMP-like coiled coil. Neuron 21:479-480.

Matos MF, Mukherjee K, Chen X, Rizo J, Sudhof TC (2003) Evidence for SNARE zippering during Ca2+-triggered exocytosis in PC12 cells. Neuropharmacology 45:777-786.

Matthew WD, Tsavaler L, Reichardt LF (1981) Identification of a synaptic vesicle-specific membrane protein with a wide distribution in neuronal and neurosecretory tissue. J Cell Biol 91:257-269.

McEwen JM, Madison JM, Dybbs M, Kaplan JM (2006) Antagonistic regulation of synaptic vesicle priming by Tomosyn and UNC-13. Neuron 51:303-315.

Montecucco C, Schiavo G, Pantano S (2005) SNARE complexes and neuroexocytosis: how many, how close? Trends Biochem Sci 30:367-372.

Oyler GA, Higgins GA, Hart RA, Battenberg E, Billingsley M, Bloom FE, Wilson MC (1989) The identification of a novel synaptosomal-associated protein, SNAP-25, differentially expressed by neuronal subpopulations. J Cell Biol 109:3039-3052.

Pan PY, Tian JH, Sheng ZH (2009) Snapin facilitates the synchronization of synaptic vesicle fusion. Neuron 61:412-424.

Pang ZP, Shin OH, Meyer AC, Rosenmund C, Sudhof TC (2006) A gain-of-function mutation in synaptotagmin-1 reveals a critical role of Ca2+-dependent soluble N-ethylmaleimide-sensitive factor attachment

protein receptor complex binding in synaptic exocytosis. J Neurosci 26:12556-12565.

Perin MS, Brose N, Jahn R, Sudhof TC (1991) Domain structure of synaptotagmin (p65). J Biol Chem 266:623-629.

Plemel RL, Lobingier BT, Brett CL, Angers CG, Nickerson DP, Paulsel A, Sprague D, Merz AJ Subunit organization and Rab interactions of Vps-C protein complexes that control endolysosomal membrane traffic. Mol Biol Cell 22:1353-1363.

Pobbati AV, Stein A, Fasshauer D (2006) N- to C-terminal SNARE complex assembly promotes rapid membrane fusion. Science 313:673-676.

Pobbati AV, Razeto A, Boddener M, Becker S, Fasshauer D (2004) Structural basis for the inhibitory role of tomosyn in exocytosis. J Biol Chem 279:47192-47200.

Poirier MA, Xiao W, Macosko JC, Chan C, Shin YK, Bennett MK (1998) The synaptic SNARE complex is a parallel four-stranded helical bundle. Nat Struct Biol 5:765-769.

Poskanzer KE, Marek KW, Sweeney ST, Davis GW (2003) Synaptotagmin I is necessary for compensatory synaptic vesicle endocytosis in vivo. Nature 426:559-563.

Price A, Wickner W, Ungermann C (2000) Proteins needed for vesicle budding from the Golgi complex are also required for the docking step of homotypic vacuole fusion. J Cell Biol 148:1223-1229.

Raymond CK, Howald-Stevenson I, Vater CA, Stevens TH (1992) Morphological classification of the yeast vacuolar protein sorting mutants: evidence for a prevacuolar compartment in class E vps mutants. Mol Biol Cell 3:1389-1402.

Richmond J (2009) Dissecting and recording from the C. Elegans neuromuscular junction. J Vis Exp.

Richmond JE, Jorgensen EM (1999) One GABA and two acetylcholine receptors function at the C. elegans neuromuscular junction. Nat Neurosci 2:791-797.

Richmond JE, Davis WS, Jorgensen EM (1999a) UNC-13 is required for synaptic vesicle fusion in C. elegans. Nat Neurosci 2:959-964.

Richmond JE, Davis WS, Jorgensen EM (1999b) UNC-13 is required for synaptic vesicle fusion in *C. elegans*. Nat Neurosci 2:959-964.

Richmond JE, Weimer RM, Jorgensen EM (2001) An open form of syntaxin bypasses the requirement for UNC-13 in vesicle priming. Nature 412:338-341.

Rickman C, Hu K, Carroll J, Davletov B (2005) Self-assembly of SNARE fusion proteins into star-shaped oligomers. Biochem J 388:75-79.

Rostaing P, Weimer RM, Jorgensen EM, Triller A, Bessereau JL (2004) Preservation of immunoreactivity and fine structure of adult *C. elegans* tissues using high-pressure freezing. J Histochem Cytochem 52:1-12.

Sakisaka T, Baba T, Tanaka S, Izumi G, Yasumi M, Takai Y (2004) Regulation of SNAREs by tomosyn and ROCK: implication in extension and retraction of neurites. J Cell Biol 166:17-25.

Sakisaka T, Yamamoto Y, Mochida S, Nakamura M, Nishikawa K, Ishizaki H, Okamoto-Tanaka M, Miyoshi J, Fujiyoshi Y, Manabe T, Takai Y (2008) Dual inhibition of SNARE complex formation by tomosyn ensures controlled neurotransmitter release. J Cell Biol 183:323-337.

Sato TK, Rehling P, Peterson MR, Emr SD (2000) Class C Vps protein complex regulates vacuolar SNARE pairing and is required for vesicle docking/fusion. Mol Cell 6:661-671.

Schiavo G, Matteoli M, Montecucco C (2000) Neurotoxins affecting neuroexocytosis. Physiol Rev 80:717-766.

Schluter OM, Basu J, Sudhof TC, Rosenmund C (2006) Rab3 superprimes synaptic vesicles for release: implications for short-term synaptic plasticity. J Neurosci 26:1239-1246.

Schoch S, Deak F, Konigstorfer A, Mozhayeva M, Sara Y, Sudhof TC, Kavalali ET (2001) SNARE function analyzed in synaptobrevin/VAMP knockout mice. Science 294:1117-1122.

Schonthaler HB, Fleisch VC, Biehlmaier O, Makhankov Y, Rinner O, Bahadori R, Geisler R, Schwarz H, Neuhauss SC, Dahm R (2008) The zebrafish mutant lbk/vam6 resembles human multisystemic disorders caused by aberrant trafficking of endosomal vesicles. Development 135:387-399.

Sollner T, Bennett MK, Whiteheart SW, Scheller RH, Rothman JE (1993a) A protein assembly-disassembly pathway in vitro that may correspond to sequential steps of synaptic vesicle docking, activation, and fusion. Cell 75:409-418.

Sollner T, Whiteheart SW, Brunner M, Erdjument-Bromage H, Geromanos S, Tempst P, Rothman JE (1993b) SNAP receptors implicated in vesicle targeting and fusion. Nature 362:318-324.

Sorensen JB, Wiederhold K, Muller EM, Milosevic I, Nagy G, de Groot BL, Grubmuller H, Fasshauer D (2006) Sequential N- to C-terminal SNARE complex assembly drives priming and fusion of secretory vesicles. EMBO J 25:955-966.

Stigloher C, Zhan H, Zhen M, Richmond J, Bessereau JL (2011) The presynaptic dense projection of the Caenorhabditis elegans cholinergic neuromuscular junction localizes synaptic vesicles at the active zone through SYD-2/liprin and UNC-10/RIM-dependent interactions. J Neurosci 31:4388-4396.

Striegel AR, Biela LM, Evans CS, Wang Z, Delehoy JB, Sutton RB, Chapman ER, Reist NE (2012) Calcium binding by synaptotagmin's C2A domain is an essential element of the electrostatic switch that triggers synchronous synaptic transmission. J Neurosci 32:1253-1260.

Sutton RB, Fasshauer D, Jahn R, Brunger AT (1998a) Crystal structure of a SNARE complex involved in synaptic exocytosis at 2.4 A resolution. Nature 395:347-353.

Sutton RB, Fasshauer D, Jahn R, Brunger AT (1998b) Crystal structure of a SNARE complex involved in synaptic exocytosis at 2.4 A resolution. Nature 395:347-353.

Tang J, Maximov A, Shin OH, Dai H, Rizo J, Sudhof TC (2006) A complexin/synaptotagmin 1 switch controls fast synaptic vesicle exocytosis. Cell 126:1175-1187.

Thakur P, Stevens DR, Sheng ZH, Rettig J (2004) Effects of PKA-mediated phosphorylation of Snapin on synaptic transmission in cultured hippocampal neurons. J Neurosci 24:6476-6481.

Tian JH, Wu ZX, Unzicker M, Lu L, Cai Q, Li C, Schirra C, Matti U, Stevens D, Deng C, Rettig J, Sheng ZH (2005) The role of Snapin in neurosecretion: snapin knock-out mice exhibit impaired calcium-dependent exocytosis of large dense-core vesicles in chromaffin cells. J Neurosci 25:10546-10555.

Trimble WS, Cowan DM, Scheller RH (1988) VAMP-1: a synaptic vesicle-associated integral membrane protein. Proc Natl Acad Sci U S A 85:4538-4542.

van den Bogaart G, Jahn R (2011) Counting the SNAREs needed for membrane fusion. J Mol Cell Biol 3:204-205.

Weimer RM (2006) Preservation of C. elegans tissue via high-pressure freezing and freeze-substitution for ultrastructural analysis and immunocytochemistry. Methods Mol Biol 351:203-221.

Weimer RM, Richmond JE, Davis WS, Hadwiger G, Nonet ML, Jorgensen EM (2003) Defects in synaptic vesicle docking in unc-18 mutants. Nat Neurosci 6:1023-1030.

Weimer RM, Gracheva EO, Meyrignac O, Miller KG, Richmond JE, Bessereau JL (2006) UNC-13 and UNC-10/rim localize synaptic vesicles to specific membrane domains. J Neurosci 26:8040-8047.

Williams AL, Bielopolski N, Meroz D, Lam AD, Passmore DR, Ben-Tal N, Ernst SA, Ashery U, Stuenkel EL (2011) Structural and functional analysis of tomosyn identifies domains important in exocytotic regulation. J Biol Chem 286:14542-14553.

Wurmser AE, Sato TK, Emr SD (2000) New component of the vacuolar class C-Vps complex couples nucleotide exchange on the Ypt7 GTPase to SNARE-dependent docking and fusion. J Cell Biol 151:551-562.

Xu J, Pang ZP, Shin OH, Sudhof TC (2009) Synaptotagmin-1 functions as a Ca2+ sensor for spontaneous release. Nat Neurosci 12:759-766.

Xu T, Rammner B, Margittai M, Artalejo AR, Neher E, Jahn R (1999) Inhibition of SNARE complex assembly differentially affects kinetic components of exocytosis. Cell 99:713-722.

Yamamoto Y, Mochida S, Kurooka T, Sakisaka T (2009) Reciprocal intramolecular interactions of tomosyn control its inhibitory activity on SNARE complex formation. J Biol Chem 284:12480-12490.

Yamamoto Y, Mochida S, Miyazaki N, Kawai K, Fujikura K, Kurooka T, Iwasaki K, Sakisaka T Tomosyn inhibits synaptotagmin-1-mediated step of Ca2+-dependent neurotransmitter release through its N-terminal WD40 repeats. J Biol Chem 285:40943-40955.

Yamamoto Y, Mochida S, Miyazaki N, Kawai K, Fujikura K, Kurooka T, Iwasaki K, Sakisaka T (2010) Tomosyn inhibits synaptotagmin-1-mediated step

of Ca2+-dependent neurotransmitter release through its N-terminal WD40 repeats. J Biol Chem 285:40943-40955.

Yang L, Huang HW (2002) Observation of a membrane fusion intermediate structure. Science 297:1877-1879.

Yao J, Kwon SE, Gaffaney JD, Dunning FM, Chapman ER (2012) Uncoupling the roles of synaptotagmin I during endo- and exocytosis of synaptic vesicles. Nat Neurosci 15:243-249.

Yizhar O, Matti U, Melamed R, Hagalili Y, Bruns D, Rettig J, Ashery U (2004) Tomosyn inhibits priming of large dense-core vesicles in a calcium-dependent manner. Proc Natl Acad Sci U S A 101:2578-2583.

Yizhar O, Lipstein N, Gladycheva SE, Matti U, Ernst SA, Rettig J, Stuenkel EL, Ashery U (2007) Multiple functional domains are involved in tomosyn regulation of exocytosis. J Neurochem 103:604-616.

Zampighi GA, Zampighi LM, Fain N, Lanzavecchia S, Simon SA, Wright EM (2006) Conical electron tomography of a chemical synapse: vesicles docked to the active zone are hemi-fused. Biophys J 91:2910-2918.

Zhang JZ, Davletov BA, Sudhof TC, Anderson RG (1994) Synaptotagmin I is a high affinity receptor for clathrin AP-2: implications for membrane recycling. Cell 78:751-760.

Zheng Q, Schaefer AM, Nonet ML (2011) Regulation of C. elegans presynaptic differentiation and neurite branching via a novel signaling pathway initiated by SAM-10. Development 138:87-96.

Zhou B, Cai Q, Xie Y, Sheng ZH (2012) Snapin recruits dynein to BDNF-TrkB signaling endosomes for retrograde axonal transport and is essential for dendrite growth of cortical neurons. Cell Rep 2:42-51.

VITA
Susan M. Klosterman, BS, MS

840 W. Taylor St. #4311* Chicago, IL 60607 *(312) 996-5190 *sklost2@uic.edu

EDUCATION

2008-Present	University of Illinois at Chicago
	Ph.D. in Molecular Cellular and Developmental Biology
	Advisor: Janet E. Richmond
2006-2008	DePaul University
	M.S. in Biology
	Advisor: Margaret E. Silliker
2003-2006	Loyola University Chicago
	B.S. in Biology

TEACHING EXPERIENCE

2006-Present	Graduate Teaching Assistant
	Courses: General Biology, Genetics, Mammalian Physiology, Molecular Biology, Microbiology, and Plant Physiology

AWARDS AND HONORS

CBC Scholar Class of 2012

DAAD Research Grant 2012

Biological Honors Society

UIC Teaching Excellence Award 2009

UIC Research Excellence Award 2012

Image of Research Finalist 2012

PUBLICATIONS AND PRESENTATIONS

Differential Roles of Snapin and Synaptotagmin in the Synaptic Vesicle Cycle. Szi-Chieh Yu, Susan Klosterman, Ashley Martin, Elena Gracheva. (Feburary 2013) PLos ONE.

VPS-39 promotes synaptic vesicle fusion in *C. elegans*. Susan Klosterman, Szi-Chieh Yu, Anna Burdina, and Janet Richmond. EMBO Conference Series *C. elegans* Neurobiology. Heidelberg Germany (June 2012).

***In vivo* analysis of conserved *Caenorhabditis elegans* tomosyn domains.** Susan M. Klosterman*, Anna O. Burdina*, Luda Shtessel, Shawn Ahmed, and Janet E. Richmond. (October 2011) PLoS ONE.

Characterization of the novel TOM-1 binding partner, VPS-39, in *C. elegans.* Susan M. Klosterman, Szi-Chieh Yu, Anna O. Burdina, and Janet E. Richmond University of Illinois at Chicago, Chicago, IL, USA 60607 18th International *C. elegans* Meeting. Los Angeles, CA (June 2011).

Regulation of tomosyn (TOM-1) trafficking in *C. elegans*. Susan M. Klosterman and Janet E. Richmond**.** University of Illinois at Chicago, Chicago, IL, USA 60607. Neuronal Development, Synaptic Function, and Behavioral *C. elegans* topic meeting. Madison, WI (June 2010).

A search for genes involved in a quorum sensing mechanism that regulates mating competency in *Didymium iridis*. Susan Klosterman[1], Peter G. Hendrickson[2], Margaret E. Silliker[2] 1Molecular, Cellular, and Developmental Biology Program, University of Illinois at Chicago,Chicago, IL 60607, USA 2Department of Biological Sciences, DePaul University, Chicago, IL 60614, USA. Annual International Dictyostelium Conference. Estes Park, CO (August 2010).

Characterization of *C. elegans* Snapin mutants. Susan M Klosterman, Ashley A Martin, Hetal Parekh, Anna O Burdina, Szi-Chieh Yu, Janet Richmond. University of Illinois at Chicago, Chicago IL. 17th International *C. elegans* Meeting. Los Angeles, CA (June 2009) and Society for Neuroscience. Chicago, IL (October 2009).

PROFESSIONAL MEMBERSHIPS

Association for Women in Science

Genetics Society of America

Society for Neuroscience

UNDERGRADUATE MENTORSHIP

Scott Paskewicz (2011-2012)

Dominick Greda (2010-2011)

Juan Abadia (2009-2010)

Peter Hendrickson (2007-2008)